# Automation of Calculations in Soft-Collinear Effective Theory


Rudi Michael Rahn
New College
University of Oxford

A thesis submitted for the degree of
*Doctor of Philosophy*

Trinity 2016

# Acknowledgements

First and foremost, I thank Guido Bell for endless patience at explaining everything I didn't immediately understand, even if some of those questions in hindsight are blatantly obvious, and endless feedback for all my ideas, even if some of those ideas in hindsight are not quite as spectacular as they first appeared, and for all the guidance when I was about to run off on tangents. It has been an honour being your DPhil student.

A big Thank You also to Uli Haisch, for graciously stepping up when I found myself without a supervisor at Oxford, for always being reachable, even across countries, and for some much needed and appreciated reality syncs about physics and the world.

I could not have imagined having better supervisors.

I gratefully acknowledge the Royal Society, the source of my funding, for making my DPhil possible, and for its flexibility that allowed me to stay in Oxford for the entire duration of my course.

As an honorary James, a big Thank You also to my office mates — James, Jim, and James — for being an awesome group. We should definitely have done the Black Tie seminar when we had the chance.

I thank my family, for encouragement when I needed it, for slowing me down when I was overzealous, for listening when I needed a sounding board, for being there when I needed to talk, and for all the support over the last years.

And finally, I thank the New College MCR, *my* MCR, and all the awesome people in it, for making the past three years so very, very special. After countless opera, bar and guest nights, the committee meetings and Freshers' Fortnights, formals and brunches, I owe a lot of who I now am to you — *"Incepit vita nova"*, in the Divine Poet's words.

# Abstract

Theoretical predictions for generic multi-scale observables in Quantum Chromodynamics (QCD) typically suffer from large Sudakov logarithms associated with the emission of soft or collinear radiation, whose presence spoils the perturbative expansion in the coupling strength which underlies most calculations in QCD. A canonical way to improve predictions wherever these logarithms appear is to resum them to all perturbative orders, which can conveniently be achieved using Effective Field Theory (EFT) methods. In an age of increasing automation using computers, this task is still mostly performed manually, observable-by-observable.

In this thesis we identify the 2-loop soft function as a crucial ingredient for the resummation of QCD Sudakov logarithms to Next-to-next-to-leading logarithmic (NNLL) accuracy in Soft-Collinear Effective Theory (SCET), for wide classes of observables involving two massless colour-charged energetic particles, such as dijet event shapes at lepton colliders, or colour singlet production at hadron colliders.

We develop a method to evaluate these soft functions using numerical methods based on sector decomposition and the choice of a convenient parametrisation for the phase space. This allows the factorisation of all implicit (real emission) and explicit (virtual correction) divergences made manifest by dimensional and analytic regularisation.

The regulator pole coefficients can then be evaluated numerically following a subtraction and expansion, and two computational tools are presented to perform these numerical integrations, one based on publicly available tools, the other based on our own code. Some technical improvements over naive straightforward numerical evaluation are demonstrated and implemented.

This allows us to compute and verify two of three colour structures of the 2-loop bare soft functions for wide ranges of observables with a factorisation theorem. A number of example results - both new and already known - are shown to demonstrate the reach of this approach, and a few possible extensions are sketched.

This thesis therefore represents a crucial step towards automation of resummation for generic observables to NNLL accuracy in SCET.

# Contents

$x$

$x$

# List of Figures and Tables

# List of abbreviations and conventions

$\bar{c}$ . . . . . One of three possibilities:

1. In the context of collinear sectors (e.g. chapter 3): anticollinear, with light cone hierarchy $k_+ \gg k_-$
2. For integration variables: $\bar{c} = 1 - c$
3. In section 7.1.1: arithmetic mean of a sample of values $c_i$

**Fourier space** . . . We use $f(k) = \int \frac{\mathrm{d}x}{2\pi}\, e^{-ikx} f(x)$ to transfer from position to momentum space, and $f(x) = \int \mathrm{d}k\, e^{ikx} f(k)$ to transform back.

**IRC** . . . . . Infrared and collinear, in the context of IRC safe observables.

**jet-collinear** . . . . To distinguish collinearity to the Wilson line directions $n$ and $\bar{n}$ from collinearity to another emitted particle, we define jet-collinearity as the former

**light cone** . . . . . We define $k_- = \bar{n} \cdot k$ and $k_+ = n \cdot k$, with light-like vectors $n$, $\bar{n}$ fulfilling $n \cdot \bar{n} = 2$.

**Metric** . . . . . We use the particle physics signature: $(+ - - -)$.

**NAE** . . . . . Non-Abelian Exponentiation

**plus distributions** Defined via

$$\int_0^1 \mathrm{d}x\, \frac{f(x)}{x^{1-n\epsilon}} = \int_0^1 \mathrm{d}x\, f(x) \left( \frac{\delta(x)}{n\epsilon} + \left[\frac{1}{x}\right]_+ + n\epsilon \left[\frac{\ln x}{x}\right]_+ + \dots \right),$$

i.e.

$$\int_0^1 \mathrm{d}x\, \left[\frac{1}{x}\right]_+ f(x) = \int_0^1 \mathrm{d}x\, \frac{f(x) - f(0)}{x},$$

and similar for the higher terms.

**Spacetime** . . . . . We assume $d = 4 - 2\epsilon$ throughout this thesis.

**X** . . . . . Placeholder for letter indices. e.g. in chapter 5 we introduce functions $F_{A1}$, $F_{A2}$, $F_{B1}$ and $F_{B2}$. $F_{X1}$ means both $F_{A1}$ and $F_{B1}$ are addressed.

*ἐγὼ δὲ οὐδὲν ἐπίσταμαι πλέον πλὴν βραχέος, ὅσον λόγον παρ᾽ ἑτέρου σοφοῦ λαβεῖν καὶ ἀποδέξασθαι μετρίως.*

*I myself know nothing, except just a little, enough to extract an argument from another man who is wise and to receive it fairly.*

— Socrates
*in Plato's Theaetetus, 161b*

# 1 Introduction

The Large Hadron Collider (LHC) at CERN near Geneva was switched on for the first time to gather data in 2009, for the explicit purpose of finding the Higgs boson, and as a general searchlight for all other types of New Physics that might exist, from Supersymmetry via Extra Dimensions to Dark Matter and new sources of CP-violation. Within three years, it had gathered enough data to achieve one of its primary design goals and the discovery of the Higgs was officially announced in July 2012[1, 2]. This means for the future that the LHC's mission will be to continue gathering data, following the planned luminosity upgrade at higher rate than ever, for both precision measurements of Higgs properties, and the continued search for New Physics.

At a proton-proton ($pp$) collider like the LHC a crucial prerequisite for any success in these focus areas is a thorough understanding of the force of nature which primarily governs the interactions of $pp$ collisions - the strong interaction - because without precise knowledge of the strong dynamics it is neither possible to make accurate measurements of the properties of the Higgs itself, nor to separate the known Standard Model backgrounds from any sign of potential New Physics.

The Standard Model (SM) we just mentioned is a gauge theory of spin-$\frac{1}{2}$ fermions and a spin-0 Higgs, whose interactions are mediated by spin-1 gauge bosons associated with the gauge group $SU(3)_c \times SU(2)_L \times U(1)$. This gauge theory attempts to describe the interactions and forces we observe in experiments. Its $SU(2)_L \times U(1)$ subgroup describes

the electroweak interactions, and $SU(3)_c$ represents Quantum Chromodynamics (QCD), the gauge theory which is used to model the strong interaction.

QCD as the correct choice for the theory describing the strong interaction is not an obvious choice, because while at least some of the particles which apparently interact via the electroweak interaction can be detected directly, the same is not true for QCD. This is due to *confinement*, the observation that colour-charged particles, i.e. the particles charged under $SU(3)_C$, are never found in isolation, as asymptotic states. The major breakthrough for QCD came when this feature was explained by *asymptotic freedom*[3]: In anti-correspondence to "screening" in electromagnetism the strong interaction gets *weaker* at higher energies, and stronger as particles are further apart. As we decrease energy the coupling strength increases until all colour-charged objects are locked together into colour-neutral objects. Asymptotic freedom follows from QCD, and this is one reason QCD is now essentially settled as the correct description of the strong interaction.

Nevertheless, problems remain, especially for us theorists. The primary tool for calculations in Quantum Field Theory is Perturbation Theory, which treats all interactions as small perturbations around the theory description for free fields. This obviously poses problems when the interaction strength is too large for the interactions to be seen as "perturbations". For QCD the energy scale at which the perturbative regime of weak interactions fades into the non-perturbative regime of strong coupling sits at $\approx 1$ GeV, well below the LHC's design centre-of-mass (CoM) energy of 14 TeV. This means that naively we could expect to be able to adequately describe the interactions of weakly coupled colour-charged quarks and gluons at the CoM energy, without ever being able to verify or falsify any of QCD's predictions, because the only objects we would find in detectors are colour-neutral mesons and baryons. The transition between the *partonic* regime of quarks and gluons and the *hadronic* regime of mesons and baryons is the transition into the non-perturbative regime, for which no analytic description exists.

Fortunately, QCD processes at high centre-of-mass energy tend to *factorise*, meaning that cross sections for hadronic collisions decompose into a partonic cross-section, convoluted with universal - i.e. process independent - *parton distribution functions* (PDFs), and can be equipped with a universal hadronisation model to arrive at the hadronic

final state. This factorisation strictly is proven only for a handful of observables[4], and assumed to generically hold for others[1].

In principle we then can measure the PDFs and build hadronisation models using a few processes, and reuse them to describe any other process we like, with a perturbatively calculable partonic cross section.

It is, however, not that easy. Although at high energies QCD is perturbative, its coupling is still comparatively large - compare $\alpha_s(M_Z) \approx 0.12$ to $\alpha_{EM}(M_Z) \approx 0.008$ - and the perturbative series does not converge well. Worse, perturbative calculations for many observables break down completely in phase space regions with radiation that is soft or collinear to energetic particles. This latter problem shows itself via the appearance of logarithms of small momentum scale fractions $r$, and takes the form of *Sudakov* double logarithms $\alpha_s^n \ln^{2n} r$ at $n$-loop order, and additional terms with fewer logarithms. If now the ratio $r$ is small enough, the logarithm is large and can cancel the smallness of the perturbative expansion parameter $\alpha_s$. As this affects all perturbative orders, the series doesn't converge. This is a common problem for many observables, which suggests generic (i.e. as observable-independent as possible) strategies to solve it are sensible. The weak convergence rate of logarithm-free or logarithm-freed perturbative QCD calculations can be addressed by increasing the loop order, leading to massive increases in numbers and complexity of the diagrams involved, and consequently computer-based strategies are by now indispensible here. To allow for possible interfacing to these computational tools, automatable procedures to account for large logarithms are therefore desirable.

In practice, this aforementioned generic task of solving the convergence rate problem via increasing the loop order of any perturbative calculations is addressed by a variety of tools that automate the computation of the first virtual and real (next-to-leading order, or NLO) corrections[7–15], often interfaced with Monte-Carlo event generators[16–20] to include *parton showers* to model the collinear and soft emission dominated regions of phase space, followed by adding hadronisation models. To avoid double counting between real emissions from NLO providers and real emissions generated in parton showers, various

[1] A necessary condition for it to hold is the absence of contributions from the Glauber region[5, 6], describing virtual transverse momentum dominated modes.

matching procedures[21–25][26, 27, standardised] are used to interface NLO providers and Monte-Carlo generators. Thanks to its flexibility this sequence of tools represents the backbone of the arsenal in current particle physics phenomenology.

Yet there are drawbacks. Matching the fixed order calculations to parton showers is a nontrivial undertaking, though progress is being made[28–31], and the probabilistic nature of parton showers makes it difficult to impossible to resum more than just the leading logarithms (LL) in the Sudakov region. Some next-to-leading logarithms(NLL) can be resummed if additional features like angular ordered emissions are implemented, but achieving full NLL accuracy is not quite feasible.

Including the higher logarithms is therefore so far the domain of *analytic resummation* methods, which usually proceed on a case-by-case basis for inclusive observables, like event shapes. The case-by-case strategy is necessary because the result is not exclusive, and the loop integrals, often 2-loop or higher, depend non-trivially on the observable's functional form. So far the only computational tools which automate the resummation of generic observables are *CAESAR*[32] for NLL resummation and *ARES*[33] for resummation to NNLL accuracy.

These tools resum large logarithms using a framework in full QCD in which soft and collinear emissions are described with universal splitting functions, which can be iterated to resum logarithms from all loop orders.

An alternative framework exists in the context of effective field theories (EFT), where the large scale separation which is responsible for the large logarithm is taken as a justification to *further factorise* by decomposing also the partonic cross section into different structures describing physics at the scales that appear in the ratio responsible for the Sudakov logarithm. This turns a weakness into a strength, as we expect the EFT to become a better approximation for small ratios just as the Sudakov problem becomes worse.

The effective theory capable of resumming Sudakov logarithms in QCD is *Soft-Collinear Effective Theory*[34–37], whose dynamical degrees of freedom are the soft and collinear modes whose emission gives rise to the large logarithms. The connection to the underlying process is, as usual in EFTs, made by matching. SCET then allows us to derive an all-order factorisation theorem, which factorises the partonic cross section

into structures describing only the hard, or the collinear, or the soft dynamics, which all live at different natural scales.

The resummation of Sudakov logarithms proceeds in SCET in typical EFT manner via the renormalisation group flow. The different fragments in the fully factorised cross section are evaluated at a common scale by evolving them from their natural scale, where there are no large logarithms, to the common scale, and the logarithms are resummed in the RG evolution kernel.

This procedure performs remarkably well, and has achieved a number of $N^3LL$ resummations for threshold production and various event shapes over the last few years[38–46].

In this thesis we present a first step towards an automated resummation tool in the framework of SCET. To this end we carve out a piece of a generic NNLL resummation project and keep it as generic as possible. The reasoning here is that this can both provide us with insights about other steps of the full NNLL resummation, but also be of use on its own. The latter point is crucial, as we find that a generic NNLL resummation project usually requires at least one NNLO calculation, which is typically performed analytically, and which hence represents a major stumbling block on the way towards automation. We therefore present here a strategy to compute NNLO soft functions for wide classes of observables involving two hard colour-charged massless legs numerically, using our own programs. This provides us with the required NNLO input to derive the soft anomalous dimensions and in many cases also the renormalised soft functions, which are crucial inputs for NNLL resummation[2].

To this purpose we first review event shapes as the rough image of the observables we have in mind in chapter 2, followed by a closer review of SCET and the SCET approach to resummation in chapter 3. In chapter 4 we first find that the resummation to NNLL accuracy requires an NNLO calculation typically performed by hand, before we list the requirements observables need to fulfil in order to fit into our strategy. In chapter 5 we list the parametrisations we use to bring the soft functions into a form amenable to numerical treatment, before we outline the programs we use and/or write to perform the numerical

[2] And NNLL', which involves matching corrections at one loop order higher than just NNLL.

integrations in chapter 6. Chapter 7 illustrates some of the technical difficulties we had to overcome, and chapter 8 lists a number of known and new results derived using our own programs, selected to show the range of acceptable observables. Finally we include a short note on Wilson lines and their generation in appendix A, list the explicit form of the Master formulae we implement in computer code in appendix B, and provide the measurement functions and actual source codes in appendices C and D.

*You don't see something until you have the right metaphor to let you perceive it.*

— James Gleick
*Chaos: Making a New Science*

# 2 Event shapes

Every collider experiment at some point needs to compare its measurements to the current understanding of nature, developed by the theorists. This is anything but a trivial task, as a collider experiment ultimately measures a distribution of individual leptons and hadrons, more or less well resolved, while theoretical predictions come in the form of differential cross-sections and derived quantities that describe parton-level physics, often somewhat inclusive to avoid divergences. One approach to bridging this gap consists of *event shapes*, observables which encode geometrical aspects of the final states in collider events, as these can generally be computed using perturbation theory with smallish hadronisation effects, but can also be measured. We will use them as the starting point from which we construct the entire endeavour outlined in this thesis.

## 2.1 Using event shapes

The main use of event shapes is straightforward and two-pronged:

First, although QCD as the correct description of the strong interaction is essentially established, details of the QCD dynamics still need to be investigated, and Standard Model (SM) constants which aren't determined by the mathematical formulation have to be measured[1]. Case in point here is the determination of $\alpha_s$, extractions using event shapes[39, 42, 48–50] form one of the contributions to its world average[51, 52].

[1] And those which *are* determined by the mathematical description can be verified[47].

And second, as event shapes classify final state geometries and topologies, they can be used in searches for New Physics, where cuts on event shape values can be used to select interesting phase space regions, which may be less troubled by background[53–56]

## 2.2 Thrust and Sphericity

The field of event shapes is vast; it includes observables used at lepton colliders and lepton-hadron machines[57] as well as hadron colliders[58], some almost ancient[59, 60], a few heavily used[59] and others lesser known[61, 62]. This makes it comparatively hard to give a clear set of criteria specifying what is an *event shape* and what isn't. For our purposes we take the definition to at least include that it is a global observable, which encodes geometric information involving a hadronic system. We will use two examples, *Thrust*[59] and *Sphericity*[60][2] and construct a working understanding of event shapes and their intricacies, without attempting to deliver a precise definition, because the set of observables we ultimately address in our computational framework also includes non-event-shape observables. A rigid demarcation is therefore unnecessary for us.

The idea underlying event shapes is the attempt to translate the geometry of a final state in a collider experiment's detector to a number, hence we should not be too reliant on the exact identification of individual particles' quantum numbers, and should instead focus on the global structure of the event. Thrust and Sphericity adhere to this principle, their definition in terms of momenta is given by

$$\begin{aligned} T &= \max_{|\vec{n}_T|=1} \frac{\sum_i |\vec{n}_T \cdot \vec{p_i}|}{\sum_i |\vec{p_i}|} & S &= \min_{|\vec{n}|=1} \frac{3}{2} \frac{\sum_i |\vec{n} \times \vec{p_i}|^2}{\sum_i |\vec{p_i}|^2} \\ &= \max_{|\vec{n}_T|=1} \frac{\sum_i |\vec{n}_T \cdot \vec{p_i}|}{Q} & &= \min_{|\vec{n}|=1} \frac{3}{2} \frac{\sum_i |\vec{p_{i\perp}}|^2}{\sum_i |\vec{p_i}|^2}, \end{aligned} \tag{2.1}$$

where the sums run over *all* particles in the final state, irrespective of their charges, and where we have taken into account in the second line that the denominator for Thrust simplifies in the centre-of-mass (CoM) frame for massless particles, and that the minimisation for Sphericity selects the axis that yields the least transverse momentum to it. We've also already labelled the *Thrust axis* $n_T$, for later convenience.

[2] For others see e.g.[57, 63]

Note that while Sphericity is dimensionless, and nontrivially so[3], Thrust looks like an observable that's artificially made dimensionless, by dividing out the event independent physical scale $Q$, which is set by the experiment parameters.

Let's take a quick look at what we're measuring here: A particle contributes significantly to $T$ if the projection of its momentum onto the Thrust axis is close to its total momentum, so we identify high-Thrust events as those for which this is true for all particles in the final state. The Thrust axis is the same for all particles, therefore pencil-like events as shown on the left in figure 2.1 have $T \approx 1$, 'messier' events are assigned lower Thrust values.

Sphericity is almost complementary, because for ideally pencil-like events the transverse momentum vanishes completely (i.e. $S = 0$), whereas an ideally isotropic event corresponds to $S = 1$.

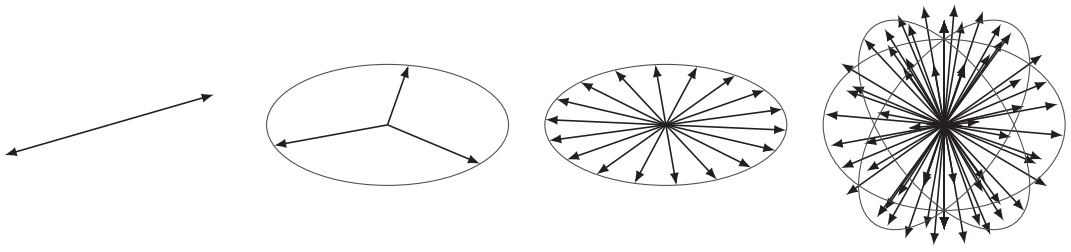

| $T = 1$ | $T = \frac{2}{3}$ | $T \geq \frac{2}{\pi}$ | $T \geq \frac{1}{2}$ |
|---|---|---|---|
| $S = 0$ | $S = \frac{3}{4}$ | $S \leq \frac{3}{4}$ | $S \leq 1$ |

**Figure 2.1:** Thrust and Sphericity values for various event geometries.

## 2.3 Fixed order calculations

So far the definition of our two event shapes only allows us to *classify* final state geometries, which obviously does not yet promote our understanding.

But as we have a precise definition in terms of momenta, we can easily start perturbative calculations of expected distributions for event shape observables, given a theory that allows us to compute S-matrix elements.

Starting with a matrix element, the differential cross section is proportional to the matrix element's square: $\mathrm{d}\sigma \sim |\mathcal{M}|^2 \, \mathrm{d}\Phi_n$ , which can be integrated to an event shape distribution:

[3],as $\sum_i |\vec{p}_i|^2$ depends non-trivially on the event geometry

$$\frac{\mathrm{d}\sigma}{\mathrm{d}e} \sim \int |\mathcal{M}|^2 \, \delta\left(e - e\left(\{k_i\}\right)\right) \prod_i \frac{\mathrm{d}^3 k_i}{2E_i} \tag{2.2}$$

The distribution is indeed differential, since integrating over the event shape placeholder $e$ on the right eliminates the $\delta$-distribution, reproducing the total cross section. Taking the constants and auxiliary factors that we've glossed over here into account, this general formula (mapped to the effective theory) is essentially the starting point for our entire project.

Let's take a closer look at Thrust:

Thrust values can in principle be assigned to any type of final state, but the ones that we are interested in are hadronic final states, and any influence Quantum Chromodynamics (QCD) might have there, so we'll limit ourselves to final states of quarks and gluons at lepton colliders.

The leading order contribution to this process is $e^+e^- \to \bar{q}q$, and momentum conservation in the centre-of-mass frame (CoM) restricts the quarks to be back-to-back, which corresponds to $T = 1$. In order to avoid singularities at non-zero values, it is convenient to define $\tau = 1 - T$. So we have at leading order

$$\frac{1}{\sigma_0}\frac{\mathrm{d}\sigma^{(0)}}{\mathrm{d}\tau} = \delta\left(\tau\right). \tag{2.3}$$

There are both virtual and real emission correction diagrams contributing at 1-loop level in full QCD, which evaluate to a corrected distribution of

$$\begin{aligned}\frac{1}{\sigma_0}\frac{\mathrm{d}\sigma^{(1)}}{\mathrm{d}\tau} = \delta\left(\tau\right) + C_F\frac{\alpha_s}{2\pi}\Bigg\{&\delta(\tau)\left(\frac{\pi^2}{3} - 1\right) - 3\left[\frac{1}{\tau}\right]_+ - 4\left[\frac{\ln\tau}{\tau}\right]_+ \\ &+ \frac{2\ln\tau}{1-\tau}\left(1 - 3\tau\right) + \frac{\left(4 - 6(1-\tau)\right)\ln(1-2\tau)}{1-\tau} + 3\left(3\tau + 2\right)\Bigg\},\end{aligned} \tag{2.4}$$

where we used the standard definition for plus-distributions[4]. To get rid of the distributions, it is a good idea to work with an integrated version of the Thrust distribution, which makes the canonical structure of the problem more apparent: The $\left[\frac{\ln\tau}{\tau}\right]_+$ term integrates to $\ln^2\tau$. This double, or *Sudakov*, logarithm is a generic feature appearing in many event

[4]Note that 3-particle states are necessarily planar, the distributions therefore have support on $\tau \in [0, \frac{1}{3}]$

shape distributions, and signals a breakdown of our ability to describe experimental outcomes adequately using straightforward perturbative quantum field theory, as can be seen in figure 2.2: The theoretical prediction matches the experimental data reasonably well, except in the region of low $\tau$, where the logarithms become dominant. Before we embark on a dynamical analysis of the physical origin of these logarithms and how to deal with them, a few more abstract remarks are in order.

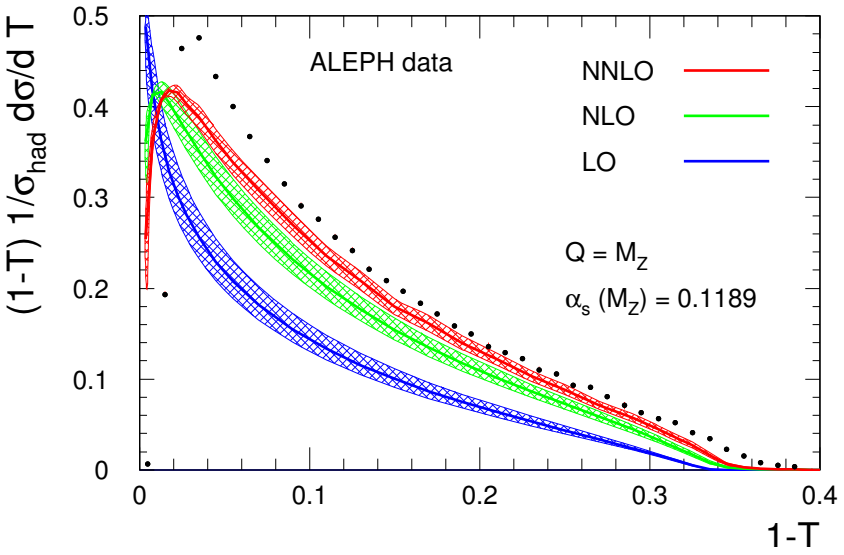


**Figure 2.2:** Comparison of the fixed-order calculations for Thrust with ALEPH data. The shaded region represents an estimate for the theoretical uncertainty. The image is taken from Gehrmann-de Ridder et al [64]'s NNLO calculation.

## 2.4 Resummation and $N^nLX$ counting

While we have only written down the 1-loop distribution, when performing calculations at various loop orders, and noting the appearance of large logarithms, we find corrections with leading terms of the structure $\alpha_s^n \ln^{2n} \tau$ at n-loop order[5]. This suggests that the usual perturbative expansion, which is assumed to be an expansion in $\alpha_s$ is actually an expansion in $\alpha_s \ln^2 \tau$, which doesn't make a difference at large values of $\tau$, but is a particularly bad choice for small $\tau$. Therefore the obvious way out of the problem is to either use a different expansion parameter, or find a way to work without the expansion, i.e without perturbation theory. The option that is usually taken, via one of two canonical

[5]This form appears in the integrated spectrum, the differential distribution exhibits matching plus-distributions.

ways, is instead to systematically construct an all-loop-order expression, which *resums* the critical terms, i.e. which expands to the pathological fixed-order result if one insists on doing so. The accuracy to which this resummed expression reproduces the fixed-order is influenced by its *logarithmic counting*, usually abbreviated as $N^nLL$, in contrast to the fixed-order $N^nLO$ loop counting. The differences between loop and logarithmic counting are not entirely straightforward — the logarithmic counting is constructed as follows:

A suitably defined fixed-order expansion of the observable that is to be resummed has (trivially) the loop-counting as the underlying ordering principle:

$$\begin{aligned} O(\tau) = a_{00} & && \text{tree} \\ &+ \alpha_s \left(L^2 a_{12} + L a_{11} + a_{10}\right) && \text{1-loop} \\ &+ \alpha_s^2 \left(L^4 a_{24} + L^3 a_{23} + L^2 a_{22} + L a_{21} + a_{20}\right) && \text{2-loop} \\ &+ \ldots + D(\alpha_s), \end{aligned} \tag{2.5}$$

where $L = \ln \tau$ stands in for the logarithm of the generic observable $\tau$ whose smallness requires resummation, and we define *suitably defined* above to mean that we somehow get rid of plus-distributions, e.g. by transforming to Laplace space or integrating the distribution to a cumulant. $D(\alpha_s)$ contains the terms that vanish as $\tau \to 0$.

We find that we can rearrange this generic expansion into an exponentiated version instead (note the *exp* in the expressions below), which reduces the severity of the problem to leading terms of $\alpha_s^n L^{n+1}$, and reshuffles terms - expanding the exponential at some order reproduces terms which would arise at different loop-orders:

$$\begin{aligned} O(\tau) &=: C(\alpha_s) \exp \Sigma(\tau) + D(\tau) \\ &= (c_0 + \alpha_s c_1 + \ldots) \\ &\times \exp\Big(\alpha_s \left[L^2 g_{12} + L g_{11} + g_{10}\right] \\ &\quad + \alpha_s^2 \left[L^3 g_{23} + L^2 g_{22} + L g_{21} + g_{20}\right] \\ &\quad + \alpha_s^3 \left[L^4 g_{34} + L^3 g_{33} + L^2 g_{32} + L g_{31} + g_{30}\right] \\ &\quad + \ldots\Big) + D(\alpha_s), \end{aligned} \tag{2.6}$$

where $D(\alpha_s)$ contains contributions which vanish as $\tau \to 0$ and we follow the notation of [65, 66].

We can now group the terms of same colour above, and end up with

$$\Sigma(\tau) = L \underbrace{g_1(\alpha_s L)}_{LL} + \underbrace{g_2(\alpha_s L)}_{NLL} + \frac{1}{L}\underbrace{g_3(\alpha_s L)}_{NNLL} + \ldots, \tag{2.7}$$

where the functions $g_i$ resum towers of $\alpha_s \ln \tau$. Constructing an expression for $g_0$ to $g_k$ now means achieving *resummation to (next-to)$^k$-leading logarithmic accuracy.*

The connection to the fixed-order result is then reestablished by *matching*, whereby a matched result is constructed as

$$X_{\text{matched}} = X_{\text{resummed}} - X^{\text{expanded}}_{\text{resummed}} + X_{\text{fixed-order}} \tag{2.8}$$

The point here is that near the critical region the fixed-order expansion is a bad expansion, so $X_{\text{resummed}}$ and $X^{\text{expanded}}_{\text{resummed}}$ are different, but the singular parts of $X^{\text{expanded}}_{\text{resummed}}$ and $X_{\text{fixed-order}}$ match, which means the surviving terms in $X_{\text{matched}}$ are the resummed quantity $X_{\text{resummed}}$ and the non-singular remainder of $X_{\text{fixed-order}}$, whereas away from the critical region the fixed-order expansion is adequate, such that $X_{\text{resummed}}$ and $X^{\text{expanded}}_{\text{resummed}}$ cancel, and the full fixed-order result survives.

## 2.5 Infrared and collinear safety

A second point of order concerns Sphericity. We've cited a result for Thrust only, with reason. We are looking at QCD-corrections to $\bar{q}q$ production on matrix element level, and this is a purely partonic affair. The detector ultimately will detect hadrons, and the transition from the partonic to the hadronic picture can so far not be described from first principles. However, due to the structure of QCD, partons will undergo splitting involving preferably soft and collinear fragments. This poses a problem for Sphericity, since replacing any particle with e.g. two collinear particles with momenta $x\vec{p}_i$ and $(1-x)\vec{p}_i$, respectively, will amount to replacing $\vec{p}_i^{\,2}$ with $\left(x^2 + (1-x)^2\right)\vec{p}_i^{\,2}$ in numerator and denominator. Since there are other terms in the sums, no cancellations occur, and the result for Sphericity changes.

For Thrust on the other hand, the splitting of one parton into perfectly collinear fragments doesn't change the Thrust value of the overall event (same for the soft splitting), so any hadronisation model that replaces one parton with a collimated jet of hadrons will only have a small effect.

In more detail there is a three-step process at work: Infrared and collinear divergences cancel in partonic calculations of the Thrust distribution. This means that no input from hadronisation is needed to arrive at a well-defined expression, and the Thrust observable is therefore not particularly sensitive to hadronisation effects. For Sphericity this is not the case. Rather, the first attempts to compute loop corrections to Sphericity had to introduce decay functions which include infrared divergences[67], which are heavily dependent on hadronisation models.

A convenient way to avoid this sort of problems is to redefine the observable and to pull the squares in equation 2.1 outside the sums. The resulting observable is called *Spherocity*[68], and is, like Thrust, an *infrared and collinear safe* observable.

Infrared and collinear safety (IRC safety) constrains observables in various nontrivial ways, and we will require it for the observables in our approaches' scope.

As for Spheri/ocity: The Spherocity axis can be difficult to determine, and although this has pushed Spherocity out of view, a variation of it has been reintroduced quite recently, so we will work with this newly defined version, and change notation accordingly. So from now on, instead of Spherocity (with a globally defined Spherocity axis), we will consider *Broadening-axis* (or *Recoil-free) Broadening*[69] as a completely generic and of course absolutely non-special second example besides Thrust. It measures particles' momentum components transverse to a suitably defined axis in each hemisphere, and naturally also suffers from large logarithms in the region of small Broadening values. Here, for each hemisphere as determined by the thrust axis, a broadening axis $\hat{b}$ is defined as the choice for $\hat{n}$ which minimises $\sum_i |\hat{n} \times \vec{p}_i|$. Broadening itself is then defined as

$$b = \sum_{i \in left} \frac{E_i}{Q} \sqrt{2(1 - \hat{b} \cdot \vec{p}_i)} + \sum_{i \in right} \frac{E_i}{Q} \sqrt{2(1 - \hat{b} \cdot \vec{p}_i)} \tag{2.9}$$

## 2.6 Origin of the large logarithms

In order to solve the problem of large logarithms we need to understand why they appear in the first place, so let's look at Thrust (or Broadening, it works just as well) in the limit $\tau \to 0$, i.e. the dijet limit.

For two particle final states momentum conservation dictates $\tau = 0$, so we need at least a third particle in order to generate non-zero Thrust values, but even then, not all configurations give rise to small $\tau$, see e.g. the second example in figure 2.1. Rather, the projection of the particles' momenta on the Thrust axis has to be close to the scalar sum of the momenta, which means a third particle in the final state must either be almost parallel to the Thrust axis, or be so low-energetic that its contribution, absent for momenta perpendicular to the Thrust axis, is not relevant. In other words, the third particle must either be either collinear to the primary partons, or soft in comparison.

The appearance of the Sudakov logarithm can then be seen as the consequence of an incomplete cancellation[70]. It is well known that the 1-loop virtual corrections to $\bar{q}q$ production exhibit infrared and collinear divergences which cancel against corresponding divergences in the $\bar{q}qg$ cross section, so that inclusive $\bar{q}q$ production at NLO is perfectly finite. The inclusive cross section involves an integral over the entire phase space for the third particle real emission, which we severely restrict when we compute event shapes like Thrust or Broadening at low values of the observable, precisely because large regions of the phase space for the third particle would correspond to unacceptably large values for the observable.

## 2.7 Resummation

Now that we have identified the source of the problem there are two main ways of setting up a framework capable of solving our dilemma open to us. It turns out they arrive at essentially the same result[66], but their outset is completely different.

### 2.7.1 Iterative soft and collinear emissions

The underlying idea of resummation for $(e^+e^-)$ event shapes in full QCD is the observation that because the double logarithm arises by virtue of an emitted gluon becoming soft (one

logarithm) and collinear (the second logarithm), higher powers of the Sudakov logarithms come associated with multiple soft and collinear gluon emissions.

However, the structure of soft and collinear emissions is universal in QCD, and can be described using a DGLAP-type splitting kernel, which means that a suitable iteration approach can be used to compute contributions from arbitrarily high order in $\alpha_s$ for any event shape which requires resummation. The vanilla template for this type of resummation framework is usually denoted as the Catani-Trentadue-Turnock-Webber or *CTTW* scheme[65], after its authors, and forms the basis for the state of the art resummation techniques in full QCD.

While a purely analytic approach, it has found a computational realisation in the form of the *CAESAR*[32] (NLL resummation) and *ARES*[33] (NNLL resummation) programs, and can therefore, unlike the second approach we're about to address, be automated.

### 2.7.2 Factorisation and the Effective theory approach

A second approach for full QCD, used for transverse momentum[6] and threshold[7] resummation especially in hadron collisions is based on QCD factorisation, followed by RG evolution of the individual factors to resum large logarithms. This is generically referred to as the Collins-Soper-Sterman/*CSS*[71] resummation scheme. While we focus on event shapes, we will also trespass onto threshold and $q_T$ resummation.

If we don't insist on full QCD, the fact that we already know that it is only a certain type of field modes that contribute to the Sudakov phase space region suggests that an Effective Field Theory (EFT) approach in which only these modes are dynamical is sensible. This is augmented by the observation that we can restate the observable whose smallness requires resummation as a ratio of scales: For Thrust, these were $\min_{\vec{n}_T} \sum_i |\vec{p}_i \cdot \vec{n}|$ and $Q$, and for Broadening $\min_{\vec{n}_\perp} \sum_i |\vec{p}_{\perp i}|$ and $Q$. Likewise, for threshold and $q_T$ resummation the (squares of the) small scales are $Q^2 - p^2$ and $q_T^2$, compared to the large $Q^2$. The problematic region is that of small values of the observable (here

[6] i.e. logarithms of $\frac{q_T}{Q}$

[7] logarithms of $(1 - \frac{p^2}{Q^2})$, where the invariant mass $p^2$ of a produced system takes up all available energy

the ratio of the scales), which is precisely the region in which an effective theory using this ratio as its expansion parameter is expected to excel.

This effective theory, which we will construct in the next chapter, is called *Soft-Collinear Effective Theory* (SCET), and will be the overarching framework under which we build our project. SCET allows its user to derive factorisation theorems which separate the theoretical description for processes to which it is applicable into different structures describing physics that plays out at different scales. Resummation in SCET is then achieved by RG flowing the constituent structures to a common scale where they are assembled to the full cross section/spectrum/expression. The RG flow shifts large logarithms into the exponents of evolution kernels, where they can't do any harm.

*Alles Gescheite ist schon gedacht worden.*
*Man muss nur versuchen, es noch einmal zu denken.*

*All intelligent thoughts have already been thought;*
*what is necessary is only to try to think them again.*

— Johann Wolfgang von Goethe
*Wilhelm Meisters Wanderjahre*

# 3 Soft-Collinear Effective Theory

In this section we'll construct the effective theory roughly outlined in the last section, and we'll use it to motivate the derivation of factorisation theorems, followed by a quick overview of the details of resummation in a SCET context. There is an almost non-exhaustive pile of literature on SCET and various complications that can arise in more or less obscure applications, but we'll stick to the bare minimum necessary to understand the basics on which we anchor our numerical approach. For more information, lecture notes[72], reviews[73], books[74, 75] and the original papers[34–37] can be readily found out in the wild.

## 3.1 Momentum modes

SCET is an effective theory for QCD and therefore a 'top-down' EFT, and in any top-down effective theory the first step is to identify the field modes which shall be retained as dynamical, and which modes are to be integrated out. The usual pedagogical examples contain entire fields which are classified as "heavy", and integrated out[1], which makes SCET slightly unusual as here only certain modes of the QCD fields are integrated out, while others are retained. We therefore have to first identify the modes which need to be kept.

[1]Examples are of course Fermi Theory[76], the Euler-Heisenberg Lagrangian[77] or some applications of Chiral Perturbation Theory[78].

### 3.1.1 Mode analysis for Thrust - SCET$_I$

We again turn to Thrust, to try to find out which modes we need to include in our EFT, and we start with fixing a few notational and conventional issues:

We'll take the CoM energy to be $Q$, and the primary partons in the dijet case to be emitted along lightlike vectors $n$ and $\bar{n}$, whose normalisation we fix such that $n \cdot \bar{n} = 2$.

We can then decompose any four-vector $q$ into lightcone components as

$$\begin{aligned} q &= q \cdot \bar{n}\frac{n}{2} + q \cdot n\frac{\bar{n}}{2} + q_\perp \\ &=: q_-\frac{n}{2} + q_+\frac{\bar{n}}{2} + q_\perp, \end{aligned} \tag{3.1}$$

where $q_\perp$ is a four-vector encoding the (two) three-momentum components transverse to the spatial components of $n$ and $\bar{n}$, i.e. $q_\perp = (0, \vec{q}_\perp)$. We will often adopt the notation that

$$q = (q_-, q_+, q_\perp). \tag{3.2}$$

In this notation, $q^2 = q_+q_- + q_\perp^2$, as can easily be seen from eq. 3.1.

Near the dijet case the definition for Thrust simplifies[65] to

$$\tau \approx \frac{p_L^2 + p_R^2}{Q^2}, \tag{3.3}$$

where $p_L$ and $p_R$ are the sums of all momenta of particles emitted in the hemispheres defined by the spatial directions of $n$ or $\bar{n}$.

Now look at explicit additional emissions, and assume we emit them only into the left hemisphere for now:

We already know that the acceptable radiation is collinear or soft, so if we emit collinear radiation to the left, we find that

$$p_L^2 \overset{!}{\sim} Q^2\tau. \tag{3.4}$$

Momentum conservation enforces that the large lightcone component must be of order $Q$, which means that $p_L^2 \sim Q^2\tau$ fixes the scaling of the (on-shell) collinear modes to be

$$k_{collinear} = Q(1, \tau, \sqrt{\tau}). \tag{3.5}$$

Adding now soft fields to the mix we find that their scaling should be

$$k_{soft} = Q(\tau, \tau, \tau), \tag{3.6}$$

lest we introduce terms in $p_L^2$ which are bigger than $Q^2\tau$, like e.g. $Q^2\sqrt{\tau}$.

For emissions into the second hemisphere the + and − components are swapped.

### 3.1.2 Mode analysis - broadening

Before we continue with our construction of SCET, we should first look at the modes that need to be included in the case of broadening.

Here we measure the transverse momentum with respect to the *broadening axis*[69], the axis which minimises the scalar sum of all momentum components perpendicular to it, which coincides with the axis laid out by the $n$ and $\bar{n}$ vectors in the dijet case and near it. The primary partons' momenta $p_1$ and $p_2$ are again oriented as for Thrust, so for any small value of broadening $b$:

$$b = \frac{\sum_{partons} |q_T|}{Q} = \frac{|p_{c\perp}| + |p_{\bar{c}\perp}| + |k_\perp|}{Q}, \tag{3.7}$$

and taking masslessness into account we find that the two acceptable scalings are

$$\begin{aligned} k_{soft} &= Q(b, b, b), \text{ and} \\ k_{collinear} &= Q(1, b^2, b), \end{aligned} \tag{3.8}$$

and the ±-swapped versions.

### 3.1.3 SCET$_I$ and SCET$_{II}$

We see that the momentum modes for broadening and Thrust are not the same, for broadening the soft mode's components scales like the transverse component of the collinear mode, and for Thrust it scales like the smaller of the ±-components. This is a main feature of SCET: The version of the theory that is used depends on the observable in question. Depending on what type of observable is to be described we may have any number of collinear sectors, and different sectors may have different virtualities. For our purposes we find that there are two types of SCET appropriate, which we call SCET$_I$ (Thrust-like) and SCET$_{II}$ (broadening-like). The precise definition we use, illustrated in figure 3.1, is that SCET$_{II}$ is the version of SCET in which the virtualities of the soft and collinear modes match, and SCET$_I$ is just the version where they don't match.

This difference between SCET$_I$ and SCET$_{II}$ causes problems, since we want to use SCET to derive factorisation theorems, and the coinciding scaling of soft and collinear

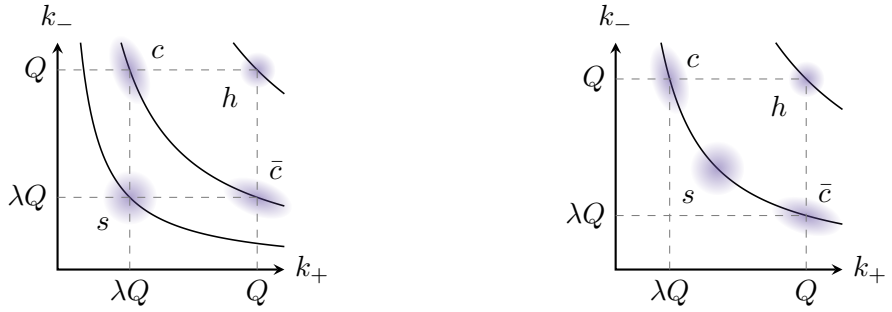


**(a)** SCET$_I$
Thrust-like

**(b)** SCET$_{II}$
Broadening-like

**Figure 3.1:** Different possible momentum scalings and their classification, using $\lambda$ as the expansion parameter. $h$, $c$, $\bar{c}$ and $s$ denote hard, collinear, anticollinear and soft scaling. Cases interpolating between these example cases are possible, see section 8.5.

modes in SCET$_{II}$ makes it difficult to separate the two sectors. If virtuality alone is not enough to classify an emission as being either soft or collinear, a second characteristic has to be used, the easiest being rapidity, which encodes the ratio between + and − components of an emission. In the straightforward calculation this shows up as an unregularised divergence, which remains even after dimensional regularisation is applied.

To solve this problem two main approaches can be found in the literature. The factorisation of the observable into collinear and soft structure requires the introduction of an additional regulator like e.g. an analytic regulator[79] or the $\Delta$-regulator[80], the dependence on which cancels when the soft and collinear structures are put together. Large logarithms remain as a remnant of this cancellation.

One approach is now to resum these large logarithms in the spirit of an RGE, and is subsequently referred to as *rapidity renormaliation group*[81].

The second approach, which we will use, is called the *Collinear Anomaly*[82], and exponentiates the large logarithms directly by deriving the form of the product of collinear and soft functions from the regulator independence of the final result.

We will deal with this in more detail when it is time to actually resum large logarithms, but for now...

## 3.2 The SCET Lagrangian

We start with the construction of the SCET Lagrangian, to learn more about the dynamics and interactions of the theory, and to see how we can derive factorisation theorems.

We will first deal with a SCET$_I$-type theory, with one soft and one collinear sector, with scaling $(\lambda, \lambda, \lambda)$ and $(1, \lambda, \sqrt{\lambda})$ in a generic expansion parameter $\lambda$, respectively, and we'll add a second, anticollinear, sector a bit later, when we need it. For this purpose we will mostly follow the approaches in [74] and [72, 83].

To begin, we split the QCD fields for quarks and gluons into soft, collinear and hard modes, where hard modes are the far off-shell modes which are integrated out and don't appear as dynamical degrees of freedom:

$$\begin{aligned} A^\mu(x) &= A_s^\mu(x) + A_c^\mu(x) + A_h^\mu(x) \\ \psi(x) &= \psi_s(x) + \psi_c(x) + \psi_h(x). \end{aligned} \tag{3.9}$$

The QCD Lagrangian has two structures of interest, the kinetic part for the gluons $(G \wedge *G)$ and that for the quarks $(\bar{\psi} \not{D} \psi)$, we begin with the gluons.

### 3.2.1 The gluon kinetic terms

The pure kinetic part of the Yang-Mills term trivially decomposes into the kinetic parts for soft and collinear gluons - momentum conservation forbids kinetic mixing between the fields - but the triple and quartic gauge interactions can include interactions like $g_s f_{ijk} (\partial_\mu A^i_{s\,\nu}) A_c^{j\mu} A_c^{k\nu}$, where the indices $s$ and $c$ denote soft and collinear field modes[2]. We do not explictly list the structure of these interactions here and denote them just symbolically by $ccs$, $ccss$ and $cccs$, as they will be eliminated at a later step (see section 3.3). Therefore we find that the gluon kinetic term translates from QCD to SCET as

$$\begin{aligned} \mathcal{L}_{A-QCD} &= -\frac{1}{4} G^a_{\mu\nu} G^{a\mu\nu} \\ &\Downarrow \\ \mathcal{L}_{A-SCET} &= -\frac{1}{4} G^a_{s\,\mu\nu} G_s^{a\mu\nu} - \frac{1}{4} G^a_{c\,\mu\nu} G_c^{a\mu\nu} + \text{Interactions}\, ccs,\ ccss,\ cccs. \end{aligned} \tag{3.10}$$

[2]Note that some interactions are forbidden by momentum conservation, e.e. the interaction of a collinear with two soft fields is not allowed, since the large energy of the collinear field cannot be carried by the soft modes.

### 3.2.2 The quark kinetic terms

It is clear that the kinetic term for the soft quarks is just the QCD version of the quark kinetic term with an additional $s$-subscript, there can again be no kinetic mixing and the covariant derivative can't contain a collinear field as there are only soft fields around: there is nothing to carry its large momentum component away.

The collinear quark Lagrangian on the other hand contains interactions between the sectors, because the suppressed momentum component of the collinear fields is of the same order as the corresponding soft gluon field momentum[3]:

$$\begin{aligned}\mathcal{L}_c &= i\bar{\psi}_c \left(\not{\partial} + igT^a \left[\not{A}_c + \not{A}_s\right]\right) \psi_c \\ &= i\bar{\psi}_c \left(\not{\partial} + igT^a \left[\not{A}_c + \frac{\not{\bar{n}}}{2} n \cdot A_s\right]\right) \psi_c,\end{aligned} \tag{3.11}$$

where we've neglected the soft gluon components which are suppressed compared to their collinear counterparts in the second line.

To continue we remember that on-shell massless Dirac spinors decompose into two two-component Weyl spinors, and realise that collinear quarks are supposed to be near on-shell. In other words we expect them to have two dominant components, and two suppressed ones. In order to identify them we define projection operators $P = \frac{\not{n}\not{\bar{n}}}{4}$ and $\bar{P} = \frac{\not{\bar{n}}\not{n}}{4}$, and decompose the quark field as

$$\xi = P\psi \qquad \phi = \bar{P}\psi. \tag{3.12}$$

To find out which of the two spinors is suppressed compared to the other, we look at their propagators. They are defined as the 2-point correlators, and hence we can derive the $\lambda$-scaling for the fields from that of the momenta. We have

$$\begin{aligned}&\int e^{-ipx} \left\langle T\, \xi(x)\bar{\xi}(0)\right\rangle \, \mathrm{d}^4x && \int e^{-ipx} \left\langle T\, \phi(x)\bar{\phi}(0)\right\rangle \, \mathrm{d}^4x \\ &= \int e^{-ipx}\, P \left\langle T\, \psi(x)\bar{\psi}(0)\right\rangle \bar{P} \, \mathrm{d}^4x && = \int e^{-ipx}\, \bar{P} \left\langle T\, \psi(x)\bar{\psi}(0)\right\rangle P \, \mathrm{d}^4x \\ &= \frac{i}{p^2+i\epsilon} \frac{\not{n}\not{\bar{n}}}{4} \not{p} \frac{\not{\bar{n}}\not{n}}{4} && = \frac{i}{p^2+i\epsilon} \frac{\not{\bar{n}}\not{n}}{4} \not{p} \frac{\not{n}\not{\bar{n}}}{4} \\ &= \frac{i}{p^2+i\epsilon} \frac{\not{n}}{2} \underbrace{\bar{n}\cdot p}_{\sim\lambda^0} && = \frac{i}{p^2+i\epsilon} \frac{\not{\bar{n}}}{2} \underbrace{n\cdot p}_{\sim\lambda^2}\end{aligned} \tag{3.13}$$

[3]Note that gauge field components need to scale like their corresponding momenta, to have equal footing between the two components of a covariant derivative

We can read off: $\phi$ is suppressed compared to $\xi$. At leading order production of $\xi$ dominates, and we will therefore not expect $\phi$s in the final state. We therefore don't include sources for the $\phi$ field in the path integral and will integrate it out. To do so, we rewrite the collinear Lagrangian using the fields $\xi/\phi$, and use the projector properties and explicit definitions of $P$ and $\bar{P}$:

$$\begin{aligned}\mathcal{L}_c &= i\left(\bar{\xi}+\bar{\phi}\right)\left(\frac{\not{n}}{2}\bar{n}\cdot D+\frac{\bar{\not{n}}}{2}n\cdot D+\not{D}_\perp\right)(\xi+\phi)\\ &= i\bar{\xi}\frac{\bar{\not{n}}}{2}n\cdot D\xi+i\bar{\xi}\not{D}_\perp\phi+i\bar{\phi}\not{D}_\perp\xi+i\bar{\phi}\frac{\not{n}}{2}\bar{n}\cdot D\phi,\end{aligned} \tag{3.14}$$

where we've used that $\not{n}\xi=\bar{\not{n}}\phi=0$ due to the definition of the projectors, and that $\xi=P\xi$ and similar for $\phi$, and that $\{P,\not{D}_\perp\}=0$, because the projectors only make use of $n$ and $\bar{n}$, and never use any of the transverse components of the lightcone basis. The unindexed covariant derivative signifies that both collinear and soft fields appear in it.

Note that the naive expectation that the terms with $\phi$ fields might be suppressed compared to the $\xi^2$-term is incorrect, the different covariant derivative components bring all four terms to the same parametric scaling/suppression: From equation 3.13 we know that $\phi$ is $\lambda^1$ suppressed compared to $\xi$, but e.g. the quadratic term in $\phi$ comes with $\bar{n}\cdot D$, which is $\lambda^2$ enhanced with respect to the $n\cdot D$ in the quadratic $\xi$-term.

Integrating out a field that only appears quadratic in the Lagrangian is not really a challenge, apart from the ordeal of sorting through a heap of terms which ultimately vanish. What one finds after the integration is a determinant which can be shown to be irrelevant[74], and a remaining Lagrangian for $\xi$ only, which can be found by deriving and solving the equations of motion for $\phi$, before plugging them back into the Lagrangian. The result, after dropping all vanishing terms is

$$\begin{aligned}\mathcal{L}_c &= i\bar{\xi}\frac{\bar{n}}{2}n\cdot D\xi+i\bar{\xi}\frac{\bar{n}}{2}\not{D}_\perp\frac{1}{\bar{n}\cdot D}\not{D}_\perp\xi\\ &= i\bar{\xi}\frac{\bar{n}}{2}\left(n\cdot D_c+ign\cdot A_s\right)\xi+i\bar{\xi}\frac{\bar{n}}{2}\not{D}_{\perp c}\frac{1}{\bar{n}\cdot D_c}\not{D}_{\perp c}\xi\end{aligned} \tag{3.15}$$

where we've made the sole remaining interaction between soft and collinear modes in the collinear Lagrangian explicit in the second line.

To arrive at a consistent EFT power counting we now need to multipole expand this Lagrangian, because the typical length scales over which the collinear fields vary -

conjugate to their typical momenta - can be much shorter than those over which soft fields vary. We therefore write at leading effective order

$$\mathcal{L}_c = i\bar{\xi}\frac{\bar{n}}{2}\left(n\cdot D_c + ign\cdot A_s(x_+)\right)\xi + i\bar{\xi}\frac{\bar{n}}{2}\not{D}_{\perp c}\frac{1}{\bar{n}\cdot D_c}\not{D}_{\perp c}\xi, \tag{3.16}$$

as the $-$ and $\perp$ components of collinear momenta are parametrically larger than their soft counterparts, which means collinear fields vary over shorter length scales in these directions, so that the soft fields are essentially constant.

As two quick comments we add that the operators in equation 3.16 are not renormalised at loop order, and that although it may not look like it, there is still a remnant of gauge invariance present.

### 3.2.3 Matching of the current

Before we deal with the last remaining soft-collinear interaction, we should turn to the current and see how it arises in SCET.

So far we've derived an EFT for QCD with only either soft modes or modes which are collinear to one lightlike direction. In practice, we will want to use it to derive results at collider experiments, in particular to describe the QCD corrections to some hard process. This means that the underlying hard Standard Model process defines an external operator of colour-charged fields, which encodes the QCD aspect of this process. The rest of the SM physics is ignored here, maybe shuffled off into a leptonic tensor. Examples are e.g. the quark vector current in the process $e^+e^- \to \bar{q}q$, or operators using the fields $\bar{q}qg$ or $qqg$ for electroweak boson production at large transverse momentum.

We then associate each of the hard colour-charged legs with a light cone vector and define a sector of collinear fields for it.

As an example, strategically chosen as it will be the most important underlying process for us, we take the quark vector current $\bar{\psi}\gamma\psi$, originating from $e^+e^-$ annihilation. In typical EFT fashion we now match this QCD current to its SCET version, which involves one collinear and one anticollinear quark[4] field.

[4] i.e. one collinear quark as before, and a quark from a second collinear sector, whose characteristic lightcone direction is not $n$, but $\bar{n}$.

Let's try to find the appropriate SCET operator, then. A naive choice would be the direct translation $\bar{\psi}\Gamma\psi \to \bar{\xi}_{\bar{n}}\Gamma\xi_n$, where the subscripts denote the collinear fields in the two different sectors, and $\xi_n$ shall be the collinear field from before. We would then compute virtual and real corrections to this operator using the Feynman rules derived from equation 3.16. But there is a problem: The collinear gauge field has one component which scales as $\lambda^0$, which means that as soon as we include the external operator above into our theory, we also generate versions of this operator with additional large gluon components attached to it. This can easily be understood from an EFT point of view:

Any Standard Model diagram which generates the current operator we want can be modified to include an additional emission of a collinear gluon off the outgoing anticollinear quark. If the outgoing anticollinear quark is to remain anticollinear, the internal quark propagator is pushed off-shell and integrated out in the transition to SCET. Diagrammatically, this is illustrated in figure 3.2. In a typical EFT we would simply expand the internal propagator, observe that the higher orders are suppressed by $\frac{p^2}{M^2}$, and conclude that effective operators with additional derivatives are suppressed.

In SCET this isn't the case, because one component of the collinear momentum is large: We start with the QCD diagram with an additional emission, and then transition to SCET:

$$\begin{aligned}
&\bar{\psi}\, ig\not{A}^a T^a \frac{\not{p}+\not{k}}{(p+k)^2+i\epsilon}\Gamma\psi \\
&\to \bar{\xi}_{\bar{n}} ig\not{A}_n{}^a T^a \frac{\not{p}+\not{k}}{(p+k)^2+i\epsilon}\Gamma\xi_n \\
&= \bar{\xi}_{\bar{n}} ig\frac{\not{n}}{2}\bar{n}\cdot A_n^a T^a \frac{\frac{\not{\bar{n}}}{2}n\cdot p+\frac{\not{n}}{2}\bar{n}\cdot k}{\bar{n}\cdot k\, n\cdot p+i\epsilon}\Gamma\xi_n \\
&= \bar{\xi}_{\bar{n}} ig\frac{\not{n}\not{\bar{n}}\not{n}}{4}\bar{n}\cdot A_n^a T^a \frac{n\cdot p}{\bar{n}\cdot k\, n\cdot p+i\epsilon}\Gamma\xi_n \\
&= \frac{igT^a}{\bar{n}\cdot k+i\epsilon\,\mathrm{sgn}\, n\cdot p}\,\bar{n}\cdot A_n^a\,\bar{\xi}_{\bar{n}}\Gamma\xi_n
\end{aligned} \tag{3.17}$$

where we dropped subleading terms in the third line, and used projector and Dirac matrix properties in the fourth and fifth line. In the result there is no parametric suppression apparent, and the operator structure to the right in the last line is what we put into the translation, plus one additional gluon.

If one takes care to include the correct non-abelian diagrams[83], this can even be generalised to multi-gluon emission, and a whole tower of operators with any number

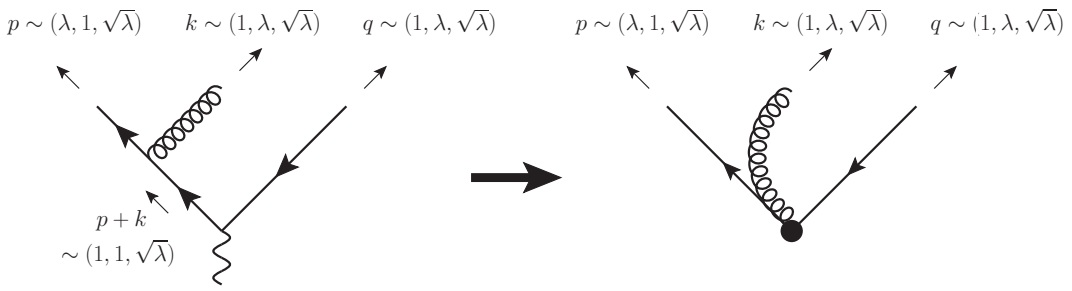


**Figure 3.2:** A QCD diagram which contributes to the collinear Wilson line. The particles going to the right are collinear, those going to the left anticollinear.

of $\bar{n} \cdot A_n$ gluons can be generated, and the coefficient will collect one more eikonal factor for each additional gluon.

As it turns out the additional emissions can be grouped into a Wilson line, i.e. an object of the form

$$W_n^\dagger(x) = \mathrm{P} \exp\left( igT^a \int_0^\infty \mathrm{d}s \ \bar{n} \cdot A_n^a(x + s\bar{n}) \right), \tag{3.18}$$

where $P$ denotes path ordering, i.e. the requirement that the colour matrices appearing in a string of fields are ordered along the integration contour. Physically, a Wilson line accompanying a collinear field contains the collinear gluons emitted by the anticollinear field in collinear direction, i.e. backwards if the quarks are back-to-back, and whose emission cannot be described using the Feynman rules in the EFT.

The form of the Wilson line is dependent on the underlying process, emissions off incoming particles, or antiparticles rather than particles, have different Wilson lines. We explore this in more detail in appendix A. One lesson to take away is that the Wilson lines which appear in the formulae we use throughout this thesis depend on the underlying event, i.e. are different if the current annihilates a $\bar{q}q$ pair or produces it, even if the same QCD current is responsible.

So a better choice for the current seems to be $J(x) = \bar{\xi}_{\bar{n}}(x) W_{\bar{n}}(x) \Gamma W_n^\dagger(x) \xi_{n(x)}$.

But not even that is the final answer, because derivatives behave just like gauge fields. This means we can generate operators carrying any number of derivatives without punishment as well. Arbitrary numbers of derivatives are usually a sign for non-locality, and indeed that is the case here: The same principle which leaves large momentum components in the Wilson line case generates dependence on large momentum components in the

virtual diagrams appearing in the explicit calculation of the hard matching coefficients between QCD and SCET. Momentum dependence in Fourier space corresponds to non-locality in position space, and so we find[5] that rather than having local operators with multiplicative factors we need to use a current of the form

$$J^\mu(x) = \int \mathrm{d}s\ \mathrm{d}t\ C(s,t) \left[\bar{\xi}_{\bar{n}} W_{\bar{n}}\right](x+sn)\gamma^\mu \left[W_n^\dagger \xi_n\right](x+t\bar{n}). \tag{3.19}$$

This is also intuitively unsurprising, the reasoning to justify locality in EFTs is usually that the available energies are not sufficient to resolve the substructure, but in this case the lightcone components of collinear and hard modes match along the collinear directions, the assumption that we can't resolve the underlying hard physics is not valid. The emergence of Wilson lines is then almost required, because there is still residual gauge invariance in the theory, and we therefore need gauge invariant operators. From a differential geometry point of view, Wilson lines are the parallel transport of the gauge action along a path through the space-time manifold, and in this particular case we connect the gauge action at $x$ and $\infty$. So while $\xi$ and $W$ on their own are not gauge invariant, the combination $W^\dagger(x)\xi(x)$, and therefore the entire operator, is.

## 3.3 Decoupling transformation

We noted in equation 3.16 that there was a term that still allowed interactions between soft and collinear modes in the collinear quark Lagrangian. If we want to derive an all-order factorisation theorem, this interaction must be removed, as well as the interaction terms that we found at the very beginning in the gluon kinetic term.

For both of these terms the crucial insight is that we can make use of a *decoupling transformation* to eliminate the interaction. To that end we redefine the collinear fields as

$$\begin{aligned} \xi_n(x) &\to S_n(x_-)\xi_n^{(0)}(x) \\ A_n(x) &\to S_n(x_-)A_n^{(0)}(x)S_n^\dagger(x_-) \end{aligned} \tag{3.20}$$

where $S_n$ is a Wilson line of soft fields along the $n$ direction, defined analoguously to $W$ in equation 3.18.

[5] The virtual diagrams are more tedious than to simply integrate out a propagator at tree level, it is worked out in more detail in [74], where the momentum space Wilson coefficient is derived. Fourier transforming then makes the non-locality explicit.

With this definition we have

$$\begin{aligned} D\xi_n &\to \left(\partial + igS_nA_n^{(0)}S_n^\dagger + ig\frac{\bar{n}}{2}n\cdot A_s\right) S_n\xi_n^{(0)} \\ &= S_n\partial\xi_n^{(0)} + igS_nA_n^{(0)}\xi_n^{(0)} + (\partial S_n(x_-))\,\xi_n^{(0)} + ig\frac{\bar{n}}{2}n\cdot A_s S_n(x_-)\xi_n^{(0)} \\ &= S_nD_n^{(0)}\xi_n^{(0)} + \frac{\bar{n}}{2}\Big(\underbrace{\frac{\partial}{\partial\bar{n}\cdot x} + ign\cdot A_s(\bar{n}\cdot x)}_{n\cdot D_sS_n=0}\Big)S_n(x_-)\xi_n^{(0)} \end{aligned} \tag{3.21}$$

Here we suppressed the $x$-dependence of $S$ wherever we didn't need it, used that $SS^\dagger = \mathbb{1}$, that the derivative acting on $S$ pulls gauge fields out of the exponential, and finally that the covariant derivative of a Wilson line vanishes along its integration contour[6].

From this it is immediately clear that the interaction in the quark term vanishes, but it also kills the interaction in the gluon term, as here the transformation of the covariant derivative implies that the field strength tensor transforms as $G^{\mu\nu} \to S_nG_n^{(0)\mu\nu}S_n^\dagger$, and the cyclicity of the trace then takes care of the rest.

This decoupling transformation of course also affects the external operator we found earlier, so for the last time we now have to add an "actually", and point out that the actual current, and the one that we definitely are going to use has the form

$$J^\mu(x) = \int \mathrm{d}s\mathrm{d}t\;\; C(s,t,\mu)\;\left[\bar{\xi}_{\bar{n}}W_{\bar{n}}\right](x+sn)\,S_{\bar{n}}^\dagger(x_+)\gamma^\mu S_n(x_-)\;\left[W_n^\dagger\xi_n\right](x+t\bar{n}). \tag{3.22}$$

The dependence on $s$ and $t$ drops out of the soft Wilson lines as $(x+t\bar{n})_- = \bar{n}\cdot(x+t\bar{n}) = x_-$.

## 3.4 Generic matching

If we try to apply this procedure to other momentum scalings than the Thrust-like case we just went through, we find that what we derived is just one special case, albeit an important and very instructive one:

We assumed that the smallest component of the collinear modes' momenta scales like the soft momentum. This of course does not need to be true, in fact it certainly isn't true for SCET$_{II}$ observables, whose soft and collinear modes share the scaling in the *transverse* momentum components. Another example we will encounter later is the angularities

[6] This is trivially true, the Wilson line is the parallel transport of the gauge action along a certain trajectory, and therefore defined as the unique section for which the covariant derivative vanishes along that trajectory.

observable, its soft and collinear modes scale as $(\lambda, \lambda, \lambda)$ and $(1, \lambda^{1+A}, \lambda^{\frac{1+A}{2}})$ with $A < 2$, respectively. In other words, it interpolates between the Thrust case[7] we covered over the last few pages and the SCET$_{II}$ case[8], and is only of the form we assumed if $A = 0$.

Fortunately, everything is a bit easier in the non-special case. Take broadening: An interaction between collinear modes and a soft mode would shift the outflowing momentum to $(1, \lambda, \lambda)$, which has a different virtuality than both soft and collinear modes and also cannot be on-shell, because the contribution to the virtuality from transverse and lightcone components have different parametric weight.

This of course means this mode is integrated out, and therefore there can't be any interactions between soft and collinear modes right from the start. The structure of the effective current operator 3.22 will nevertheless still be generated, the same mechanism that generates the collinear Wilson lines can in this case generate the soft Wilson lines - internal propagators in the full QCD diagrams give rise to eikonal factors.

## 3.5 Factorisation for Thrust

There are now no more interactions between soft and collinear sectors, and we can start to derive factorisation theorems, and as an instructive example we will now derive the factorisation theorem for Thrust.

We closely follow the derivation in [75], with some modifications and variable relabelling wherever we feel the need to highlight crucial points.

The cross section for $e^+e^- \to$ dijet in the Standard Model produces the final state partons via an electroweak current, we assume for now there's only the photon. The QCD dynamics then takes the form

$$\mathrm{d}\sigma = \sigma_0 \frac{-2\pi}{NQ^2} \sum_X \mathrm{d}\Pi_X \, (2\pi)^4 \delta^{(4)}(q - p_X) \, \langle\Omega| \, J_\mu^\dagger(0) \, |X\rangle \, \langle X| \, J^\mu(0) \, |\Omega\rangle \, . \tag{3.23}$$

Here $\sigma_0$ is the tree-level electromagnetic cross section for $q\bar{q}$-production of all flavours and $N$ colours, $q = (Q, Q, 0)^T$ is the momentum of the $s$-channel photon, and $J^\mu$ is the electromagnetic quark current. Dijet production means that any radiation apart from the primary quarks has to be collinear or soft, therefore using SCET is appropriate.

[7] $A = 0$
[8] $A = 1$

The quark current is then replaced by the external operator in equation 3.22 in the transition to SCET. $X$ are the QCD final states, which will be weighted/restricted by the $\delta$-distribution defining Thrust.

In the SCET copy for Thrust there are no interactions between soft, collinear and anticollinear sectors following decoupling, and hence the sum over the states $|X\rangle$ decomposes into a sum over individual soft, collinear and anticollinear final states:

$$\begin{aligned} \sum_X &\to \sum_{X_s, X_c, X_{\bar{c}}} \\ |X\rangle &\to |X_s\rangle \otimes |X_c\rangle \otimes |X_{\bar{c}}\rangle \,, \end{aligned} \tag{3.24}$$

which allows us to decompose $\langle\Omega| J_\mu^\dagger(0) |X\rangle \langle X| J^\mu(0) |\Omega\rangle$ using 3.22 to

$$\begin{aligned} \langle\Omega| J_\mu^\dagger(0) |X\rangle \langle X| J^\mu(0) |\Omega\rangle \to \int \mathrm{d}s' \,\mathrm{d}t' \,\mathrm{d}s \,\mathrm{d}t \, C^*(s',t') C(s,t) \\ \cdot \langle\Omega| \left[S_n^\dagger(0) S_{\bar{n}}(0)\right]_{cd} |X_s\rangle \langle X_s| \left[S_{\bar{n}}^\dagger(0) S_n(0)\right]_{ab} |\Omega\rangle \\ \cdot \langle\Omega| (\bar{\xi}_{n,k} W_n)_c(t'\bar{n}) |X_c\rangle \langle X_c| (W_n^\dagger \xi_{n,j})_b(t\bar{n}) |\Omega\rangle \, \gamma_{kl}^\mu \\ \cdot \langle\Omega| (W_{\bar{n}} \xi_{\bar{n},l})_d(s'n) |X_{\bar{c}}\rangle \langle X_{\bar{c}}| (\bar{\xi}_{\bar{n},i} W_{\bar{n}})_a(sn) |\Omega\rangle \, \gamma_{\mu,ij} \\ = \int \mathrm{d}s' \,\mathrm{d}t' \,\mathrm{d}s \,\mathrm{d}t \, C^*(s',t') C(s,t) \, \mathrm{tr}\left[\gamma_\mu \frac{\not{n}}{8} \gamma^\mu \frac{\not{\bar{n}}}{8}\right] \\ \cdot \langle\Omega| \left[S_n^\dagger S_{\bar{n}}\right]_{cd}(0) |X_s\rangle \langle X_s| \left[S_{\bar{n}}^\dagger S_n\right]_{ab}(0) |\Omega\rangle \\ \cdot \frac{\delta_{bc}}{N} \,\mathrm{tr}\, \langle\Omega| (\bar{\xi}_n W_n)(t'\bar{n}) |X_c\rangle \langle X_c| \not{\bar{n}} (W_n^\dagger \xi_n)(t\bar{n}) |\Omega\rangle \\ \cdot \frac{\delta_{ad}}{N} \,\mathrm{tr}\, \langle\Omega| (W_{\bar{n}} \xi_{\bar{n}})(s'n) |X_{\bar{c}}\rangle \langle X_{\bar{c}}| \not{n} (\bar{\xi}_{\bar{n}} W_{\bar{n}})(sn) |\Omega\rangle \,, \end{aligned} \tag{3.25}$$

where we made the colour indices $a, \ldots, d$ manifest, and used the fact that the structures containing collinear and anticollinear fields can be trivially rearranged if we include spinor indices $i, \ldots, l$. In the transition over the equality we used that

- The collinear structures describe the propagation of only one sector, and there are no interactions between sectors, so the "input" colour at the hard interaction is conserved, and these structures must be colour diagonal. Averaging over colours then produces the factor $\frac{1}{N}$.

- Lorentz invariance dictates the proportionality of the collinear and anticollinear structures to $\not{\bar{n}}$ and $\not{n}$, which yields the Dirac trace near the $C$-factors and the traces in the last two lines. The details can be found in [75, p.797-800].

Next we get rid of the explicit non-locality. We introduce the Fourier transform of $C(s,t,\mu)$:

$$C(s,t,\mu) = \int \mathrm{d}k\,\mathrm{d}l\, e^{iks} e^{ilt}\, \tilde{C}(k,l,\mu) \tag{3.26}$$

Using the translation operator we find that

$$\langle X_c|\, \mathcal{O}(t\bar{n})\, |\Omega\rangle = \langle X_c|\, e^{i\hat{\mathcal{P}}\cdot t\bar{n}} \mathcal{O}(0) e^{-i\hat{\mathcal{P}}\cdot t\bar{n}}\, |\Omega\rangle = e^{it\bar{n}\cdot p_{X_c}} \langle X_c|\, \mathcal{O}(0)\, |\Omega\rangle \tag{3.27}$$

Plugging $C$ in terms of its Fourier transform and this translation into equation 3.25 allows us to perform the $s$, $s'$, $t$ and $t'$ integrations, which each yield one $\delta$-distribution, which fix $k$ and $l$ to the large components of the collinear and anticollinear momenta: $\bar{n}\cdot p_c$ and $n\cdot p_{\bar{c}}$

With this we can turn to the momentum conservation enforcing $\delta$-distribution in equation 3.23. Here we realise that $p_X$ is nothing but the sum of radiated momenta from all relevant sectors, i.e. $p_X = p_c + p_{\bar{c}} + p_s$. We know the typical scaling of these modes, so the Dirac $\delta$ falls apart accordingly:

- For the $n$-components we find $\delta(\bar{n}\cdot q - \bar{n}\cdot p_X) = \delta(Q - \underbrace{\bar{n}\cdot p_c}_{\sim\lambda^0} - \underbrace{\bar{n}\cdot p_{\bar{c}}}_{\sim\lambda^2} - \underbrace{\bar{n}\cdot p_s}_{\sim\lambda^2}) = \delta(Q - \bar{n}\cdot p_c)$, which *fixes* this component[9]. Likewise $\delta(Q - n\cdot p_{\bar{c}})$ fixes the $n$-component.
- As $\vec{q}_\perp = \vec{0}$, and $\vec{p}_{s\perp} \sim \lambda \vec{p}_{c\perp,\bar{c}\perp}$, the $\perp$-component is determined by $\delta(\vec{p}_{\bar{c}\perp} + \vec{p}_{c\perp})$. This can be further simplified by realising that we integrate over the relative orientation between incoming leptons and outgoing partons when computing the cross section, which means that the final result can't depend on our choice for the axis $\vec{n}$ we use to define "collinear". We can therefore choose our coordinate system for a collinear sector such that the $z$-axis points along $\vec{n}$. This forces the transverse components of this sector to vanish, which we compensate for by introducing a new constraint $4\pi\frac{Q^2}{4}\delta^{(2)}(p_{c\perp})$. An alternative take on this is that we perform the integration $\mathrm{d}^2 p_{c\perp}$ (which is implicit in the sum over $X_c$) directly, because we know via symmetry that it can only contribute a constant factor. This also explains the prefactor $4\pi\frac{Q^2}{4}$, it is the area covered by this integration, momentum conservation enforces $|\vec{p}_c| = \frac{Q}{2}$.

[9] Before this we only assumed a rough magnitude of $\sim Q$ for this component, this Dirac $\delta$ nails the value down to Q exactly.

Overall momentum conservation therefore reads

$$\delta^{(4)}(q - p_X) \to 2\pi Q^2 \delta(Q - \bar{n}\cdot p_c)\delta(Q - n\cdot p_{\bar{c}})\delta^{(2)}(p_{c\perp})\delta^{(2)}(p_{\bar{c}\perp}), \tag{3.28}$$

where the factor of 2 appears due to the transition to lightcone coordinates.

We can see here that this constraint fixes three of four components of both the $p_c$ and $p_{\bar{c}}$ vectors. This can be made explicit by defining new vectors

$$r_c^\mu = \frac{n^\mu}{2}Q + \frac{\bar{n}^\mu}{2}x_c \qquad r_{\bar{c}}^\mu = \frac{\bar{n}^\mu}{2}Q + \frac{n^\mu}{2}x_{\bar{c}}, \tag{3.29}$$

which obey the same constraints from momentum conservation trivially and highlight the freedom in the smaller lightcone component in each sector. Adding a superfluous constraint for the suppressed $n\cdot p_c$ and $\bar{n}\cdot p_{\bar{c}}$ to identify them with $x_c$ and $x_{\bar{c}}$ yields

$$\begin{aligned}\delta^{(4)}(q - p_X) &\to 2\delta(Q - \bar{n}\cdot p_c)\delta(Q - n\cdot p_{\bar{c}})\pi Q^2\delta^{(2)}(p_{c\perp})\delta^{(2)}(p_{\bar{c}\perp}) &(3.30)\\ &\quad\cdot\int \mathrm{d}x_c\,\mathrm{d}x_{\bar{c}}\,\delta(x_c - n\cdot p_c)\delta(x_{\bar{c}} - \bar{n}\cdot p_c) &(3.31)\\ &= 2\pi Q^2\int \mathrm{d}x_c\,\mathrm{d}x_{\bar{c}}\,\frac{1}{2}\delta^{(4)}(r_c^\mu - p_c^\mu)\,\frac{1}{2}\delta^{(4)}(r_{\bar{c}}^\mu - p_{\bar{c}}^\mu) &(3.32)\end{aligned}$$

As a last step we use that $r_c^2 = \frac{Q}{2}x_c$, and hence $\mathrm{d}r_c^2 = \frac{Q}{2}\mathrm{d}x_c = \frac{\bar{n}\cdot r_c}{2}\mathrm{d}x_c$ , and write

$$\begin{aligned}\frac{1}{\sigma_0}\frac{\mathrm{d}\sigma}{\mathrm{d}\tau} = \left|\tilde{C}(-Q,-Q,\mu)\right|^2 &\int \mathrm{d}r_c^2\,\mathrm{d}r_{\bar{c}}^2\\ &\cdot\sum_{X_s}\frac{1}{N}\,\mathrm{tr}_{SU(3)}\,\langle\Omega|\left[S_n^\dagger S_{\bar{n}}\right](0)\,|X_s\rangle\,\langle X_s|\left[S_{\bar{n}}^\dagger S_n\right](0)\,|\Omega\rangle\\ &\cdot\sum_{X_c}\frac{1}{N}\frac{1}{4\pi(\bar{n}\cdot r_c)}(2\pi)^4\delta^{(4)}(r_c^\mu - p_c^\mu)\\ &\qquad\mathrm{tr}_{Dirac}\,\langle\Omega|\,(\bar{\xi}_n W_n)(0)\,|X_c\rangle\,\langle X_c|\,\bar{\not{n}}(W_n^\dagger\xi_n)(0)\,|\Omega\rangle\\ &\cdot\sum_{X_{\bar{c}}}\frac{1}{N}\frac{1}{4\pi(n\cdot r_c)}(2\pi)^4\delta^{(4)}(r_{\bar{c}}^\mu - p_{\bar{c}}^\mu)\\ &\qquad\mathrm{tr}_{Dirac}\,\langle\Omega|\,(W_{\bar{n}}\xi_{\bar{n}})(0)\,|X_{\bar{c}}\rangle\,\langle X_{\bar{c}}|\,\not{n}(\bar{\xi}_{\bar{n}}W_{\bar{n}})(0)\,|\Omega\rangle\\ &\cdot\delta(\tau - \tau(p_X)),\end{aligned} \tag{3.33}$$

where we collected $\delta$-distributions into traces, used that the Dirac trace in 3.25 evaluates to $-\frac{1}{4}$, and reinstated the Thrust constraint on the phase spaces.

This is as far as we can get with just the scaling information, before we continue a few words are in order:

- The $|C^2|$ in the first line encodes the matching from QCD to SCET, and is generic for any $0 \to 2$ QCD process. It includes virtual vertex corrections at higher loop orders. As befitting a function determined by the integrating out of the hard modes, its natural scale is $Q$. It is typically called the *Hard function*.

- The second line gives rise to the *Soft function*, it encapsulates the emission of soft isotropic radiation from the colour-charged particles in the process. Here the sum over $X_s$ implicitly contains phase space integrations for any emissions off the Wilson lines sandwiched between the bras and kets.

- The two integral structures in the last four lines are identified as the progenitors for the *Jet functions*[10], which describe the collinear radiation off the energetic outgoing primary particles. The sum here also includes phase space integrations, and a sum over all colours is assumed.

Now we look at the form of the Thrust definition as it enters in equation 2.2 in detail: Thrust reduces in the dijet limit to $\tau = \frac{p_L^2 + p_R^2}{Q^2}$, where $p_{L/R}$ is the total 4-momentum into the left or right hemisphere, and the hemispheres are defined by the jet axis $\vec{n}$. This means particles in $X_c$ always contribute to $p_L$, and those in $X_{\bar{c}}$ always contribute to $p_R$. Soft emissions can contribute to either, depending on whether they are more collinear ($\bar{n} \cdot p_s > n \cdot p_s \Rightarrow p_L$) or anticollinear.

So assuming that there is a total soft momentum of $k_L$ comprised of particles going into the left hemisphere ($\bar{n} \cdot k_L > n \cdot k_L$), we can estimate

$$p_L^2 = (p_c + k_L)^2 = \underbrace{p_c^2}_{\sim\lambda^2} + \underbrace{2 p_c k_L}_{\sim\lambda^2} + \underbrace{k_L^2}_{\sim\lambda^4} = r_c^2 + Q\, n \cdot k_L, \tag{3.34}$$

where we used the relative scaling of the collinear and soft components to eliminate $k_L^2$ and the subleading component of $p_c k_L$, as well as the form of $p_c$ as we'll find it in the factorisation theorem for the dijet cross section. For emission to the right we find a similar form:

$$p_R^2 = (p_{\bar{c}} + k_R)^2 = \underbrace{p_{\bar{c}}^2}_{\sim\lambda^2} + \underbrace{2 p_{\bar{c}} k_R}_{\sim\lambda^2} + \underbrace{k_R^2}_{\sim\lambda^4} = r_{\bar{c}}^2 + Q\, \bar{n} \cdot k_R \tag{3.35}$$

[10] Technically there is an extension of the sum over final states still missing, but as we aren't going to look at jet functions in detail we omit this detail.

Combining these two we find

$$\tau = \sum_{L,R} \frac{p_L^2 + p_R^2}{Q^2} = \frac{r_c^2 + r_{\bar{c}}^2 + Qn \cdot k_L + Q\bar{n} \cdot k_R}{Q^2} = \tau_c + \tau_{\bar{c}} + \tau_s, \tag{3.36}$$

where in the last equality we highlight that the observable decomposes into a sum of contributions from the different sectors. This additive behaviour near the dijet case is what allows us to derive the factorisation theorem, and is therefore a crucial requirement. In fact, this decomposition into independent contributions to the observable from the individual sectors is a necessary requirement for any observable to allow factorisation. Plugging this into the factorisation theorem we find that the phase space integrations in the $X_s$ and $X_{c,\bar{c}}$ are now linked, because all sectors contribute and relative sizes of the contributions matter. We therefore modify 3.33 by explicitly highlighting the contribution from the soft sector in the relevant line when plugging in the $\delta$-constraint to arrive at the factorisation theorem for Thrust:

$$\begin{aligned}
\frac{1}{\sigma_0}\frac{\mathrm{d}\sigma}{\mathrm{d}\tau} = \left|\tilde{C}(-Q,-Q,\mu)\right|^2 \int \mathrm{d}r_c^2\, \mathrm{d}r_{\bar{c}}^2\, \mathrm{d}k\, \delta(\tau - \frac{r_c^2 + r_{\bar{c}}^2 + Qk}{Q^2}) \\
\cdot \sum_{X_s} \frac{1}{N} \operatorname{tr} \langle\Omega| \left[S_n^\dagger S_{\bar{n}}\right](0) |X_s\rangle \langle X_s| \left[S_{\bar{n}}^\dagger S_n\right](0) |\Omega\rangle\, \delta(k - \bar{n}\cdot k_R - n \cdot k_L)) \\
\cdot \sum_{X_c} \frac{1}{N} \frac{1}{2\pi(\bar{n}\cdot r_c)} (2\pi)^4 \delta^{(4)}(r_c^\mu - p_c^\mu) \\
\operatorname{tr} \langle\Omega| (\bar{\xi}_n W_n)(0) |X_c\rangle \langle X_c| \not{\bar{n}} (W_n^\dagger \xi_n)(0) |\Omega\rangle \\
\cdot \sum_{X_{\bar{c}}} \frac{1}{N} \frac{1}{2\pi(n\cdot r_c)} (2\pi)^4 \delta^{(4)}(r_{\bar{c}}^\mu - p_{\bar{c}}^\mu) \\
\operatorname{tr} \langle\Omega| (W_{\bar{n}} \xi_{\bar{n}})(0) |X_{\bar{c}}\rangle \langle X_{\bar{c}}| \not{n} (\bar{\xi}_{\bar{n}} W_{\bar{n}})(0) |\Omega\rangle
\end{aligned} \tag{3.37}$$

We can again identify $\left|\tilde{C}\right|^2$ as the hard function, the second line as the soft function for Thrust, and the latter two structures as the relevant jet functions.

Each of these can be computed individually in perturbation theory, and subsequently convoluted with the others to arrive at the full distribution.

Assigning the obvious letter choices to the different functions, the factorisation theorem takes the simple form

$$\frac{1}{\sigma_0}\frac{\mathrm{d}\sigma}{\mathrm{d}\tau} = H(Q,\mu) \int \mathrm{d}r_c^2\, \mathrm{d}r_{\bar{c}}^2\, \mathrm{d}k\, \delta(\tau - \frac{r_c^2 + r_{\bar{c}}^2 + Qk}{Q^2})\, J(r_c^2,\mu)\, J(r_{\bar{c}}^2,\mu)\, S(k,\mu) \tag{3.38}$$

## 3.6 The soft function

Highlighting the details works best when dealing with a concrete example, for which we pick the Thrust soft function - since we will focus on soft functions for generic observables later, this seems like a good choice.

As in any perturbative calculation, the soft function (as well as the jet and hard functions) is ill defined in the absence of a suitable regularisation and renormalisation procedure. In dimensional regularisation the bare soft function for Thrust can be computed, the 1-loop result is[84]

$$\begin{aligned} S_b(k,\mu) = \delta\left(k\right) + \frac{\alpha_s C_F}{\pi}\Big[ &- \frac{1}{\epsilon^2}\delta(k) + \frac{2}{\epsilon}\frac{1}{Q\tau}\left[\frac{Q\tau}{k}\right]_+ - \frac{2}{\epsilon}\ln\frac{\mu}{Q\tau}\delta(k) \\ &- \frac{4}{Q\tau}\left[\frac{Q\tau\ln\frac{k}{Q\tau}}{k}\right]_+ + \frac{4}{Q\tau}\ln\frac{\mu}{Q\tau}\left[\frac{Q\tau}{k}\right]_+ + \frac{1}{2}\left(\frac{\pi^2}{6} - 4\ln\frac{\mu}{Q\tau}\right)\delta(k)\Big], \end{aligned} \tag{3.39}$$

where we've chosen the reference scale $\kappa_2$ introduced in [84] as $\kappa_2 = Q\tau$, to map the range of the plus-distributions to the maximal domain for $k$, which is constrained to $0 \leq k \leq Q\tau$ by the Dirac delta in (3.37). At $\mathcal{O}(\alpha_s)$ in the $\overline{MS}$ scheme, renormalising via the introduction of a Z-factor has the same effect as dropping the $\epsilon$-poles.

The appearance of Dirac-delta and plus-distributions here is a problem, for two main reasons. First, renormalising this soft function requires convoluting it with an appropriate $Z$-factor, rather than multiplying it, which ultimately leads to non-local renormalisation group equations (RGE), which makes solving them obviously difficult. Second, since we at some point want to switch to numerical evaluation, distribution valued results are problematic, we'd much prefer regular functions.

Fortunately there is a way out: If we work in Laplace space, where each function $f$ has an associated Laplace space version:

$$\tilde{f}(\rho) = \int_0^\infty \mathrm{d}x\, e^{-\rho x} f(x), \tag{3.40}$$

we find that the factorisation theorem becomes

$$\tilde{\sigma}(\rho,\mu) = \int_0^\infty \mathrm{d}\tau\, e^{-\rho\tau}\,\frac{\mathrm{d}\sigma}{\mathrm{d}\tau} = H(Q,\mu)\tilde{J}^2(\frac{\rho}{Q^2},\mu)\tilde{S}(\frac{\rho}{Q},\mu), \tag{3.41}$$

and the tilde'd functions are regular and non-distributive.

Multiplicative renormalisation for any function $F$ leads to RGE of the form

$$\frac{\mathrm{d}F_R(\mu)}{\mathrm{d}\ln\mu} = \gamma_F F_R(\mu), \tag{3.42}$$

and the easiest way to find the anomalous dimension $\gamma_F$ is to derive the renormalised function, and realise that the $\mu$-dependence that the perturbative $F_R$ exhibits is a crude approximation of the RG flow near the natural scale for the function. Linearising, viz. deriving the function with respect to $\ln\mu$ at the natural scale, can therefore reproduce the anomalous dimension[11].

For our soft function above, the easiest way to find the Laplace space anomalous dimension is to derive $\frac{\mathrm{d}S_R}{\mathrm{d}\ln\mu}$ and subsequently Laplace transform the result to the Laplace space parametrised by the variable $\frac{\rho}{Q}$ we find in the factorisation theorem above.

We find that for the soft function

$$\gamma_{soft} = \frac{\alpha_s}{4\pi}(-16C_F)\ln\frac{\mu\rho e^{\gamma_e}}{Q}, \tag{3.43}$$

which is the first perturbative order of

$$\gamma_{soft} = -4\Gamma_{Cusp}[\alpha_s]\ln\frac{\mu\rho e^{\gamma_e}}{Q} + \gamma_S[\alpha_s], \tag{3.44}$$

where we defined the all-order *Cusp anomalous dimension* $\Gamma_{Cusp}$ and *soft anomalous dimension* $\gamma_s$. $\Gamma_{Cusp}$ is related to the renormalisation of Wilson lines with a kink or cusp, and therefore universal for all observables which share the same underlying Wilson line structure, it is also the same for hard, jet and soft functions. The fact that it comes with a $\ln\frac{\mu\rho}{Q}$ attached is the reason we can resum double logarithms using RGE methods. $\gamma_S$ is observable dependent, and different from $\gamma_J$ and $\gamma_H$. If we define the perturbative expansion for both gammas as

$$\Gamma_{Cusp} = \sum_{n=0}^{\infty}\left(\frac{\alpha_s}{4\pi}\right)^{n+1}\Gamma_n \qquad \gamma_S = \sum_{n=0}^{\infty}\left(\frac{\alpha_s}{4\pi}\right)^{n+1}\gamma_S^{(n)}, \tag{3.45}$$

we can read off $\Gamma_0 = 4C_F$ and $\gamma_S^{(0)} = 0$

[11]The idea is that $\mu$-independence of $F_B$ links the anomalous dimension to the $\mu$-dependence in $F_R$, and the solution for the RGE matches the perturbative result $F_R$ at the natural scale. Therefore linearisation of $F_R$ around this value for $\mu$ reproduces the anomalous dimension, as it there coincides with the linearisation of the RGE solution.

We can now solve the RGE for the Laplace space soft function and conclude that it runs between any scales $\mu$ and $\mu_0$ as

$$\begin{aligned}\tilde{S}(\frac{\rho}{Q},\mu) &= \tilde{S}(\frac{\rho}{Q},\mu_0)\exp\left(\int_{\mu_0}^{\mu}\mathrm{d}\ln\mu'\,\gamma_S(\frac{\rho}{Q},\mu')\right)\\ &= \tilde{S}(\frac{\rho}{Q},\mu_0)\exp\underbrace{\int_{\mu_0}^{\mu}\frac{\mathrm{d}\mu'}{\mu'}\Big(-4\Gamma_{Cusp}\ln\frac{\mu'}{\mu_0}+\gamma_S}_{=:K_S(\mu,\mu_0)}-4\Gamma_{Cusp}\ln\frac{\mu_0\rho e^{\gamma_e}}{Q}\Big)\\ &= \tilde{S}(\frac{\rho}{Q},\mu_0)\cdot e^{K_S(\mu,\mu_0)}\cdot(\frac{\mu_0\rho e^{\gamma_e}}{Q})^{-4\int_{\mu_0}^{\mu}\frac{\mathrm{d}\mu'}{\mu'}\Gamma_{Cusp}}\end{aligned} \tag{3.46}$$

The only $\mu$-dependence is now either manifest, or contained in the $\alpha_s$ of the Gammas' expansions, and we can therefore conclude that this integral is calculable, in a perturbative sense, if the running of the coupling is known. That this is enough, and that the "perturbative sense" is good enough here, although perturbation theory got us into the entire mess in the first place, is part of the next section.

## 3.7 Resummation in SCET

Before we turn to its accuracy, however, we should first perform the resummation.

We have the RGE and possible solution for the soft function, there are of course also equivalent ones for hard and jet functions:

$$\begin{aligned}\tilde{J}(\frac{\rho}{Q^2},\mu) &= \tilde{J}(\frac{\rho}{Q^2},\mu_0)\cdot e^{K_J(\mu,\mu_0)}\cdot(\frac{\mu_0^2\rho e^{\gamma_e}}{Q^2})^{2\int_{\mu_0}^{\mu}\frac{\mathrm{d}\mu'}{\mu'}\Gamma_{Cusp}}\\ H(Q,\mu) &= H(Q,\mu_0)\cdot e^{K_H(\mu,\mu_0)}\cdot(\frac{\mu_0}{Q})^{-4\int_{\mu_0}^{\mu}\frac{\mathrm{d}\mu'}{\mu'}\Gamma_{Cusp}}\end{aligned} \tag{3.47}$$

We can now see why resummation is necessary in Laplace space. When we transitioned to Laplace space the $r_c^2$- and $k$-integrals we used to transform the soft and jet functions to Laplace space fixed the mass dimensions and therefore also the relative weight of $\rho$ and $\mu$. This is why we find $\frac{\mu_0\rho}{Q}$ as the dimensionless parameter in the last factor of the soft function, as well as $\frac{\mu_0^2\rho}{Q^2}$ for the jet function. They are the only dimensionless quantities built from $\frac{\rho}{Q^n}$ and $\mu$, the only other scale in the problem[12]. If we didn't run, i.e. if we set $\mu=\mu_0$, any choice for $\mu_0$ which causes one of these combinations to be $\sim 1$ will cause the other to be $\sim\rho^n$ for some $n$. As the renormalised functions contain logarithms of these scale ratios, we find large logarithms again.

[12]Needless to say that for the hard function there is only one dimensionless combination of $Q$ and $\mu$.

If we do run, however, and choose $\mu_0$ to be $\mu_H \sim Q$ for the hard, $\mu_J \sim \frac{Q}{\sqrt{\rho}}$ for the jet and $\mu_S \sim \frac{Q}{\rho}$ for the soft function, the functions as evaluated at the inital scale of the running in (3.46) and (3.47) will be free of large logarithms. The exponents $K_i$ and - for choices of the $\mu_0$ away from the natural scales - that of the third factor, will then resum all the logarithms we can wish for.

As one last comment before we turn to perturbativity, note that the final result should be independent of the scale $\mu$ that we evolved the individual functions to. We find logarithms of the form $\ln \frac{\mu_i}{\mu}$ in the anomalous dimensions, so this independence requirement sets stringent bounds on what is allowed. It enforces the equality of the Cusp anomalous dimension between soft, hard and jet functions, and prohibits quadratic or higher powers of the logarithms. Also, it forces the non-Cusp anomalous dimensions to obey

$$\gamma_S + \gamma_{J_c} + \gamma_{J_{\bar{c}}} + \gamma_H = 0. \tag{3.48}$$

Finally, the establishment of the accuracy level. In line with the scheme for N$^n$LL counting we established in eq. 2.6 we expect the exponents $K_S$, $K_J$ and $K_H$ to resum logarithms. Let's take a closer look. Any $\mu$-dependence in e.g. $K_S$ is either manifest as a $\ln \mu$, or is hiding inside $\alpha_s(\mu)$. If we know the QCD $\beta$-function, we can express $\alpha_s(\mu)$ in terms of $\alpha_s$ at some other scale.

The QCD $\beta$-function is known to 4-loop[85], for our purposes fewer than this will suffice. The 2-loop running for $\alpha_s$, if the $\beta$-function is parametrised as

$$\beta(\alpha_s) = -2\alpha_s \sum_{n=0}^{\infty} \left(\frac{\alpha_s}{4\pi}\right)^{n+1} \beta_n \tag{3.49}$$

has the solution

$$\begin{aligned} \alpha_s(\mu) = \alpha_s(\mu_0) - \frac{\alpha_s^2(\mu_0)}{2\pi}\beta_0 \ln\frac{\mu}{\mu_0} + \frac{\alpha_s^3(\mu_0)}{8\pi^2}\left(2\beta_0^2 \ln^2\frac{\mu}{\mu_0} - \beta_1 \ln\frac{\mu}{\mu_0}\right) \\ + \frac{\alpha_s^4(\mu_0)}{32\pi^3}\left(-4\beta_0^3 \ln^3\frac{\mu}{\mu_0} + 5\beta_0\beta_1 \ln^2\frac{\mu}{\mu_0} + \mathcal{O}(\beta_2 \ln\frac{\mu}{\mu_0})\right). \end{aligned} \tag{3.50}$$

Note that the three terms of the form $\alpha_s^n L^{n-1}$ appear exclusively with $\beta_0$, the two $\alpha_s^n L^{n-2}$ terms require $\beta_1$ as well. This pattern generalises to higher order.

As the last ingredient, look at the anomalous dimension terms. At the first few orders, using 3.45, we have

$$K_S(\mu, \mu_0) = \int_{\mu_0}^{\mu} \mathrm{d}\ln\mu \left[\ln\frac{\mu}{\mu_0}\Gamma_{Cusp} + \gamma_s\right] \tag{3.51}$$

$$= \int_{\mu_0}^{\mu} \mathrm{d}\ln\mu \left[ \ln\frac{\mu}{\mu_0}\frac{\alpha_s(\mu)}{4\pi}\Gamma_0 \right. \tag{3.52}$$

$$+ \ln\frac{\mu}{\mu_0}\left(\frac{\alpha_s(\mu)}{4\pi}\right)^2\Gamma_1 + \frac{\alpha_s(\mu)}{4\pi}\gamma_s^{(0)} \tag{3.53}$$

$$\left. + \ln\frac{\mu}{\mu_0}\left(\frac{\alpha_s(\mu)}{4\pi}\right)^3\Gamma_2 + \left(\frac{\alpha_s(\mu)}{4\pi}\right)^2\gamma_S^{(1)} + \dots \right] \tag{3.54}$$

Now we can collect logarithms. From eq. 3.50 we know that each power of $\alpha_s(\mu)$ denies us least one logarithm, because $\alpha_s(\mu)$ at best contributes $\alpha_{s0}^n \ln^{n-1}\frac{\mu}{\mu_0}$, and taking powers makes this worse. The integration itself yields one logarithm, one is already present, and if we include only the $\alpha_{s0}^n \ln^{n-1}$ series in (3.50), we generate all possible terms of the form $\alpha_{s0}^n \ln^{n+1}$. In other words, we achieve leading logarithmic accuracy, and we only need $\Gamma_0$ and $\beta_0$ for it. If we also want to capture the $\alpha_{s0}^n \ln^n$ terms, we need to sacrifice one logarithm, which we can do by including the $\alpha_{s0}^n \ln^{n-2}$ terms in the running of $\alpha_s$, which means we need $\beta_1$, or by giving up one logarithm in the anomalous dimension, which means we'll need $\Gamma_1$ and $\gamma_S^{(0)}$.

So to recap: for LL resummation we needed only the 1-loop $\alpha_s$ running and 1-loop cusp anomalous dimension, NLL requires 2-loop $\alpha_s$ running and cusp, and 1-loop non-cusp anomalous dimensions. There are also contributions from jet and hard functions, so any order in $\gamma_S$ needs to be matched by $\gamma_J$ and $\gamma_H$, while keeping eq. 3.48 in mind.

One last comment: While the logarithmic counting strictly doesn't make statements about the renormalised functions, a typical guideline is to assume that $\alpha_s \ln\frac{\mu}{\mu_0} \sim 1$, which implies that the perturbative expansion of $\tilde{S}$, $\tilde{J}$ and $H$ can be mapped to the logarithmic counting. This series then starts at tree level without logarithmic enhancement or suppression, and gains inverse logarithm-powers as more $\alpha_s$-orders are added. We'd therefore formally require $\alpha_s^n$-terms at $\mathrm{N}^{n+1}\mathrm{LL}$ level.

Recognising that oftentimes the renormalised functions are available if the anomalous dimensions are known, and in order to avoid some subtleties in the counting, a modified counting scheme is introduced: $\mathrm{N}^n\mathrm{LL}$' accuracy requires renormalised functions to $\alpha_s^n$-order.

## 3.8 SCET$_{II}$ and the collinear anomaly

Before we can lay out the basics of our framework, we need to review SCET$_{II}$, added complications arise in this case.

To recapitulate: SCET$_{II}$ observables are those for which soft and collinear modes lie on the same virtuality hyperbola. This implies that contributions from the overlap regions between soft and collinear modes lead to large — in fact unconstrained — integrations over rapidity, leading to divergences unregularised by dimensional regularisation.

SCET$_{II}$ observables' distributions can therefore not be computed using solely dimensional regularisation.

The solution is to introduce a second regulator which introduces a rapidity bias, which allows us to calculate soft and jet functions, both of which show divergences in the new regulator, in addition to the usual $\epsilon$. The second regulator can be introduced in two major ways, by modifying matrix elements[80, 81], or by changing the phase space[79][86, 87].

We will choose the latter, in which case both the soft and jet functions have poles in this new regulator, usually denoted $\alpha$. This $\alpha$-dependence cancels as soon as all soft and collinear sectors are added up, but as a residue large logarithms remain.

As the regulator is implemented by modifying the phase space integrals and introduces additional dimensionful factors to break the equal scaling of soft and collinear modes in the calculation, a 't Hooft-like scale $\nu$ must be introduced into the theory, similar to the appearance of $\mu$ in dimensional regularisation. Naturally the product of the relevant jet and soft functions must be independent of the artificially introduced scale $\nu$. Therefore the logarithm of this product must obviously be $\nu$-independent as well:

$$\frac{\mathrm{d}}{\mathrm{d}\ln\nu}\Big(\ln J_c(p_c^2,\mu,\nu)+\ln J_{\bar{c}}(p_{\bar{c}}^2,\mu,\nu)+\ln S(k_s,\mu,\nu)\Big)=0, \tag{3.55}$$

from which can be argued that this expression must be at most linear in $\ln\nu$[82].

Then this implies that the terms which give rise to large logarithms when the regulator cancels in the product of the two functions, actually exponentiates. Once this exponentiation has occurred, the remaining structures are free from large logarithms, and the usual SCET procedures of running hard and collinear-and-soft-product functions to a common scale can be set up.

千里之行始於足下。

*The journey of a thousand li starts from where one stands.*

— Lǎozi
*Dàodéjīng*

# 4 Defining the boundaries

We understand now the mechanisms that are used in SCET to resum large logarithms, so it is time to lay out the exact boundaries of our project. We therefore will list in this chapter all the properties we require of any observable to mark it as compatible with our approach, and motivate them.

## 4.1 Perturbative orders

First we need to determine what we want to achieve, and what needs to be computed for it.

We saw in section 3.7 that to achieve NLL resummation for Thrust, a SCET$_I$ observable, we needed the 2-loop cusp anomalous dimension $\Gamma_{cusp}$, the 1-loop hard, jet and soft anomalous dimensions $\gamma_{H,J,S}$, as well as the tree-level matching coefficients $c_{H,J,S}$. This can be generalised[66] to N$^n$LL, for which the required quantities and their respective perturbative order are listed in table 4.1. The listed tokens illustrate that NLL is the current state-of-the-art, that some full and many partial sets of the required ingredients for NNLL resummed observables exist, and that N$^3$LL is only achieved for very few observables. The entries for $F$ and $W$ refer to the SCET$_{II}$-equivalent of the soft and jet anomalous dimensions and finite terms, respectively, with $F$ the anomaly coefficient and $W$ the remainder function.

The colour coding of table 4.1 is as follows:

| Accuracy | $\Gamma_{cusp}$ | $\gamma_H, \begin{cases} \gamma_J, \gamma_S \\ F \end{cases}$ | | $c_H, \begin{cases} c_J, c_S \\ W \end{cases}$ | | $\beta$ |
|---|---|---|---|---|---|---|
| LL | $\alpha_s^1$ | - | - | tree | tree | $\alpha_s^1$ |
| NLL | $\alpha_s^2$ | $\alpha_s$ | $\alpha_s$ | tree | tree | $\alpha_s^2$ |
| NNLL | $\alpha_s^3$ | $\alpha_s^2$ | $\alpha_s^2$ | $\alpha_s$ | $\alpha_s$ | $\alpha_s^3$ |
| NNLL' | $\alpha_s^3$[88] | $\alpha_s^2$ | $\alpha_s^2$ | $\alpha_s^2$ | $\alpha_s^2$ | $\alpha_s^3$ |
| N$^3$LL | $\alpha_s^4$ | $\alpha_s^3$[89] | $\alpha_s^3$ | $\alpha_s^2$ | $\alpha_s^2$ | $\alpha_s^4$[85] |

**Table 4.1:** Required perturbative orders of the resummation ingredients for different logarithmic accuracy levels. The colour coding is explained in the text.

1. The N$^3$LO cusp anomalous dimension, required for N$^3$LL resummation, is unknown and therefore marked in red. Due to its small effect, published N$^3$LL analyses have resorted to e.g. Padé approximations.

2. Quantities marked in orange require observable dependent NNLO or higher calculations, and are therefore known on a case-by-case basis.

3. Green highlighted objects are either outright known ($\beta$, $\Gamma_{cusp}$, $\gamma_H$; $c_H$ partially), or can be extracted using automated tools ($c_H$ at NLO), or are 1-loop calculations, which we generically treat as feasible.

To clarify a bit more: The hard anomalous dimension $\gamma_H$ and matching coefficient $c_H$ reflect EFT level knowledge as Wilson coefficients, they are the same for all observables which have the same underlying hard scattering process. For $\gamma_H$ there is a result in terms of known quark and gluon form factors[89][89], and $c_H$ is either known (e.g.[89]), or can at least for up to NNLL resummation be extracted using tools that automate hard scattering processes which are available[90, 91].

The striking feature is that NNLL resummation generically requires an NNLO calculation, which is observable dependent and therefore generically not known, and then usually performed analytically. This analytic part is a major stumbling block on the way to automated resummation to NNLL.

This is therefore the point we attack, we set out to cover generic observables and provide this NNLO input for NNLL resummation, i.e. anomalous dimensions in an automated framework. It turns out that there is almost no additional effort required

to compute the full soft function, we therefore *de facto* always compute the full bare soft function, including the $\epsilon$-finite terms.

With the hard anomalous dimension known [89], and (3.48) at the back of our mind we note that the only missing NNLO input for generic NNLL resummation is either the jet *or* soft anomalous dimension[1].

For SCET$_{II}$ observables the picture is similar, here we need to compute the 2-loop anomaly exponent $F$. For this we need again one of soft and jet functions to 2-loop.

As soft functions are required for both processes at lepton and hadron colliders, i.e. with both beam or jet functions, and because the matrix elements tend to be a bit easier, we choose to focus on soft functions.

## 4.2 Principal motivation

We now know what we want to compute, now we need to explain why we believe that an extended framework that covers many observables in one go is even possible.

For this we recall from chapters 2 and 3 that the starting point formula for the evaluation of event shape distributions is of the schematic form

$$\frac{\mathrm{d}\sigma}{\mathrm{d}e} \sim \int |\mathcal{M}|^2 \, \delta\left(e - e\left(k_i\right)\right) \prod_i \frac{\mathrm{d}^3 k_i}{2E_i} \tag{4.1}$$

which, following a factorisation theorem gives rise to a soft function of similar form

$$S(\omega) \sim \int |\mathcal{M}_{soft}|^2 \, \delta\left(\omega - \omega\left(\{k_i\}\right)\right) \prod_i \frac{\mathrm{d}^3 k_i}{2E_i}, \tag{4.2}$$

The crucial detail here is that the matrix element contains all the explicit regularised divergences originating from virtual contributions and the implicit divergences associated with real radiation, and these are the same for all observables that share the same hard scattering process. The observable only enters though the measurement function[2], which acts as a weight function on the phase space, and is generically harmless, i.e. does not contribute regulator divergences.

[1] Assuming there are no sectors besides soft and collinear, which is not always necessarily the case, but will be true for the observables we accept.

[2] Here a Dirac delta.

This means that an approach in which we isolate all divergences in the matrix element analytically and make them explicit, followed by an expansion in the regulator, can be used to compute the bare soft function expansion for in principle any observable at negligible effort. Once the divergences are analytically isolated, changing the observable only means that integrals which evaluate to pure numbers, and which serve as coefficients for the different orders in the regulator expansion, are swapped for different integrals. Therefore, as all divergences will have been treated, these remaining integrals can then be safely performed numerically, regardless of their form — and therefore covering all manner of different observables.

## 4.3 "Generic" in detail

Although we want to be as all-encompassing as possible, some constraints need to be set. In order to be able to explain and motivate these constraints properly, we use the NLO computation for a schematic soft function as a template slate.

We will cover the exact form for the NLO soft function, including all constants in chapter 5, but here, where we need to be able to see the implications physical choices have on the form of the soft function, we boil it down to its bare bones structure.

Combining the definition of the soft function via Wilson lines with the form above and a Laplace transform, we require the soft function to be

$$S(\tau,\mu) = \sum_{i\in X_s} \exp(-\tau e(\{k_i\}))\, \frac{1}{N}\, \mathrm{tr}_c \left\langle\Omega\right| \left[S_n^\dagger S_{\bar n}\right](0) \left|X_s\right\rangle \left\langle X_s\right| \left[S_{\bar n}^\dagger S_n\right](0) \left|\Omega\right\rangle \tag{4.3}$$

$$\Rightarrow S_{NLO}(\tau,\mu) \sim \int \underbrace{\frac{\mathrm{d}^d k}{(2\pi)^{d-1}}\theta(k^0)\delta(k^2)}_{\text{phase space}}\ \underbrace{\mathcal{R}^\alpha(k)}_{\substack{\text{analyt.}\\ \text{regulator}}}\ \underbrace{\exp(-\tau\omega(k))}_{\substack{\text{measurement}\\ \text{function}}}\ \underbrace{\frac{\alpha_s\mu^{2\epsilon}}{(k_+k_-)}}_{\text{Matrix element}} \tag{4.4}$$

For the physical discussion we can for now neglect the analytic regulator, we therefore set $\alpha = 0$, with the understanding that in chapter 5 we reinstate it, we will also take a closer look at SCET$_{II}$ observables in section 4.4 below.

For on-shell radiation we have

$$\begin{aligned}\int \mathrm{d}^d k\, \theta(k^0)\delta(k^2) &= \frac{1}{2}\int \mathrm{d}k_-\mathrm{d}k_+\mathrm{d}^{d-2}k_\perp\, \delta(k_+k_- + k_\perp^2)\theta(k_+ + k_-)\\ &= \frac{1}{2}\int \mathrm{d}^{d-3}\Omega_T \int_0^\infty \mathrm{d}k_-\mathrm{d}k_+\mathrm{d}k_T\, \delta(k_+k_- - k_T^2)\, k_T^{d-3}\\ &= \frac{1}{4}\int \mathrm{d}^{d-3}\Omega_T \int_0^\infty \mathrm{d}y\, \mathrm{d}k_T\, y^{-1} k_T^{d-3}\end{aligned} \tag{4.5}$$

Here we first transitioned to lightcone coordinates in the first line, switched from Minkowski vector $k_\perp$ to the Euclidean $\vec{k}_T$ and immediately continued to spherical coordinates in the second line, and eliminated $k_-$ in the last, followed by a substitution $k_+ \to k_T\sqrt{y}$.

Note that by using the delta distribution and $k_+$ substitution we now have new variables

$$k_T = \sqrt{k_+ k_-} \qquad\qquad y = \frac{k_+}{k_-}, \tag{4.6}$$

of which $y$ is an exponentiated form of the canonical rapidity variable.

Using these variables we write

$$S_{NLO}(\tau,\mu) \sim \int \mathrm{d}^{d-3}\Omega_T \int_0^\infty \mathrm{d}y\, \mathrm{d}k_T\, \exp(-\tau\omega(k))\, k_T^{-1-2\epsilon} y^{-1} \tag{4.7}$$

We now *demand* that the observable is of a form such that

$$S_{NLO}(\tau,\mu) \sim \int \mathrm{d}^{d-3}\Omega_T \int_0^\infty \mathrm{d}y \mathrm{d}k_T\, \exp(-\tau\, k_T\, y^{\frac{n}{2}} f(y,\vartheta))\, k_T^{-1-2\epsilon} y^{-1} \tag{4.8}$$

with observable dependent parameter $n$ and function $f$, where the latter is positive, and nonvanishing for $y \to 0$.

Going forward we use the physical exchange symmetry $\bar{n} \leftrightarrow n$ to restrict the $y$-integration to the interval $[0,1]$, as under this exchange $y \to \frac{1}{y}$, which allows us to map the integration domain $[1,\infty[$ to $[0,1]$. Finally, we perform the $k_T$-integration, which yields

$$S_{NLO}(\tau,\mu) \sim \tau^{2\epsilon}\,\Gamma(-2\epsilon) \int \mathrm{d}^{d-3}\Omega_T \int_0^\infty \mathrm{d}y\, y^{-1+n\epsilon} f(y,\vartheta)^{2\epsilon}. \tag{4.9}$$

Following a subtraction

$$y^{-1+n\epsilon} = \frac{\delta(y)}{n\epsilon} + \left[\frac{1}{y}\right]_+ + n\epsilon \left[\frac{\ln y}{y}\right]_+ + \dots \tag{4.10}$$

the $\epsilon$-divergences are explicit, and we can perform an expansion in $\epsilon$, and integrate the coefficients numerically.

We're now in a position to list the assumptions we made and again state why we made them:

1. The form of the matrix element is dependent on the underlying structure of the Wilson lines, from whose expansion it is derived. We assume in (4.4) and later for NNLO that the matrix element derives from a structure corresponding to

two massless back-to-back colour-charged initial or final state particle. It can be shown[92] that the changes in the Wilson lines' $i\epsilon$ prescription, dependent on whether particles are incoming or outgoing[3], only affects the imaginary part of the real-virtual amplitude, which does not contribute at NNLO. We can therefore cover observables with **two jets and no beams** (e.g. leptonic dijet event shapes), **two beams and no jets** (hadronic 0-jet observables) or **one beam and one jet** (Deep inelastic scattering). As the soft anomalous dimensions appearing in hadronic dijet observables can be derived from the leptonic dijet and hadronic 0-jet cases (as shown explicitly for Transverse Thrust[111]), we can also cover the anomalous dimensions for **two beams and two jets.** Exceptions to this constraint are possible, see e.g. 8.8, and multiple Wilson line representation choices are possible, yielding colour structures $C_S^2$, $C_S C_A$ and $C_S T_F n_f$, with $C_S = C_F$ for the Wilson lines in the fundamental representation, and $C_S = C_A$ for the adjoint. We will by default assume $C_S = C_F$, which can be mapped to the adjoint, if necessary.

2. The **measurement function** is present in an **exponential form**. How we arrive at this exponential is of almost no consequence for the numerics. For typical event shape type observables a Laplace transform will yield the exponential form, as it did between (4.2) and (4.3), but in some cases a Fourier transform might be required, or no transform at all.

3. The measurement function's exponential is **linear in mass dimension**. Without this, the $k_T$-integration would not have been possible or yielded a different result. This constraint is compatible with any observable that directly measures energy or mass like quantities, and observables with are artificially dimensionless, as we observed for Thrust in section 2.2.

4. The observable dependent function $f$ must be **nonvanishing and positive**, otherwise the $k_T$-integration is not allowed. This can be slightly relaxed, as it is easy to check that $f$ only appears as $\ln f$ in the $\epsilon$-expanded formula, which is an integrable

[3]See appendix A

divergence if only isolated points[4] are affected, and as long as these zeroes do not interfere with any plus-distribution. This means that at NNLO some critical limits must be nonzero, which will be covered in sections 5.6 and 5.8. This is to some extent enforced by the factorisation theorem — if a soft contribution to an observable vanishes identically, it shouldn't even appear in the factorisation in the first place.

5. $f$ should also be **$\epsilon$-independent**, as with additional $\epsilon$-dependence the expansion obviously changes, but we take it as fixed: The only observable dependence is in $f$ and $n$, not in the structure of the expansion.

   This can be a nontrivial restriction thanks to the requirement that the measurement function has exponential form, because creative ways of arriving at an exponential can introduce $\epsilon$-dependence.

6. The function $f$ can in principle depend on any angle in the solid transverse space angle $\mathrm{d}^{d-3}\Omega_T$. We allow **dependence on one angle in the transverse space per particle**, measured with respect to the same reference vector, and perform the other angular integrations analytically. This means we have at NLO

$$\begin{aligned}\int \mathrm{d}^{d-3}\Omega_T &= \frac{2\pi^{\frac{1}{2}-\epsilon}}{\Gamma\frac{1}{2}-\epsilon}\int_{-1}^{1}\mathrm{d}\cos\vartheta\,\sin^{-1-2\epsilon}\vartheta \\ &= \frac{4\pi^{\frac{1}{2}-\epsilon}}{\Gamma\frac{1}{2}-\epsilon}\int_{0}^{1}\mathrm{d}t\,(4t\bar{t})^{-\frac{1}{2}-\epsilon}.\end{aligned} \tag{4.11}$$

   with $\cos\vartheta = 1-2t$, $\bar{t} = 1-t$. Explicit examples for such a reference vector would be a third jet direction[5] or the direction of a lepton pair in the initial or final state[6]

7. **In principle,** the soft function should only have **one function variable**. In (4.9) we see that the Laplace space variable, the conjugate to the position space variable $\omega$ with which we started here, factorises from the integral. This must be the case, because the only surviving dimensionful quantities are $\tau$ and $\mu$, and they must

[4] Integration subdomains of measure zero, to be precise. We can have observables which vanish if e.g. an angle which is not tied to a plus-distribution, vanishes.

[5] See e.g. production of W at large $p_T$ in section 8.8

[6] See See e.g. Transverse Thrust in section 8.9

combine to the dimensionless combination $\tau\mu$. For multiple variables[7], the integral now can depend on combinations of these variables. We can still accommodate soft functions with e.g. $N$ variables in a rasterised manner: We take one combination of the variables to be $\tau$, and express the others through $\tau$ and $N-1$ parameters, which we assign at compile time. Rasterising values for the $N-1$ parameters then allows us to determine individual values, or the shape of the soft function by fitting.

## 4.4 SCET$_I$ and SCET$_{II}$ observables

We already have the parts of the 1-particle parametrisation which allow us to cover the SCET$_I$/SCET$_{II}$ topic in (4.6), and so since this is the chapter outlining the broad properties of acceptable observables, it is a good moment to say a few words about SCET$_{II}$ vs. SCET$_I$ observables, and about the interplay between the definition of the observable and the contributing sectors.

For this, we assume that there is a soft sector of scaling $(\lambda, \lambda, \lambda)$, and collinear/anti-collinear sectors of as of yet undetermined scaling.

The soft sector contribution $\omega$ that appears in a factorisation theorem, which we already saw when we set up the framework in (4.2), depends on lightcone variables $k_+$ and $k_-$ and a discussion-irrelevant angle. Any possible $k_\perp$-dependence is fixed by the on-shell-ness of the emission. $\omega$ is by assumption linear in mass dimension, so $\omega \sim \lambda$ necessarily for any soft mode.

Now let us move along the soft sector's virtuality hyperbola towards the sides, i.e. we look at the collinear edges of the soft region. This means one of the two lightcone components dominates over the other, — we take without loss of generality $k_- > k_+$ — which allows us to expand the definition of $\omega$ in this limit, and we find that

$$\omega \sim k_-^s k_+^{(1-s)}, \tag{4.12}$$

for some observable-dependent $s$.

[7] As they appear in e.g. the hemisphere soft function $S(k_L, k_R)$ and its Laplace conjugate, respectively.

To extract more information, use the parametrisation we already saw in (4.6). Then

$$\omega \sim (k_T\sqrt{y})^{1-s}\left(\frac{k_T}{\sqrt{y}}\right)^s = k_T y^{\frac{1}{2}-s}, \tag{4.13}$$

where the strict jet-collinear[8] limit is $y \to 0$, and we see that the observable can vanish ($s < \frac{1}{2}$), diverge ($s > \frac{1}{2}$) or run towards a constant ($s = \frac{1}{2}$) in the jet-collinear limit, depending on the value for $s$.

Note that this also makes no statement about the absolute scaling of any components, this is a purely relative statement about how the observable responds to a change in rapidity, and should therefore also hold for other momentum scalings.

We can therefore make statements about the relevant sectors, based on this knowledge. If we know that there are high-energetic, collinear modes in the theory, but not the scaling they should exhibit, we can just take them to scale as[9] $(1, \lambda^{2a}, \lambda^a)$, and demand that they contribute to the observable an $\mathcal{O}(\lambda^1)$-term, on par with the soft modes. This order is necessary because one consequence of the factorisation theorem is that an observable gets contributions from all relevant sectors - we saw the equivalent of $\delta(\omega - \omega_c - \omega_{\bar{c}} - \omega_s)$ in the factorisation theorem for Thrust - at the same suppression. Were one sector's contribution suppressed we could just drop the entire sector from the theory.

Plugging the scaling above into the definition of the observable in the collinear limit yields

$$\omega_c \sim \lambda^{0\cdot s}\lambda^{2a\cdot(1-s)} \overset{!}{\sim} \lambda^1, \tag{4.14}$$

and therefore $a = \frac{1}{2(1-s)}$.

If we plug in as examples the usual suspects — Thrust and Broadening — we find

$$\begin{aligned}
&\omega_T = \min(k_+, k_-) \underset{\text{limit}}{\overset{\text{coll.}}{\to}} k_+ && \Rightarrow s = 0 \Rightarrow a = \frac{1}{2} && \Rightarrow (1, \lambda^1, \lambda^{\frac{1}{2}}) && \Rightarrow \text{SCET}_I \\
&\omega_B = k_T = \sqrt{k_+k_-} \underset{\text{limit}}{\overset{\text{coll.}}{\to}} \sqrt{k_+k_-} && \Rightarrow s = \frac{1}{2} \Rightarrow a = 1 && \Rightarrow (1, \lambda^2, \lambda^1) && \Rightarrow \text{SCET}_{II}
\end{aligned} \tag{4.15}$$

We've now tied the value of $s$ to the contributing sectors, so we can identify $s = \frac{1}{2}$ as the $\text{SCET}_{II}$ case. In other words: $\text{SCET}_{II}$ observables don't vanish or diverge in the jet-collinear limit.

[8] We define jet-collinear to mean "collinear to the axes $n$ or $\bar{n}$", since for NNLO we can also have particles collinear to each other.

[9] The general form would be $(1, \lambda^{2a}, \lambda^b)$, but for on-shell modes $b \overset{!}{=} a$.

Also note that following (4.13) $\omega \sim y^{\frac{1}{2}-s}$, but in the derivation of the NLO formula (4.8) we factor out the leading $y$-scaling in the exponential: $-\tau\omega(k) = -\tau k_T y^{\frac{n}{2}} f(y,\vartheta)$. We therefore can identify

$$n = 1 - 2s \tag{4.16}$$

and immediately see that $s = \frac{1}{2}$ corresponds to $n = 0$ and is common for all SCET$_{II}$ observables. We then see that there is now a problem for these observables, because the $y$-integration is regularised by $n$, which doesn't happen for $n = 0$. So we learn that the analytic regulator *must* provide some scaling in $y$ to properly do its job: $\mathcal{R}^\alpha(k) \overset{!}{\sim} y^{N\alpha}$, for some non-zero $N$. This is exactly what we expect, as the analytic regulator must differ between collinear and soft sectors, and the only difference is tied to rapidity.

As a small caveat note that this mode assignment discussion is not valid for all observables, we will in particular discuss observables for which $s = 1$, in which case we'd conclude that the collinear sector should scale as $(1, \lambda^\infty, \lambda^\infty) \to (1, 0, 0)$. The reason for this failure is the assumption of *high-energetic* collinear modes: we assumed that there is only one suppression factor (i.e. $\lambda$) in the theory and that collinear modes scale as $\lambda^0$ in their large component. An example is threshold Drell-Yan[10], where we don't have collinear modes but emissions originating from PDFs, which contribute large logarithms at their endpoints. These modes scale as $(\lambda, \epsilon, \sqrt{\lambda\epsilon})$[93] in the "collinear" sector, where $\epsilon = \frac{\Lambda_{QCD}}{Q}$. Even with $\epsilon \to 0$, which we have done so far implicitly, the form is not as assumed above. The classification into SCET$_I$ and SCET$_{II}$ based on $n$ is unaffected, though, in e.g. Drell-Yan we find $\omega = k_+ + k_-$, which leads to the correct $n = -1$ for the correct collinear mode.

[10] Covered in section 8.7

*If you look the right way,*
*you can see that the whole world is a garden.*

— Frances Hodgson Burnett & Caroline Thompson
*The Secret Garden*

# 5 Parametrisations

In this chapter we cover the parametrisations we use to bring the soft function's definition in (4.3) to a form suitable for subtraction, regulator expansion and subsequent integration.

As a short disclaimer right at the start we need to point out that the expressions we derive here are not the final functions we feed to the numerical integrator, but they are qualitatively the same, and are listed alongside the master formulae in appendix B. We decided against deriving the final formulas explicitly here, as several of the steps we use to improve numerical convergence or to reduce the number of terms arising from the regulator expansion do not help to highlight the analytically interesting points, and in some cases actively increase the complexity enough to drown out all interesting physics. These steps will be explained qualitatively and using simplified examples in the following chapters. The results of implementing them, however, are banished to the appendices.

## 5.1 The starting point

To quickly recap, we assume that (4.3) represents the starting point, with an exponential form measurement function, which can usually be achieved via a Laplace transform or similar procedures.

The main point of this chapter will now be to identify the matrix elements which contribute at NLO and NNLO loop orders and to set up the parametrisation in such a way that all regulator divergences factorise cleanly from the rest of the expression.

First, note that because the measurement function is not dependent on the form of the matrix element, but only on the final state multiplicity, a perturbative expansion is not as useful as an ordering in terms of final states. We therefore write

$$S(\tau,\mu)=\sum_{i=0}^{\infty}\int\left|\mathcal{M}^{(i)}(\{k_i\})\right|^2\exp(-\tau\omega(\{k_i\}))\prod_{j=1}^{i}2\pi\,\theta(k_j^0)\,\delta(k_j^2)\,\mathcal{R}^{\alpha}(k_j)\,\tilde{\mu}^{4-d}\frac{\mathrm{d}^d k_j}{(2\pi)^d},\tag{5.1}$$

where each term in the sum receives contributions from different perturbative orders, depending on the number of particles in the final state: The $i=0$ term collects all purely virtual contributions, $i=1$ collects all contributions with 1 particle in the final state, etc.

Here we also already included the analytic regulator $\mathcal{R}$ necessary for SCET$_{II}$ type observables, introduced as a deformation of the phase space.

In order to preserve the physical exchange symmetries $n\leftrightarrow\bar{n}$ and $k\leftrightarrow l$, which arise from the arbitrary assignment of the labels "collinear"/"anticollinear" and the fact that the two final state particles should be treated on equal footing, we deviate slightly from [79], and define our analytic regulator to be

$$\mathcal{R}(k)=\frac{\nu}{n\cdot k+\bar{n}\cdot k}=\frac{\nu}{k_++k_-}\tag{5.2}$$

Note that this regulator treats collinear and soft modes differently, as soft modes scale as $\lambda^1$ in all components and hence $\mathcal{R}\sim\lambda^{-1}$, but collinear modes scale as $(1,\lambda,\sqrt{\lambda})$, and so for them $\mathcal{R}\sim 1$. It therefore qualifies as an analytic regulator for our purposes.

Also, unlike in chapter 3 we no longer wish to highlight the difference between the $n$- and $\bar{n}$-projections, so we will generically switch back to denoting light cone components as $k_+$ and $k_-$.

We are interested in NNLL resummation, so from counting of $\alpha_s$-powers we see that we need all contributions up to $i=2$ in equation 5.1 for the soft functions of a given observable, i.e. 1-loop and 2-loop virtual ($i=0$), 1-loop real and 2-loop virtual-real ($i=1$) and 2-loop real ($i=2$) emissions.

The purely virtual corrections turn out to be scaleless, so we only need the 1-loop real, and 2-loop interference and double real contributions.

In general the 1-loop contributions are comparatively simple, and for many observables can be solved analytically, but we already used the NLO case to determine the shape of the soft functions we compute, and so we will now fill in the gaps in that derivation:

## 5.2 The NLO case

The NLO real emission case receives contributions from the four cut diagrams in fig. 5.1, corresponding to the combinations of one emission off two Wilson lines. Diagrams 5.1 (c) and (d) vanish, as they are proportional to the products $n \cdot n$ or $\bar{n} \cdot \bar{n}$, which vanish. The other diagrams yield identical contributions, so that the matrix element reads

$$\mathcal{M}^{(1)}(k) = \frac{\alpha_s C_F}{2\pi} \frac{1}{k_+ k_-}, \tag{5.3}$$

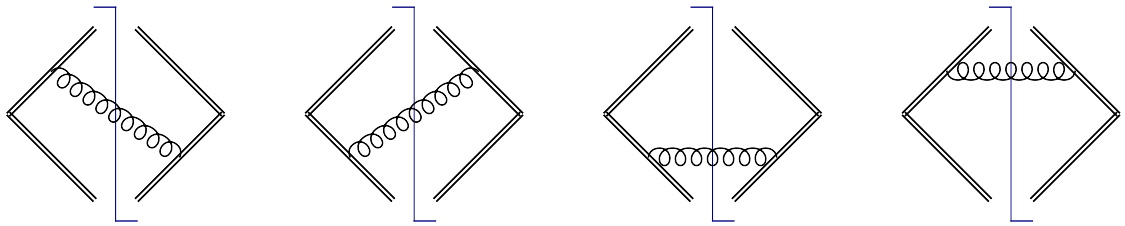


**Figure 5.1:** Cut 1-loop diagrams. Diagrams (a) and (b) yield identical results, (c) and (d) vanish.

This yields a starting formula of

$$S^{(1)}(\tau, \mu) = \frac{\alpha_s C_F}{2\pi} \int_{\mathbb{R}^d} \frac{\mathrm{d}^d k}{(2\pi)^d} \, \tilde{\mu}^{4-d} \, 2\pi \, \theta(k^0) \, \delta(k^2) \, \left( \frac{\nu}{k_+ + k_-} \right)^{\alpha} \frac{1}{k_- k_+} \, \exp(-\tau \omega(k)), \tag{5.4}$$

where we included powers of $\tilde{\mu}^2 = \frac{\mu^2 e^{\gamma_e}}{4\pi}$ to restore the correct mass dimension and signify that we work in $\overline{MS}$ scheme.

We already showed how the phase space for one on-shell particle looks like in (4.5), where we also defined the working set of variables as

$$k_T = \sqrt{k_+ k_-} \qquad\qquad y = \frac{k_+}{k_-}. \tag{5.5}$$

The reasoning here is that we expect divergences associated with the emission becoming soft or jet-collinear (i.e. collinear to the $n$, $\bar{n}$ directions), and these two variables encode these limits for $k_T \to 0$ and $y \to 0 \vee \infty$, respectively.

Integrating over all but one of the angles in the transverse space

$$\int \mathrm{d}^{d-3}\Omega_T = \frac{4\pi^{\frac{1}{2}-\epsilon}}{\Gamma(\frac{1}{2}-\epsilon)} \int_0^1 \mathrm{d}t\, (4t\bar{t})^{-\frac{1}{2}-\epsilon}. \tag{5.6}$$

with $\cos\vartheta = 1-2t$, $\bar{t} = 1-t$, we find

$$\begin{aligned} S^{(1)}(\tau,\mu) &= \frac{\alpha_s C_F}{2^{4-2\epsilon}\Gamma(\frac{1}{2}-\epsilon)\pi^{\frac{7}{2}-\epsilon}} \nu^\alpha \tilde{\mu}^{2\epsilon} \int_0^\infty \mathrm{d}k_T \int_0^\infty \mathrm{d}y \int_0^1 \mathrm{d}t\, \exp\left(-\tau\omega(k_T,y,t)\right) \\ &\quad \times k_T^{-1-2\epsilon-\alpha}\, y^{-1+\frac{\alpha}{2}}\, (1+y)^{-\alpha}\, (t\bar{t})^{-\frac{1}{2}-\epsilon} \\ &= \frac{\alpha_s C_F}{2^{3-2\epsilon}\Gamma(\frac{1}{2}-\epsilon)\pi^{\frac{7}{2}-\epsilon}} \nu^\alpha \tilde{\mu}^{2\epsilon} \int_0^\infty \mathrm{d}k_T \int_0^1 \mathrm{d}y \int_0^1 \mathrm{d}t\, \exp\left(-\tau\omega(k_T,y,t)\right) \\ &\quad \times k_T^{-1-2\epsilon-\alpha}\, y^{-1+\frac{\alpha}{2}}\, (1+y)^{-\alpha}\, (t\bar{t})^{-\frac{1}{2}-\epsilon} \end{aligned} \tag{5.7}$$

Here we used the $n \leftrightarrow \bar{n}$ exchange symmetry to map the $y$-integration over the interval $[1,\infty[$ to the interval $[0,1]$ in the second equality, as $y \to \frac{1}{y}$ under $n \leftrightarrow \bar{n}$ exchange.

Next we assumed in (4.8) that the exponent is linear in mass dimension, and write

$$\omega(k_T,y,t) = k_T\, y^{\frac{n}{2}}\, f(y,t), \tag{5.8}$$

where we also factored out the leading scaling in $y$ such that $f$ is finite in the limit $y \to 0$. This is important because we already saw in section 4.4 that $\mathrm{SCET}_I$ observables tend to vanish in the jet-collinear limit, the significance of which becomes clear after we perform the $k_T$-integration analytically, and subsequently find as the final formula

$$\begin{aligned} S^{(1)}(\tau,\mu) &= \frac{\alpha_s C_F \Gamma(-\alpha-2\epsilon)}{2^{3-2\epsilon}\Gamma(\frac{1}{2}-\epsilon)\pi^{\frac{7}{2}-\epsilon}} \tau^{\alpha+2\epsilon} \nu^\alpha \tilde{\mu}^{2\epsilon} \\ &\quad \times \int_0^1 \mathrm{d}t\, \mathrm{d}y\, y^{-1+\frac{n+1}{2}\alpha+n\epsilon}\, f(y,t)^{\alpha+2\epsilon}\, (1+y)^{-\alpha}\, (t\bar{t})^{-\frac{1}{2}-\epsilon}. \end{aligned} \tag{5.9}$$

First, note that for non-zero $n$, i.e. the $\mathrm{SCET}_I$ case, we can set $\alpha = 0$ as expected. If $n = 0$, $\alpha$ must remain non-zero, otherwise the $y$-integration is unregularised, again as expected for the $\mathrm{SCET}_{II}$ case. Moreover, the correct value for $n$ is important, because the $y$-monomial is decomposed as

$$y^{-1+n\epsilon} = \frac{\delta(y)}{n\epsilon} + \left[\frac{1}{y}\right]_+ + n\epsilon \left[\frac{\ln y}{y}\right]_+ + \ldots, \tag{5.10}$$

so we would get the $\epsilon$-pole wrong if we don't capture the full leading scaling. Equally important, note that $f$ appears with a purely regulator determined exponent, the regulator

expansion generates terms $\ln^n f$. Acting with a plus-distribution on such a term generates $\ln^n f|_{y=0}$ expressions over the entire integration region, and these should not diverge.

A quick look shows that the divergences are now fully accounted for, the soft divergence is encoded in $\Gamma(-\alpha - 2\epsilon)$, the collinear limit is explicit after the subtraction and expansion are performed on the $y$-monomial. For SCET$_I$ both the Gamma and $y$-structure contribute a $\frac{1}{\epsilon}$-pole, so that the leading divergent term is an $\epsilon^{-2}$-term. For SCET$_{II}$ the $\alpha$-expansion needs to be performed first, here the $y$-structure contributes a $\frac{1}{\alpha}$-pole, and the Gamma can contribute both $\frac{1}{\epsilon}$- and $\frac{\alpha}{\epsilon^2}$-terms, such that both $\frac{1}{\alpha\epsilon}$ and $\frac{1}{\epsilon^2}$-terms appear as leading divergent structures.

Finally observe that the remaining integral is perfectly well-behaved and integrable over the canonical domain for our numerical integrators, the interval $[0, 1]$. There are integrable divergences[1] at $t = 0 \vee 1$, and there will be a plus-distribution in $y$, but no additional complications. $f$ cannot vanish in the $y \to 0$ limit, we captured any such scaling using $n$. If it vanished in any other limit[2], this would contribute an integrable logarithmic divergence, and again not pose a problem. The integrations also all already run over the interval $[0, 1]$, the canonical integration domain for our numerical integrators.

## 5.3 The NNLO case

The NNLO case follows in its general outline the NLO case, albeit with additional pitfalls in the form of overlapping divergences, more integrations and a non-trivial divergence structure.

First note that for the NNLO case the number of diagrams which can contribute is larger than for NLO, and comes in various classes. It is advisable to treat different classes, especially colour structures, separately.

[1] These will be the main protagonists of chapter 7.
[2] Think $y \to 1$, or $t \to 0$

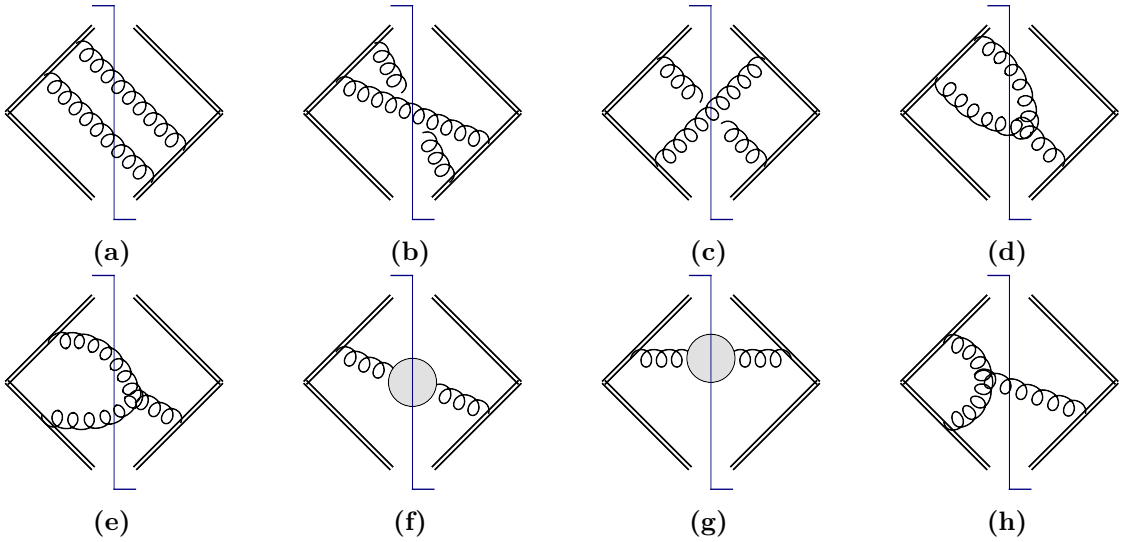


**Figure 5.2:** The diagram topologies contributing to the NNLO soft function. (a)-(c) contribute to $C_F^2$ and $C_F C_A$, (d) and (e) contribute to $C_F C_A$ only, (f) and (g) contribute to $C_F C_A$ and $C_F T_F n_f$, and (h) is the 1-particle cut contributing to $C_F C_A$.

## 5.4 NNLO: The 1-particle cut

The real-virtual emission (h) in figure 5.2 is structurally identical to the NLO case, the only difference is the matrix element, which again is similar to the NLO case, it reads

$$\left|\mathcal{M}^{(1PC)}\right|^2 = -64\pi^2 C_F C_A \frac{\pi^2 \Gamma(-\epsilon)\cot(\pi\epsilon)}{\Gamma(-2\epsilon)\sin(\pi\epsilon)} k_-^{-1-\epsilon} k_+^{-1-\epsilon} \tag{5.11}$$

Since the only difference is located in the prefactors, any NLO strategy immediately is applicable to the 1-particle cut as well. Thanks to the additional Gamma and trigonometric functions, the leading divergence for the 1-particle cut is $\epsilon^{-4}$ for SCET$_I$ observables, SCET$_{II}$ has both $\epsilon^{-4}$ and $\alpha^{-1}\epsilon^{-3}$ as the leading poles.

The NNLO 1-particle cut is the only virtual-real contribution, so we might expect the $i\epsilon$ prescription to be relevant here, especially since different Wilson line configurations give rise to different $i\epsilon$ prescription, as ingoing and outgoing particles and antiparticles lead to different Wilson lines. The $i\epsilon$ prescription can, however, be shown to be irrelevant[92], the matrix element is therefore the same for two colour-charged massless external legs in either initial or final states, as declared in section 4.3.

## 5.5 Implications from IRC safety and non-abelian exponentiation

Before we turn to the NNLO 2-particle case, it is advisable to first take a look at the constraints that IRC safety enforces on the measurement function, especially when combined with Non-Abelian Exponentiation.

Think of a generic observable and its 1-particle and 2-particle realisations. What can we say about its general form, and how are the two cases related?

From IRC safety we know that the 2-particle case must reduce to the 1-particle case in certain limits, and we know that observables which are compatible with non-abelian exponentiation (NAE) must be the sum of two 1-particle instances of the observable. The latter is due to the fact that the matrix element's $C_F^2$ colour structure is essentially a product of two 1-particle emissions, and the observable definition appears in an exponential multiplied to it. In other words, observables which respect NAE measure the two emissions as independent, NAE-breaking observables allow relative dependence.

This implies that a generic observable can be written as a sum of two 1-particle terms, and a term which is only present in NAE-breaking observables. This latter term is heavily constrained by IRC safety, as it cannot survive in any limit which reduces the observable to its 1-particle version.

We therefore claim that generic observables can be written as

$$\begin{aligned}\omega^{(2)}(k,l) &= \omega^{(1)}(k) + \omega^{(1)}(l) + g(k,l) \\ &= k_T y_k^{\frac{n}{2}} f(y_k, \vartheta_k) + l_T y_l^{\frac{n}{2}} f(y_l, \vartheta_l) + g(k,l)\end{aligned} \tag{5.12}$$

where g must vanish in the limits $k_T \to 0$, $l_T \to 0$ and the collinear limit for the two emissions. The functions $f$ are the dimensionless functions we found in the 1-loop case exponent, and $g$ has mass dimension 1 and is only present for observables which break NAE.

Note now that for SCET$_I$ observables the first two terms can only vanish if both particles become jet-collinear, having one jet-collinear particle is in general not enough to cause the observable as a whole to vanish. This is the equivalent of the NLO observable vanishing as $y \to 0$. We will therefore need a "rapidity"-type variable which captures the jet-collinear limit the same way the 1-loop variable $y$ did for NNLO.

Second, we see that this "rapidity" variable must scale as $y_k$ in the soft limit for particle $l$ and as $y_l$ in the soft limit for particle $k$, because the NNLO leading scaling must revert to the 1-loop scaling for the surviving emission in the soft limit for either particle. This in particular means that a $\text{SCET}_I$ observable at NLO doesn't magically turn into a $\text{SCET}_{II}$ observable at NNLO, and at a more detailed level, that the sectors contributing EFT degrees of freedom scale the same for NLO and NNLO. Physically that is clearly true, this here is the technical statement.

Next, note that the positivity requirement for the function which is left *after* leading scaling in the "rapidity" variable is factored out, is a non-trivial requirement here. This is best seen in an example: Let a hypothetical observable be

$$\omega(k,l) = k_T y_k f_k + l_T y_l f_l + \sqrt{y_k\, y_l}\,\hat{g} \tag{5.13}$$

Then we would conclude that the leading scaling in either emissions' rapidities is $\sqrt{y}$, and we factor this out using our as-of-yet unknown variable. But now make one emission (e.g. $l$) soft. Then the only term which survives in the remainder[3] is $k_T\sqrt{y_k}f_k$, which vanishes in the limit $y_k \to 0$. The positivity requirement therefore enforces that for NAE breaking observables it is the 1-particle terms which set the leading scaling, *not* the NAE breaking term $g$.

We suspect that there may be physical constraints which enforce this scaling constraint independently, but in full generality it is difficult to make such broad statements, therefore we require this scaling as a restriction on our framework.

And finally, note that IRC protects many limits of vanishing variables and ensures that the observable stays finite. As an example, take the angle between the projection of emission $k$ onto the transverse space and the reference vector that we allowed in section 4.3.

Assume that the observable vanishes if this angle tends to zero, independent of the alignment of the other emission $l$. If now the $k$-emission becomes soft, the observable has a discontinuous jump from 0 at any positive, even infinitesimal energy for emission $k$, to a nonzero value at $E_k = 0$, because IRC safety demands that the observable reproduces the 1-particle value for emission $l$ in this limit. This clearly violates the spirit of IRC safety.

Armed with this we can now turn towards NNLO.

[3]Remember, we factored out $\sqrt{y_k}$.

## 5.6 NNLO: $C_F T_F n_f$

The easiest and simplest of the structures in the 2-particle contributions is the $T_F n_f$ colour structure. It arises from diagrams which involve cut fermion bubbles, as pictured in figure 5.2(f) and (g).

Collecting the contributions to the $T_F n_f$ structure from the different relevant diagrams, we find that the matrix element for equation 5.1 with $i = 2$ is

$$\mathcal{M}^{(2)}_{n_f} = \frac{\alpha_s^2 C_F T_F n_f}{8\pi^2} \left[ \frac{1}{(k\cdot l)^2} \left( \frac{2k\cdot l}{(k_+ + l_+)(k_- + l_-)} - \frac{(k_+ l_- - k_- l_+)^2}{(k_+ + l_+)^2 (k_- + l_-)^2} \right) \right] \tag{5.14}$$

for two emissions with momenta $k$ and $l$. Here we can already see that the divergence structure is a lot more complicated than the NLO or 1-particle cut cases. In particular the collinear divergence due to $k\cdot l = \frac{k_+ l_-}{2} + \frac{k_- l_+}{2} - k_T l_T \cos\vartheta_{kl}$ requires special attention, it makes a straightforward factorisation of the divergence impossible. Still, we start as before: transform to lightcone coordinates, and use the on-shell conditions to eliminate the transverse momentum integrations. The remaining integrations then are the surviving lightcone components $k_\pm$ and $l_\pm$, as well as the angular integrations.

We'll shelve the angular integrations for now, and cover the lightcone variables first.

We introduce the *physical parametrisation* in terms of collective variables $p_T$ and $y$, as well as relative variables $a$ and $b$ as follows:

$$\begin{aligned} p_T &= \sqrt{(k_+ + l_+)(k_- + l_-)} & y &= \frac{k_+ + l_+}{k_- + l_-} \\ a &= \sqrt{\frac{l_+ k_-}{l_- k_+}} = \sqrt{\frac{y_l}{y_k}} & b &= \sqrt{\frac{k_+ k_-}{l_+ l_-}} = \frac{k_T}{l_T} \end{aligned} \tag{5.15}$$

The variable $y$ here has its name not in vain, as expressed in 1-particle rapidities it is

$$y \sim \sqrt{y_k y_l}\, \frac{k_T\sqrt{y_k} + l_T\sqrt{y_l}}{k_T\sqrt{y_l} + l_T\sqrt{y_k}}, \tag{5.16}$$

and therefore — just make one of the particles soft — has the scaling we saw was necessary for the NNLO "rapidity" variable.

Nevertheless, as mentioned above, this will not be the parametrisation we ultimately use for the numerical evaluation, although it is qualitatively similar. It is far more intuitive and approachable than the actual "computing parametrisation", though, so

some of the input will be required in this form, as physical interpretations are easier and expressions are shorter.

Still, using this parametrisation we find for the soft function

$$\begin{aligned} S(\tau,\mu)^{(2)}_{n_f} = \frac{1}{16}\frac{\alpha_s C_F T_F n_f}{2(2\pi)^{2d}} \int_0^\infty \mathrm{d}p_T\,\mathrm{d}a\,\mathrm{d}b\,\mathrm{d}y \int \mathrm{d}^{d-3}\Omega_k\,\mathrm{d}^{d-3}\Omega_l\,\frac{2abp_T^3}{(a+b)^2(1+ab)^2 y} \\ \cdot \frac{4a([1-a]^2[1-b]^2+4t[1+ab][a+b])}{bp_T^4([1-a]^2+4at)^2} \\ \cdot \left(\frac{abp_T^2}{(a+b)(1+ab)}\right)^{-2\epsilon} \tilde{\mu}^{4\epsilon} \cdot \exp(-\tau\omega(k,l)) \\ \cdot \left(\frac{\nu^2(a+b)^2(1+ab)^2 y}{bp_T^2(a+b+ay[1+ab])(a[a+b]+y[1+ab])}\right)^{\alpha} \end{aligned} \tag{5.17}$$

where the first line lists constant prefactors and Jacobians, the second line is the square bracket part of the matrix element from equation 5.14 translated to this parametrisation, the third line consists of the $\epsilon$-dependent remnants of the transverse momentum integration and the observable dependence, and the fourth line is the analytic regulator.

Just as for the NLO case we can now restrict some of the integration ranges which at the moment run over the entire positive real axis, namely those for $a$, $b$ and $y$:

The symmetries we have at our disposal here are $k \leftrightarrow l$ exchange and $n \leftrightarrow \bar{n}$ exchange, which map $a \to \frac{1}{a}$, $b \to \frac{1}{b}$, $y \to y$, and $a \to \frac{1}{a}$, $b \to b$, $y \to \frac{1}{y}$, respectively. In figure 5.3 we have illustrated the effect of these mappings on select regions of the integration domain. We can concatenate the symmetries to identify different regions of the integration domain, and find that the entire domain of $\mathbb{R}_+ \times \mathbb{R}_+ \times \mathbb{R}_+$ decomposes into two subdomains (the blue and white regions in figure 5.3(c)), which are fourfold multiples of unit cubes $[0,1] \times [0,1] \times [0,1]$, which in turn are related by the inversion of one of the variables $a$, $b$ and $y$. In the illustration one such unit cube is highlighted by dashed lines, the second can be found as any of the adjacent white cubes[4] From now on, we will denote these two relevant integration regions by "A" and "B", respectively.

With this done we can now take a look at the divergence structure of the soft function in its current form:

[4]Strictly speaking the second relevant integration region has one integration which runs over the interval $[1,\infty]$, but following the inversion of this variable it maps back onto a unit cube.

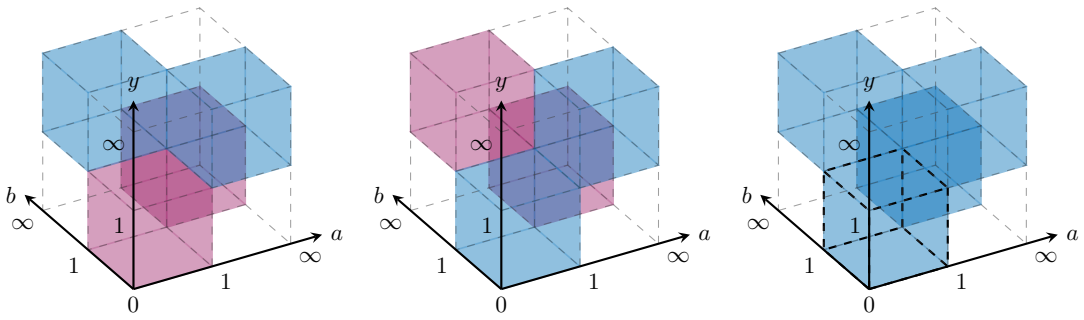


**(a)** $k \leftrightarrow l$ exchange **(b)** $n \leftrightarrow \bar{n}$ exchange **(c)** Reduced integration region

**Figure 5.3:** Cubes of the same colour in (a) and (b) must yield the same result in the integration as required by the stated symmetries, concatenating these symmetries then allows the reduction of the integration domain to two unit cubes, one of which is highlighted in (c), the second emerges from it by inversion of one variable.

1. There is a divergence from $p_T^{-1-4\epsilon-2\alpha}$, which is regularised by $\epsilon$ even in the absence of the analytic regulator $\alpha$, which we identify as corresponding to the radiated system becoming soft collectively.

2. A divergence from $y^{-1+\alpha}$ seems so far only regularised by $\alpha$, and is associated with the radiated particles becoming jet-collinear in the non-trivial manner outlined in section 5.5.

3. And there is an divergence at $a \to 1$, $t \to 0$, whose regularisation status is unclear, and which we identify as a collinear divergence associated with the two particles becoming collinear to each other[5].

Armed with this knowledge we again finally turn to the measurement function. In analogy to the NLO case we write it as

$$\exp(-\tau\omega(k,l)) = \exp(-\tau y^{\frac{n}{2}} p_T F(a,b,y,t,\vartheta_k,\vartheta_l)), \tag{5.18}$$

where $\vartheta$, $\vartheta_k$ and $\vartheta_l$ are all angles which we haven't yet resolved but may still appear, and now $p_T$ is the only remaining mass scale. The $p_T$ integration can again be performed

[5] $a \to 1$ corresponds to the rapidities becoming equal, $t \to 0$ means the angle between the emissions' transverse momentum vectors vanishes.

analytically, and we find for the overall formula

$$\begin{aligned} S(\tau,\mu)^{(2)}_{n_f} = \frac{1}{4}\frac{\alpha_s C_F T_F n_f}{2(2\pi)^{8-4\epsilon}} \int_0^1 \mathrm{d}a\,\mathrm{d}b\,\mathrm{d}y \int \mathrm{d}^{d-3}\Omega_k\,\mathrm{d}^{d-3}\Omega_l\,\frac{2ab}{(a+b)^2(1+ab)^2 y} \\ \cdot \frac{4a([1-a]^2[1-b]^2+4t[1+ab][a+b])}{b([1-a]^2+4at)^2} \\ \cdot y^{n(2\epsilon+\alpha)}\Gamma(-4\epsilon-2\alpha)\left(F_A(a,b,y,t,\vartheta_k,\vartheta_l)^{4\epsilon+2\alpha}+F_B(a,b,y,t,\vartheta_k,\vartheta_l)^{4\epsilon+2\alpha}\right) \\ \cdot \left(\frac{ab}{(a+b)(1+ab)}\right)^{-2\epsilon} \tilde{\mu}^{4\epsilon}\tau^{4\epsilon+2\alpha} \\ \cdot \left(\frac{\nu^2(a+b)^2(1+ab)^2 y}{b(a+b+ay[1+ab])(a[a+b]+y[1+ab])}\right)^{\alpha}, \end{aligned} \tag{5.19}$$

where the middle line remains after the $p_T$ integration, and we used that all terms are invariant under the inversion of either $a$, $b$ or $y$, but the measurement function $F$ may be different in the two integration regions.

### 5.6.1 Angular parametrisation

Finally, we turn to the last white spot on our parametrisation's atlas: The angles.

We stated in section 4.3, that we'd grant dependence on one angle per particle measured with respect to a shared reference vector in transverse space, i.e. two angles in the NNLO case. In addition, we need already in the matrix element[6] the angle in the transverse space *between* the emissions themselves. In other words we need to parametrise a 3-dimensional subspace of $(d-2)$-dimensional transverse space (spanned by the vectors $\vec{k}_T$, $\vec{l}_T$ and $\vec{n}_j$), in such a way that these three angles are accessible.

So how do we set up the coordinate systems for $\vec{k}_T$ and $\vec{l}_T$? It may at first glance appear sensible to measure the polar angles for $k$ and $l$ both with respect to $\vec{n}_j$, to remain symmetric under $k \leftrightarrow l$ exchange, but it turns out that this entails very cumbersome reparametrisations to arrive at unit cube integrations. It is more sensible to choose an arrangement as in figure 5.4, even though $k \leftrightarrow l$ exchange symmetry appears to be broken here.

By choosing the angles this way, we parametrise $\vec{l}_T$ as $\hat{\vec{l}}_T = (0,\ldots,0,0,1)^T$, $\hat{\vec{k}}_T = (0,\ldots,0,\sin\vartheta,\cos\vartheta)^T$ and $\vec{n}_j = (0,\ldots,\sin\vartheta_l\sin\vartheta_5,\sin\vartheta_l\cos\vartheta_5,\cos\vartheta_l)^T$.

[6] In the overlapping collinear divergence.

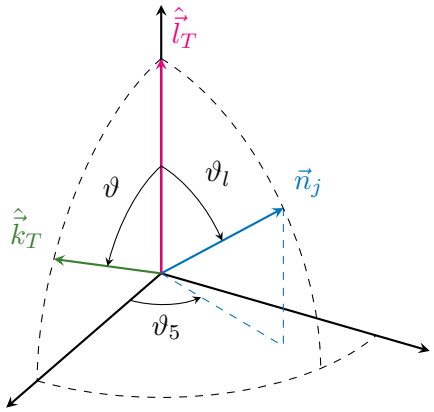


**Figure 5.4:** The angular parametrisation of the transverse space.

This ensures that the product $k \cdot l$, which always appears in e.g. the $T_F n_f$ matrix element has a simple angular dependence on the angle $\vartheta$, and only the angular dependence on the reference vector, which is not present for all observables, is difficult.

For the angular integration measure this means that we have

$$\begin{aligned}\int \mathrm{d}^{d-3}\Omega_k \mathrm{d}^{d-3}\Omega_l &= \int \mathrm{d}^{d-4}\Omega \mathrm{d}^{d-5}\Omega \cdot \int_0^\pi \mathrm{d}\vartheta\, \mathrm{d}\vartheta_l\, \mathrm{d}\vartheta_5\, \sin^{d-4}\vartheta\, \sin^{d-4}\vartheta_l\, \sin^{d-5}\vartheta_5 \\ &= \frac{2\pi^{\frac{1}{2}-\epsilon}}{\Gamma(\frac{1}{2}-\epsilon)} \frac{2\pi^{-\epsilon}}{\Gamma(-\epsilon)} \int_{-1}^1 \mathrm{d}\cos\vartheta\, \mathrm{d}\cos\vartheta_l\, \mathrm{d}\cos\vartheta_5 \\ &\quad \cdot \sin^{d-5}\vartheta\, \sin^{d-5}\vartheta_l\, \sin^{d-6}\vartheta_5 \\ &= \frac{-2^{1-6\epsilon}\pi^{\frac{1}{2}-2\epsilon}\epsilon}{\Gamma(\frac{1}{2}-\epsilon)\Gamma(1-\epsilon)} \int_0^1 \mathrm{d}t\, \mathrm{d}t_5\, \mathrm{d}t_l (t\bar{t})^{-\frac{1}{2}-\epsilon} (t_l\bar{t}_l)^{-\frac{1}{2}-\epsilon} (t_5\bar{t}_5)^{-1-\epsilon}\end{aligned} \tag{5.20}$$

which is almost complete except for one modification: The integration over $t_5$ is problematic, it seems at first glance as if it could contribute an $\epsilon$-pole, but it also comes with a global factor $\epsilon$, which cancels said pole. For the numerical integration it is sensible to shift this $\epsilon$ to the $\Gamma$ function we generate from the $p_T$ integration, and treat $t_5$ as a regularised divergent variable. This leaves us with the problem that the $t_5$ integration is divergent at both 0 and 1, which we solve by splitting the integration domain at $\frac{1}{2}$, and rescaling the two halves as $t_5 \to \frac{t_5}{2}$ and $t_5 \to 1 - \frac{t_5}{2}$, respectively. This yields for both

$$\int \mathrm{d}^{d-3}\Omega_k \mathrm{d}^{d-3}\Omega_l \to \frac{-2^{2-4\epsilon}\pi^{\frac{1}{2}-2\epsilon}\epsilon}{\Gamma(\frac{1}{2}-\epsilon)\Gamma(1-\epsilon)} \int_0^1 \mathrm{d}t\, \mathrm{d}t_5\, \mathrm{d}t_l (t\bar{t})^{-\frac{1}{2}-\epsilon} (t_l\bar{t}_l)^{-\frac{1}{2}-\epsilon} (t_5[2-t_5])^{-1-\epsilon}, \tag{5.21}$$

where now we have to pay attention that we integrate two copies of the actual integrand, one with the substitution $t_5 \to \frac{t_5}{2}$, the second with $t_5 \to 1 - \frac{t_5}{2}$. The matrix element and

Jacobians are independent of $t_5$ and therefore invariant, but again the observable might not be, so the sum $F_A^{4\epsilon+2\alpha} + F_B^{4\epsilon+2\alpha}$ now becomes a sum $F_{A1}^{4\epsilon+2\alpha} + F_{B1}^{4\epsilon+2\alpha} + F_{A2}^{4\epsilon+2\alpha} + F_{B2}^{4\epsilon+2\alpha}$, where the subscripts 1 and 2 denote the two possible substitutions for $t_5$.

Finally, to conclude the angle discussion, we point out that technically we broke $k \leftrightarrow l$ exchange symmetry with our choice of angles, but we note that we can work with angles $\vartheta_k$ and $\vartheta_l$ up until the very last moment before the numerical integration, and then as the last step choose which of them is left as an integration variable, and which is replaced by a combination of $\vartheta$, $\vartheta_5$ and the other emission's $\vartheta_i$ angle. Then $k \leftrightarrow l$ exchange symmetry is still present for all analytic steps, and only lost when we don't need it anymore, anyway.

The explicit replacements should also be listed, if we define $\cos\vartheta_k = 1 - 2t_k$ and $\cos\vartheta_l = 1 - 2t_l$, with the choice to treat $t_l$ as an integration variable, and resolve the angle variable $t_k$, then the substitutions are

$$\begin{aligned} &t_l \to t_l \\ &t_k \to t + t_l - 2tt_l - 2\sqrt{t\bar{t}t_l\bar{t}_l}\,(1 - t_5) \text{ in region 1,} \\ &t_k \to t + t_l - 2tt_l - 2\sqrt{t\bar{t}t_l\bar{t}_l}\,(t_5 - 1) \text{ in region 2,} \end{aligned} \tag{5.22}$$

where we could just as well have switched the $k$ and $l$ labels, the result of the integration would be the same.

This is a good place to worry about limits, now, as we might be concerned that the function $F_{A1}$ and its variations in other regions might vanish in some limits.

The critical limits surely are those associated with a plus-distribution, as we would have to factor out leading scaling (as for $y$) if the measurement function vanished. These are the limits:

1. There's an overlapping divergence at $(a, t) \to (1, 0)$, in which the functions $F_{Xi}$ have to be non-zero via collinear safety, da this limit must reproduce the 1-particle case, which is assumed to be non-zero.

2. The factor $y^{-1+\cdots}$ generates an $\epsilon$-pole, and we already factored out the leading scaling in $y$, so this limit is finite.

3. The angle variable $t_5$ generates a pole after a subtraction, and the measurement function is finite in this limit according to the reasoning outlined at the end of section 5.5: Taking $t_5 \to 0$ followed by a soft limit for any of the emissions reproduces the non-zero 1-particle observable, hence the $t_5 \to 0$ limit can't vanish on its own.

4. All other limits do not come with a pole-generating monomial, and therefore at best produce integrable divergences[7]

### 5.6.2 Removing the overlapping divergence

To allow the factorisation of all divergences, the next explicit analytic step is to introduce another reparametrisation to resolve the overlapping divergence at $a = 1$, $t = 0$: We define

$$a = 1 - u(1 - v) \qquad t = \frac{u^2 v}{1 - u(1 - v)}. \tag{5.23}$$

This substitution introduces enough complexity to turn the expression for the $T_F n_f$ structure rather ugly. Because it is not what we feed to the numerical integrator, as will be explored in chapter 7, we will not explicitly derive the intermediate results here. Nevertheless, to see what happens to the collinear divergence, we can isolate it in 5.19: The analytic regulator and $\epsilon$-dependent structures cannot contain initially a divergence requiring a subtraction due to their exponents, and also cannot generate one after the substitution, therefore we can restrict ourselves to the Jacobians of all substitutions we made so far and the matrix element itself, and we find that these structures change under the reparametrisation as

$$\begin{aligned} &\frac{2ab}{(a+b)^2(1+ab)^2 y} \cdot \frac{4a([1-a]^2[1-b]^2 + 4t[1+ab][a+b])}{b([1-a]^2+4at)^2} \frac{1}{\sqrt{t\bar{t}}} \\ &\quad \to \frac{\mathcal{N}(u,v,b)}{[1+b(1-u[1-v])]^2[1+b-u(1-v)]^2(1+v)^3 y} \frac{\sqrt{1-u(1-v)}}{u\sqrt{v(1-u)(1+uv)}}, \end{aligned} \tag{5.24}$$

where $\mathcal{N}$ is some function non-vanishing in the interesting limits, and we marked in blue the only surviving divergence[8], which emerges from the $\sqrt{t\bar{t}}$ structure originating from the angular integration. As it turns out (without showing it explicitly) this divergence is regularised by $\epsilon$ only, and therefore contributes an $\epsilon^{-1}$-pole, for both $\mathrm{SCET}_I$ and $\mathrm{SCET}_{II}$ observables.

[7], which will be the protagonists of chapter 7.

[8]Besides $y$, which was of course already present.

Combining this with the knowledge about the other divergences, we find that with $y$ contributing an $\alpha^{-1}$-pole for SCET$_{II}$ observables, and the prefactor containing the structure $\epsilon\Gamma[-4\epsilon-2\alpha] \approx \frac{-1}{4} + \frac{\alpha}{8\epsilon} + \dots$ from the $t_5$ and $p_T$ integrations, we get leading poles of $\alpha^{-1}\epsilon^{-2}$ and $\epsilon^{-3}$ for SCET$_{II}$ , and $\epsilon^{-3}$ for SCET$_I$ , originating from subtractions required for the integrations over $y$, $u$ and $t_5$.

## 5.7 NNLO: $C_F C_A$

The $C_A$ structure is quite ugly and cumbersome, but not particularly challenging from an analytic point of view. It can, in fact, be treated using the same parametrisation as the $T_F n_f$ structure, and shares most of the difficulties that $T_F n_f$ also showed.

Because we already went through the derivation for $T_F n_f$ in detail, and the $C_A$ structure turns substantially more complex once the first parametrisation substitutions are performed, we only show the matrix element to point out where a few additional points of interest originate, but again banish the full expression to the appendix.

Summing all contributions to $C_A$ from the various diagrams that exhibit this structure (see figure 5.2), we find that the matrix element is

$$\begin{aligned}\left|\mathcal{M}^{(2)}_{C_A}\right|^2 = \frac{\alpha_s^2}{8\pi^2}\Big[&\frac{k_-^2 l_+(2k_+ + l_+) + 2k_- l_-(k_+^2 - k_+ l_+ + l_+^2) + k_+ l_-^2(k_+ + 2l_+)}{(k\cdot l)k_- k_+ l_- l_+(k_- + l_-)(k_+ + l_+)} \\ &- \frac{2(k_-[2k_+ + l_+] + [k_+ + 2l_+]l_-)}{k_- k_+ l_- l_+(k_- + l_-)(k_+ + l_+)} \\ &+ \frac{(1-\epsilon)(k_+ l_- - l_+ k_-)^2}{(k\cdot l)^2(k_- + l_-)^2(k_+ + l_+)^2}\Big]\end{aligned} \tag{5.25}$$

Compared to $T_F n_f$ we find additional divergences in $k_- k_+ l_- l_+ \sim k_T^2 l_T^2$, which translates to an additional divergence in the variable $b$, corresponding to one of the particles becoming soft. The measurement function in this limit is protected by IRC safety, it must reduce to the 1-particle case in this limit and we excluded observables which vanish over wide ranges of phase space even for 1-particle final states in 4.3.

The structure in the final line is interesting, because it has the same divergence structure as $T_F n_f$ and has explicit $\epsilon$-dependence. It originates from cut gluon and ghost bubbles, which explains the similarity to $C_F T_F n_f$, which originates from cut fermion

bubbles. Together with the fourth integration over $b$, which is regularised by both[9] $\epsilon$ and $\alpha$, it is responsible for most of the complexity we face when writing computer code, as the $b$-subtraction leads to mixing of different $\epsilon$ and $\alpha$ orders, which is the main reason the $C_A$ formulas and programs will be significantly longer than the $T_F n_f$ ones, especially since $C_A$ starts at a higher power divergence, which means the regulator expansions need to be performed to higher orders, as well.

Finally, because the other divergences besides $b$ are shared with $T_F n_f$ we can already predict that we will find leading poles of $\epsilon^{-4}$ for SCET$_I$ and $\epsilon^{-3}\alpha^{-1}$ as well as $\epsilon^{-4}$ for SCET$_{II}$ .

## 5.8 NNLO: $C_F^2$

The $C_F^2$ colour structure for generic, i.e. NAE-breaking observables is not as easy as $C_A$ or $T_F n_f$. The reason lies in its divergence structure, compared to the other two structures.

The $C_F^2$ structure's matrix element is essentially the NLO matrix element squared, which means it exhibits divergences tied to either particle becoming soft or jet-collinear. This is at face value incompatible with our current approach of factoring out the leading scaling in one variable which encodes the critical limits from the measurement function $F$.

For $T_F n_f$ we already saw that factoring only the variable $y$'s leading scaling was enough to render the measurement function finite, as there were three critical limits associated with plus-distributions: $y \to 0$, $t_5 \to 0$ and the collinear limit $u \to 0$, formerly known as $a \to 1$, $t \to 0$, of which the latter two are protected by IRC safety. The observable cannot vanish or diverge in those two limits, therefore factoring out the leading scaling in the one remaining variable $y$ is sufficient to capture the behaviour of the observable in all critical limits and ensure finiteness.

For the $C_A$ structure we find the same three divergences, as well as a fourth: $b \to 0$, the soft limit for one particle, which is also protected by IRC safety. So again, factorising the leading scaling in $y$ is enough.

[9] This can already be seen in the $T_F n_f$ formula.

The $C_F^2$ structure on the other hand has several critical limits which aren't protected: any combination of one particle becoming soft and the other becoming jet-collinear leads to a vanishing observable for SCET$_I$ type problems, without being protected by IRC safety.

A second way of looking at the problem starts with the NLO case. There we performed the integration over the sole remaining energy scale $k_T$, which pulled the observable function $\omega(k)$ down from the exponent of the exponential. Only after this did the $y$-integration turn out to be regularised. For $C_F^2$ we look at the square of the NLO expression, so we'd expect that we need to perform two analytic integrations over energy scales to regularise both the $y_k$ and $y_l$ rapidity divergences. But as clustering effects may introduce nontrivial dependence on the relative energies of the emitted particles we cannot do this while maintaining full generality.

As it turns out, there is a way of parameterising the soft function's integrals that allows us to use the same strategies as before. This parameterisation differs from those used for the $T_F n_f$ and $C_F C_A$ structures in that it is observable dependent: It depends on the value of the parameter $n$, which determines whether the observable is of SCET$_I$ or SCET$_{II}$ type.

At the time of submission of this thesis we had not yet found this parameterisation and the entire project was limited to observables obeying non-abelian exponentiation, which was stated outright in this very section. As we are now no longer limited to observables obeying NAE, mentioning this restriction would be factually incorrect. So to avoid making false statements while still maintaining the submission date as a cutoff for the D.Phil. programme, we maintain the restriction to NAE-obeying observables for the programmes written and results derived in this thesis, and point to the full write-up paper (in preparation and to be published soon™) for the details and some results for observables involving clustering effects.

## 5.9 Renormalisation

Here we discuss the procedures to extract anomalous dimensions and anomaly coefficients from the bare soft functions we get after the numerical evaluation.

As they factorise cleanly from the relevant integrals, and therefore do not need to be specified during the computation, we keep certain parameters and variables — such as the Laplace variable $\tau$ and the coupling $\alpha_s$ — apart from the assumed results of the numerical evaluation when it comes to writing down the full bare soft function. This provides us with a small amount of freedom to shift unsavoury constants.

Since it is easier and more straightforward than the SCET$_{II}$ case, we start with the SCET$_I$ case.

### 5.9.1 Extractions for SCET$_I$

Denoting bare quantities with subscript $b$, we assume for the form of the soft function in terms of the numerically computed $x_i$ (NLO) and $y_i$ (NNLO)[10]:

$$\begin{aligned} S_b(\tau) = 1 &+ \left(\frac{\alpha_{s,b}}{4\pi}\right)\left(\mu^2\bar{\tau}^2\right)^{\epsilon}\left[\frac{x_2}{\epsilon^2}+\frac{x_1}{\epsilon^1}+x_0+x_{-1}\epsilon+x_{-2}\epsilon^2\right] \\ &+ \left(\frac{\alpha_{s,b}}{4\pi}\right)^2\left(\mu^2\bar{\tau}^2\right)^{2\epsilon}\left[\frac{y_4}{\epsilon^4}+\frac{y_3}{\epsilon^3}+\frac{y_2}{\epsilon^2}+\frac{y_1}{\epsilon}+y_0\right], \end{aligned} \tag{5.26}$$

where we defined $\bar{\tau} = \tau e^{\gamma_e}$. This redefinition shifts powers of $e^{\gamma_e}$ into the expressions that are evaluated numerically, which simplifies the expansion of the $\Gamma$-functions in the variable-independent prefactors. The expressions in appendix B include this contribution.

The higher order terms in the NLO part $x_{-i}$ need to be included because the renormalised soft function at NNLO receives contributions for which the $\alpha_s^1$-terms in the renormalising $Z$-factor collide with the NLO terms in $S_b$, and then pole cancellations need to be able to occur. For the NNLO terms this cannot happen, any such term would be $O(\alpha_s^3)$, but this issue provides a hint that an extension to higher regulator orders than $\epsilon^0$ might at some point become necessary.

Using for the renormalised coupling

$$\alpha_s = Z_\alpha \alpha_{s,b} \qquad\qquad Z_\alpha = 1 - \frac{\alpha_s}{4\pi}\frac{\beta_0}{\epsilon}, \tag{5.27}$$

and introducing a $Z$-factor $Z_s$ to absorb all remaining $\epsilon$-poles in the bare soft function, we find for the renormalised soft function

[10]The NLO coefficients $x_i$ can usually be computed analytically, so while we can of course produce the relevant source code for the NLO programs, we assume we don't have to.

$$
\begin{aligned}
S(\tau) &= Z_s(\tau) S_b(\tau) \\
&= 1 + \frac{\alpha_s}{4\pi}\left[2x_2 L^2 + 2x_1 L + x_0\right] \\
&\quad + \left(\frac{\alpha_s}{4\pi}\right)^2 \left[\frac{32y_4 - 10x_2^2}{3} L^4 + \frac{4}{3}\left(8y_3 - [15x_1 + \beta_0]\right) L^3\right. \\
&\quad + 2\left(4y_2 - [x_1 + \beta_0]x_1 - 3x_0 x_2\right) L^2 \\
&\quad \left. + 2\left(2y_1 - [x_1 + \beta_0]x_0 - 2x_{-1}x_2\right) L + y_0 - (x_1 + \beta_0)x_{-1}x_{-2}\right],
\end{aligned}
\tag{5.28}
$$

where the powers of $L = \ln \mu\bar{\tau}$ are generated by expanding $\left(\mu^2\bar{\tau}^2\right)^{j\epsilon}$ and cancelling $\epsilon$ against the poles before removing them.

This soft function fulfils an RGE, whose anomalous dimension convention we take to be

$$
\frac{\mathrm{d}S(\tau)}{\mathrm{d}\ln\mu} = -\frac{1}{n}\left[4\Gamma_{cusp}\ln(\bar{\tau}\mu) - 2\gamma^s\right] S(\tau), \tag{5.29}
$$

where $n$ is the exponent of the leading scaling in the rapidity variable $y$ that we encountered in section 4.4, and both anomalous dimensions $X = \Gamma_{cusp} \vee \gamma^s$ have perturbative expansions

$$
X = \sum_{i=0}^{\infty} X_i \left(\frac{\alpha_s}{4\pi}\right)^{i+1} \tag{5.30}
$$

This RGE can be solved, its NNLO solution in terms of the just defined anomalous dimensions is

$$
\begin{aligned}
S(\tau) = 1 &+ \frac{\alpha_s}{4\pi}\left[-\frac{2}{n}\Gamma_0 L^2 + \frac{2}{n}\gamma_0^s L + c_1\right] \\
&+ \left(\frac{\alpha_s}{4\pi}\right)^2 \left[\frac{2}{n^2}\Gamma_0^2 L^4 - \frac{4\Gamma_0}{3n}\left(\beta_0 + \frac{3}{n}\gamma_0^s\right) L^3\right. \\
&+ \frac{2}{n}\left(-\Gamma_1 + \frac{1}{n}\left(\gamma_0^s\right)^2 + \beta_0\gamma_0^s - \Gamma_0 c_1\right) L^2 \\
&\left. + 2\left(\frac{1}{n}\gamma_1^s + \frac{1}{n}\gamma_0^s c_1 + \beta_0 c_1\right) L + c_2\right]
\end{aligned}
\tag{5.31}
$$

Comparing coefficients between the equations 5.28 and 5.31 allows us to pin down the quantities $\gamma_1^s$ and $c_2$, which we determined to be the relevant and interesting ingredients for NNLL' resummation in section 4.1. In particular, assuming that $\Gamma_{cusp}$ is known and NLO calculations are easy enough not to require numerical treatment, we find that we need $y_1$ as the only NNLO bare soft function coefficient to determine $\gamma_1^s$, and $y_0$ as the only numerical NNLO result to fix $c_2$.

The relevant expressions for $\gamma_1^s$ and $c_2$ subsequently are

$$\begin{aligned}\gamma_1^s &= 2n\left(y_1 - x_2 x_{-1} - x_0\left(x_1 + \beta_0\right)\right)\\ c_2 &= y_0 - \left(x_1 + \beta_0\right)x_{-1} - x_2 x_{-2}\end{aligned} \tag{5.32}$$

The other coefficients are then combinations of known quantities, and can be used for consistency checks or to estimate the numerical error.

### 5.9.2 Extracting SCET$_{II}$ quantities

For SCET$_{II}$ , the appearance of the collinear anomaly[82] introduces additional difficulty, it requires the second regulator and ties soft and jet functions together.

We assume again that we have either analytic or numerical methods to derive the coefficients of the leading orders in now both regulators, and take the form of the bare soft function to be

$$\begin{aligned}S_b(\tau) = 1 &+ \left(\frac{\alpha_{s,b}}{4\pi}\right)\left(\mu^2\bar{\tau}^2\right)^{\epsilon}(\nu\bar{\tau})^{\alpha}\left[\frac{1}{\alpha}\left(\frac{x_{11}}{\epsilon} + x_{10} + x_{1-1}\epsilon + x_{1-2}\epsilon^2\right)\right.\\ &\left. + \frac{x_{02}}{\epsilon^2} + \frac{x_{01}}{\epsilon^1} + x_{00} + x_{0-1}\epsilon + \alpha\left(\frac{x_{-1,3}}{\epsilon^3} + \frac{x_{-1,2}}{\epsilon^2} + \frac{x_{-1,1}}{\epsilon^1} + x_{-1,0}\right)\right]\\ &+ \left(\frac{\alpha_{s,b}}{4\pi}\right)^2\left(\mu^2\bar{\tau}^2\right)^{2\epsilon}\left\{(\nu\bar{\tau})^{2\alpha}\left[\frac{1}{\alpha^2}\left(\frac{y_{22}}{\epsilon^2} + \frac{y_{21}}{\epsilon} + y_{20}\right)\right.\right.\\ &\left. + \frac{1}{\alpha}\left(\frac{y_{13}}{\epsilon^3} + \frac{y_{12}}{\epsilon^2} + \frac{y_{11}}{\epsilon} + y_{10}\right) + \frac{y_{04}}{\epsilon^4} + \frac{y_{03}}{\epsilon^3} + \frac{y_{02}}{\epsilon^2} + \frac{y_{01}}{\epsilon} + y_{00}\right]\\ &\left. + (\nu\bar{\tau})^{\alpha}\left[\frac{1}{\alpha}\left(\frac{z_{13}}{\epsilon^3} + \frac{z_{12}}{\epsilon^2} + \frac{z_{11}}{\epsilon} + z_{10}\right) + \frac{z_{04}}{\epsilon^4} + \frac{z_{03}}{\epsilon^3} + \frac{z_{02}}{\epsilon^2} + \frac{z_{01}}{\epsilon} + z_{00}\right]\right\},\end{aligned} \tag{5.33}$$

where we needed to separate the 1-particle cut's contributions $z_{ij}$ from that of the 2-particle cuts' $y_{ij}$ and NLO $x_{ij}$, because the analytic regulator as a phase space modification contributes differently depending on particle number, and hence the exponents of $\alpha_s$ and $\nu\bar{\tau}$ are different in these three classes. To extract interesting quantities, theoretical background is needed: The RGE for the hard function contains a cusp anomalous term which must be cancelled by corresponding running in the product of jet and soft functions, so terms involving the natural scale $Q$ of the hard function must necessarily appear in the latter. It has been shown that this dependence exponentiates as

$$J_L(\tau,\mu)J_R(\tau,\mu)S(\tau,\mu) = \left(Q^2\bar{\tau}\right)^{-F(\tau,\mu)}W(\tau,\mu), \tag{5.34}$$

where the dependence on the natural scales for the Jet and Soft functions implies that

$$\begin{aligned} J(\tau,\mu) &= \left(\frac{Q^2}{\nu^2}\right)^{-\frac{1}{2}F(\tau,\mu)} W_J(\tau,\mu) \\ S(\tau,\mu) &= \left(\nu^2\bar{\tau}^2\right)^{-F(\tau,\mu)} W_S(\tau,\mu), \end{aligned} \tag{5.35}$$

as the dependence on the analytic regulator scale $\nu$ must cancel in the product of jet and soft functions. We take this behaviour to be generic for SCET$_{II}$ observables.

This means that the *anomaly coefficient* $F$ can be determined from an observable's jet and soft functions alone, but the *remainder function* $W$ needs both, and its soft and jet contributions are in general regulator dependent.

Since we only cover soft functions in this thesis, we will therefore concentrate on the anomaly coefficient.

From the form of the soft-jet product, and the RGE of the hard function, it follows[82] that the anomaly coefficient fulfils the RGE

$$\frac{\mathrm{d}F(\tau)}{\mathrm{d}\ln\mu} = 2\Gamma_{cusp}. \tag{5.36}$$

For the anomaly exponent, more work is required. Equation 5.35 implies, as proven for broadening in [94], that

$$\ln S(\tau,\mu) = -2F(\tau,\mu)\ln(\nu\bar{\tau}) + R(\tau,\mu), \tag{5.37}$$

or with explicit analytic regulator[11]

$$\begin{aligned} \ln S(\tau,\mu) &= (\nu\bar{\tau})^{\alpha}\left[-\frac{1}{\alpha}f_1 + r_1 + \mathcal{O}(\alpha)\right] \\ &\quad + (\nu\bar{\tau})^{2\alpha}\left[-\frac{1}{\alpha}f_2 + r_2 + \mathcal{O}(\alpha)\right] \\ &= -\frac{1}{\alpha}(f_1+f_2) - 2\ln(\nu\bar{\tau})\left(\frac{1}{2}f_1 + f_2\right) + \ldots, \end{aligned} \tag{5.38}$$

from which we see that the anomaly coefficient is determined by the logarithm term, not the $\alpha$-pole, as expected from (5.35). The $f_1$-term in this expression contains both NLO and NNLO 1-particle cuts, the 2-particle cut contribution $f_2$ trivially can only contain NNLO contributions, the $r_i$ terms follow the same scheme for the non-divergent terms, and contain information about the remainder function $W$.

[11] Higher poles of $\alpha$ cannot appear without $\ln^2$ terms appearing.

Note also that we only made $\alpha$ explicit, we didn't mention $\epsilon$ yet: This form for $\ln S$ holds for bare and renormalised functions alike.

To connect back to equation 5.33 we now use that

$$S(\tau) = \exp \ln S(\tau) \approx 1 + \ln S(\tau) + \frac{1}{2} \ln^2 S(\tau) + \dots \tag{5.39}$$

Up to NNLO order for $S$ we find that both the NLO and NNLO contributions to the first expansion order are relevant, but only the NLO contributions in the $\ln^2 S$ term appear, as $\ln S$ starts at $\mathcal{O}(\alpha_s)$.

Also, because $\ln S$ in 5.38 has only a single $\alpha$-pole, we can immediately conclude that the $\alpha^{-2}$-pole in $S(\tau)$ arises from the $\ln^2 S$ term, and therefore only contains NLO information.

A short recap may be in order to avoid losing sight of the ultimate target: Equation 5.39 recovers the form of $S(\tau, \mu)$ in terms of the collinear anomaly coefficient $F$ and other stuff[12] $R$, and we can now — by comparing the coefficients of different $\alpha$-orders in equations 5.33 and 5.39 — determine the structures $f_1$ and $f_2$. As the numerical results from equation 5.33 contain $\epsilon$-poles, we can build the bare anomaly coefficient $F_b(\tau, \mu) = \frac{1}{2} f_1(\tau, \mu) + f_2(\tau, \mu)$ from them.

The explicit comparison shows that

$$\begin{aligned} f_1 &= \frac{\alpha_s}{4\pi} \left(\mu^2 \bar{\tau}^2\right)^\epsilon \left[\frac{x_{11}}{\epsilon} + x_{10} + x_{1-1}\epsilon + x_{1-2}\epsilon^2\right] \\ &\quad + \left(\frac{\alpha_s}{4\pi}\right)^2 \left(\mu^2 \bar{\tau}^2\right)^{2\epsilon} \left[-\frac{z_{13}}{\epsilon^3} - \frac{z_{12}}{\epsilon^2} - \frac{z_{11}}{\epsilon} - z_{10}\right] \\ &\quad + \left(\frac{\alpha_s}{4\pi}\right)^2 \left(\mu^2 \bar{\tau}^2\right)^{\epsilon} \frac{\beta_0}{\epsilon} \left[\frac{x_{11}}{\epsilon} + x_{10} + x_{1-1}\epsilon\right] \\ f_2 + f_1^{(NLO)} r_1^{(NLO)} &= \left(\frac{\alpha_s}{4\pi}\right)^2 \left(\mu^2 \bar{\tau}^2\right)^{2\epsilon} \left(-\frac{y_{13}}{\epsilon^3} - \frac{y_{12}}{\epsilon^2} - \frac{y_{11}}{\epsilon} - y_{10}\right), \end{aligned} \tag{5.40}$$

where the three lines for $f_1$ correspond to NLO, NNLO 1-particle cut, and the hybrid from NLO and $\alpha_s$-running due to the appearance of $\alpha_{s,b}$ in equation 5.33, respectively. For $f_2$ it is not possible to cleanly separate the actual quantity of interest $f_2$ from a contribution due to the $\ln^2 S(\tau, \mu)$ term in (5.39). For this additional term the leading NLO $\alpha^{-1}$ pole meets the subleading constant term in the square. The usual methods to distinguish contributions from NLO and NNLO or 1-particle and 2-particle cuts fail

[12] Or their 1- and 2-particle cut contributions $f_1$, $f_2$, $r_1$ and $r_2$, respectively.

here — squares of NLO 1-particle cut terms share the prefactors $[\alpha_s(\nu\bar{\tau})^\alpha]^2 = \alpha_s^2(\nu\bar{\tau})^{2\alpha}$ with the NNLO 2-particle cut terms. However, a quick look at the coinciding NLO forms for $S(\tau)$ and $\ln S(\tau)$ is enough to convince us that

$$r_1^{(NLO)} = \frac{\alpha_s}{4\pi}(\mu^2\bar{\tau}^2)^\epsilon \left[\frac{x_{02}}{\epsilon^2} + \frac{x_{01}}{\epsilon^1} + x_{00} + x_{0-1}\epsilon\right] \tag{5.41}$$

We therefore now have an expression for the bare anomaly coefficient, and we proceed similarly to the SCET$_I$ case from here.

To assume that the product of bare jet and soft functions in equation 5.34 renormalises multiplicatively implies that the bare anomaly coefficient renormalises additively:

$$F_b(\tau) = F(\tau) + Z_F(\tau). \tag{5.42}$$

The renormalised $F(\tau)$ fulfils the RGE in equation 5.36, whose NNLO exact solution is

$$\begin{aligned} F(\tau,\mu) = {} & \frac{\alpha_s}{4\pi}\left[2\Gamma_0 L + d_1 + \mathcal{O}(\epsilon)\right] \\ & + \left(\frac{\alpha_s}{4\pi}\right)^2 \left[2\Gamma_0\beta_0 L^2 + 2(\Gamma_1 + \beta_0 d_1)L + d_2 + \mathcal{O}(\epsilon)\right] \end{aligned} \tag{5.43}$$

and where we are interested in the value for $d_2$ as the NNLO non-cusp contribution to the anomaly exponent.

Comparing coefficients between this solution and equation 5.40, followed by tedious algebra, allows us to pin down

$$d_2 = -y_{10} - \frac{z_{10}}{2} + x_{0-1}x_{11} + x_{00}x_{10} + x_{01}x_{1-1} + x_{02}x_{1-2} + \frac{\beta_0}{2}x_{1-1} \tag{5.44}$$

In other words: to derive the NNLO anomaly coefficient we need the $\frac{1}{\alpha}$ poles in the bare soft function.

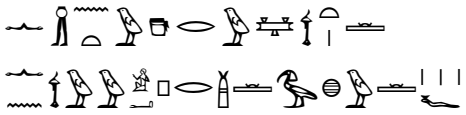

*The limits of art can't be reached,*
*and no artist's skills are perfect.*

— Ptahhotep
*The instruction of Ptahhotep, Papyrus Prisse*

# 6 Approaches

As we now have already made contact with an assumed final result of the numerical evaluation, we better proceed to the explicit description of the programs we use.

Because numerical integration almost by definition has black box characteristics, one comprehensive strategy is not enough, we need redundancy to allow for checks. We therefore have several programs, based on different languages, (to a certain extent) different numerical integrators and general levels of sophistication.

As a disclaimer again we point to the fact that the formulae we derived so far, by describing the parametrisations in chapter 5, are not the final formulae that are fed to the integrators. The reason is that using these formulae would lead to problems whose understanding presupposes knowledge about numerical integration and the specific way we implement some computations. We will address these problems in the next chapter, when we know the limitations and strengths of our programs. For now we will describe our programming efforts with the results of chapter 5 as templates, mindful of the fact that these examples are only qualitatively identical to the final integrands.

Moreover, as typesetting source code is a tedious endeavour, we will mostly describe the content in words and include the final source files in appendix D. These files are commented throughout and straightforwardly coded, the flow through the program is unobstructed by pure coding optimisations.

Finally, since the NLO case has no difficulties that the NNLO case doesn't share, and because for all the observables we compute as examples the NLO calculations are easy enough to be computed analytically, we will focus on the programs for the evaluation of the NNLO parts of the soft functions. If it turns out to be necessary, writing the NLO programs is a matter of days at the most.

## 6.1 SecDec-based approach

The first approach we present is suitable for the $C_F C_A$ and $C_F T_F n_f$ cases for SCET$_I$ observables. The starting point here is a master formula of the form as encountered in equation 5.19, combined with eq. 5.21:

1. There are factorised divergences of the form $x^{-1+i\epsilon}$, in the variables $y$ and $t_5$ for $C_F T_f n_f$, and in $y$, $b$ and $t_5$ for $C_F C_A$,

2. There is an overlapping collinear divergence in $(a, t) \to (1, 0)$,

3. There are integrable divergences in the other variables $t_l$ and (for $n_f$:) $b$.

4. The measurement function is non-divergent in the limit of any of the limits associated with a regularised divergence, and only contributes an integrable divergence in any other limit, due to its exponent.

We therefore look for a way to extract the implicit divergences and make them explicit, with special care for the overlapping divergence, subsequently expand this intermediate result in $\epsilon$, all the while keeping the measurement function generic, and then finally integrate the coefficients numerically, with the explicit form of the measurement function restored.

This is a rather generic set of problems, and we are of course not the first to encounter similar challenges, so it's not surprising that there is already a tool which does precisely that.

The tool in question is called *SecDec*[95], available in its current iteration 3.0.9 at `https://secdec.hepforge.org/`, and was developed to compute multi-loop Feynman parameter integrations. In typical integrals for virtual corrections, integrals over a set

of Feynman parameters need to be performed which often show overlapping divergences that only manifest when multiple of these parameters tend to a certain limit combined.

The SecDec program uses *iterated sector decomposition*[96] to resolve overlapping divergences, before applying a subtraction scheme, expanding, and switching to the numerical integration.

What makes SecDec an excellent program from our point of view is the fact that SecDec comes in two flavours, or "branches":

1. The *loop* branch is designed to resolve overlapping divergences in loop integrals explicitly, it uses multiple assumptions about external momenta and the form of integrands which are generically true for loop integrations, but not for the phase space integrations we perform. It is therefore not interesting for us.

2. The *general* branch on the other hand is designed to take a generic expression and it just runs its algorithm until all overlapping divergences are decomposed. What makes it interesting for us is the fact that it allows the definition of *dummy functions*, which are required to be functions which don't interfere with the decomposition, subtraction or expansion phases, and which are kept parametric during these phases, only to be reinstated just before the numerical integration.

Needless to say, the dummy function feature is precisely what we need — we know almost nothing about the measurement function, except that it is harmless in any and all of the limits which require subtractions.

### 6.1.1 Sector decomposition

Before we run through its technical aspects, we should devote a few words to the primary feature of SecDec.

SecDec is the only program we use which can deal with overlapping divergences, an issue we had to devote some time to during the early stages of our project. As we at some point may want to address Jet functions, we expect the reappearance of overlapping divergences, potentially without the fortunate discovery of a parametrisation which resolves them all. It is therefore also a good idea to quickly describe the sector decomposition method.

The starting point for sector decomposition is an integral of the form

$$I = \int_0^1 \int_0^1 \mathrm{d}x\mathrm{d}y\,(x+y)^{-2+j\epsilon}, \tag{6.1}$$

with $j \neq 0$. This integral is divergent at $(0,0)$, and regularised by the $j\epsilon$ term.

For sector decomposition we now split the integrand region into two triangles

$$I = \int_0^1 \mathrm{d}x \int_0^x \mathrm{d}y\,(x+y)^{i+j\epsilon} + \int_0^1 \mathrm{d}y \int_0^y \mathrm{d}x\,(x+y)^{-2+j\epsilon}, \tag{6.2}$$

and subsequently rescale $y = tx$ in the first triangle integral, and $x = ty$ in the second, with $t$ as the new integration variable. This changes the integrands to

$$\begin{aligned} I &= \int_0^1 \mathrm{d}x \int_0^1 x\,\mathrm{d}t\,(x+tx)^{-2+j\epsilon} + \int_0^1 \mathrm{d}y \int_0^1 y\,\mathrm{d}t\,(ty+y)^{-2+j\epsilon} \\ &= \int_0^1 \int_0^1 \mathrm{d}x\,\mathrm{d}t\,x^{-1+j\epsilon}(1+t)^{-2+j\epsilon} + \int_0^1 \int_0^1 \mathrm{d}y\,\mathrm{d}t\,y^{-1+j\epsilon}(1+t)^{-2+j\epsilon}, \end{aligned} \tag{6.3}$$

where now the divergence is fully factorised and only tied to one variable in each term. This entire procedure is illustrated in figure 6.1.

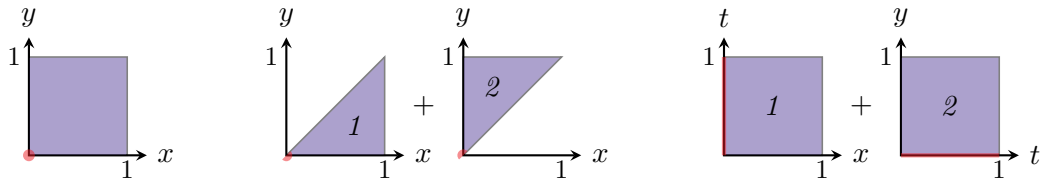


**(a)** Initial **(b)** Split **(c)** Decomposed

**Figure 6.1:** The Sector decomposition in equation 6.3 illustrated, the location of the divergence is marked in red.

For more complicated divergences, several sector decomposition steps may be required. For our collinear divergence $a^2 + 4(1-a)t$, where we sent $a \to 1-a$ to have the divergence at $(0,0)$, for example, two steps resulting in three sectors are required.

One major advantage of the Sector Decomposition method is that these steps can be iterated, the algorithm runs over a set of polynomials until all overlapping divergences are decomposed into factorised ones.

### 6.1.2 A typical SecDec run for us

SecDec uses multiple different programming languages and external auxiliaries, therefore it is most illustrative if we just trace out one typical SecDec run and describe the steps in detail.

The following step-by-step explanation is illustrated in figure 6.2.

1. The input to SecDec is provided via three different files.

   The `.input` file contains the global parameters, the most important ones are the choice of the integrator and its settings, the highest $\epsilon$-order that is computed, the required precision for the numerical integration, the variable name and choice of any parameter that is included, and of course the observable's name.

   The `.m` file contains in Mathematica list format a list of all polynomial factors appearing in the integrand and due for the sector decomposition algorithm. For us it also includes one generic entry `{F[z[1],z[2],z[3],z[4],z[5],z[6]],4 eps}` representing the measurement function $F$ that is kept parametric[1], dependent on the 6 integration variables, with the exponent as the second entry. Most of the entries in the `.m` file are static, from the point of view of the user, since these are numerator terms, Jacobians, prefactors and of course the divergent structures. The only exception is the divergent structure for $y$: $y^{-1+n\epsilon}$. As the value for $n$ is observable dependent and must be specified here, it is essential for the subtraction steps.

   The `F.f` file contains the definition of the measurement function $F$, for one integration region. The language for the numerical integration is `FORTRAN77`, hence the function `F(x1,x2,x3,x4,x5,x6)` must be provided in `FORTRAN77` form. As Dummy functions should not be $\epsilon$ dependent, the format for the dummy function in the `.m` file must be `{F[z[1],z[2],z[3],z[4],z[5],z[6]],4eps}`, and so we have to run the program four times to collect the contributions from $F^{4\epsilon}_{A1}$, $F^{4\epsilon}_{A2}$, $F^{4\epsilon}_{B1}$ and $F^{4\epsilon}_{B2}$ in section 5.6.1

2. Following the initial program call, SecDec uses Mathematica as a backend to run through the factor list in the `.m` file and seeks out any overlapping divergence it can find, and decomposes them. We do not use the working parametrisation anymore, but already have factorised divergences, so this step doesn't do anything for us.

[1] It represents one of the $F_{Xi}$ in (B.1) or (B.2).

3. Next the program looks for divergent monomials, i.e. factors of the form `{z[i],-1+ j*eps}`, and decomposes them into $\frac{\delta(z_i)}{n\epsilon}$ and plus-distribution parts.

4. Then all resulting terms are expanded in $\epsilon$, and terms of identical $\epsilon$-order are collected. The expansion is truncated at the `.input`'s `epsord` variable.

5. The Mathematica expressions are subsequently translated to `FORTRAN77`, and `FORTRAN` sources are written for the sequential integration of the required $\epsilon$-orders using the parameter settings for the numerical integrators chosen in the `.input` file. The dummy function's source file forms part of this set of sources.

6. Sequentially, starting at the highest $\epsilon$-order / least divergent term, the sources are compiled and the resulting programs executed.

7. Following their successful run, the results for the various $\epsilon$ orders are collected and written to a file.

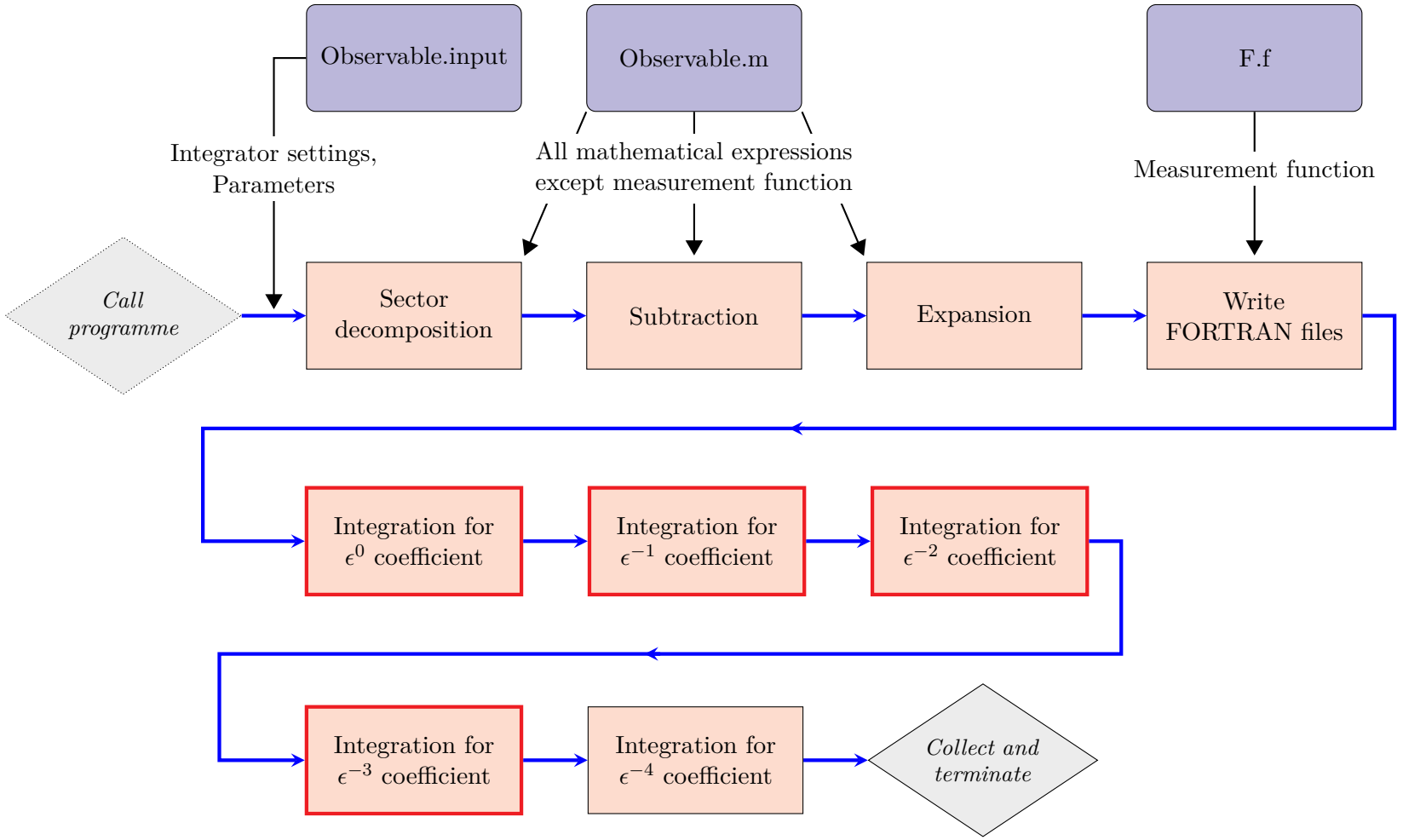


**Figure 6.2:** Program flow through the SecDec-based approach. Blue boxes denote files requiring user input, red boxes are program steps, whereby a red rim highlights time intensive ones. Blue arrows denote program flow, black arrows input data which is read in. External libraries are not included in this chart.

### 6.1.3 The numerical integrators

SecDec offers the choice between the integrators in the *Cuba*[97] library[2], and *BASES*[98]. The possibility to use BASES is one of the reasons we keep the SecDec based approach around, the second ansatz using explicit programs run on a computer uses one of the Cuba integrators (Divonne) hard coded.

We find that the Cuba integrators, in particular Cuhre and primarily Divonne yield the best results, given the right parameters, and in fact outclass BASES by far. Still, the Cuba library is a single library, written by one developer, using similar programming techniques for all its integrators, so the option of using an integrator written completely independently is welcome.

The input parameters specified in the example configuration and source files for the SecDec based ansatz have been chosen to yield results within $\approx$ 1h on a typical desktop machine.

## 6.2 Possible improvements

Although the SecDec based approach can be used to reliably compute bare soft functions, there are a few reasons why we'd like an alternative.

1. As a tool written without SCET in mind, there is only one regulator implemented, which a priori only allows the computation of $\text{SCET}_I$ obervables. Explicitly triggered by this limitation to $\text{SCET}_I$ observables, an extension to multiple regulators is on the horizon for the next major release for SecDec, *SecDec4* or *pySecDec*, but this is still in its early beta stage.

2. The input for the SecDec approach is scattered over multiple files, and mixed with static input that is the same for all of our observables. Ideally there should only be one location where user input needs to be specified.

3. The order of integrations is less than ideal for consistency checks, as the leading terms which should already be known are computed last.

[2]Vegas, Suave, Divonne and Cuhre, of which Divonne and Cuhre are our favourites.

4. Running the program four times, one time each for the four $F_{ij}$ functions is tedious and requires manual adding.

5. The decomposition, subtraction and expansion stages are essentially black boxes. While the corresponding output is in principle available, it cannot realistically be checked, and although the three intial stages will always generate similar output, they are run at each call of the program, occasionally resulting in nondeterministic bugs.

6. And finally, and most seriously, using knowledge about the structure of the integrand allows us to drastically reduce the computational effort.

The last point requires closer attention.

We have, following the reparametrisation from variables $a, t$ to $u, v$, fully factorised divergences. In particular, the full integrand is a product of multiple structures

$$\underbrace{\mathrm{Pre}(\epsilon,\alpha)}_{\text{prefactor}} \int \Big(\prod \mathrm{d}x_i\Big) \cdot \underbrace{\mathrm{Div}(\epsilon,\alpha,[x_i])}_{\text{divergences}} \cdot \overbrace{\mathrm{X}(\epsilon,\alpha,[x_i])}^{\substack{\text{numerator,}\\ \text{Jacobians,}\dots}} \cdot \underbrace{\sum_{\substack{j=A1,A2,\\ B1,B2}} F_j^{4\epsilon+2\alpha}([x_i])}_{\text{measurement function}} \tag{6.4}$$

The crucial insight is that only the divergences Div can contribute regulator poles, as they are decomposed as

$$x^{-1+j\epsilon} = \frac{\delta(x)}{j\epsilon} + \left[\frac{1}{x}\right]_+ + j\epsilon \left[\frac{\ln x}{x}\right]_+ + \dots, \tag{6.5}$$

all other structures are finite in the limit of vanishing regulators. For $\mathrm{SCET}_{II}$ there are terms in the prefactors Pre and divergences Div which are of the form

$$\frac{1}{\epsilon+\alpha} = \frac{1}{\epsilon} - \frac{\alpha}{\epsilon^2} + \frac{\alpha^2}{\epsilon^3} + \dots, \tag{6.6}$$

but even these only contribute one net pole, and otherwise just convert $\alpha$ poles into $\epsilon$ poles.

This means that every pole reduces the number of integrations by one. The leading pole for the 2-particle cut $C_F C_A$, for example, is the $\epsilon^{-4}$ pole. It must necessarily include the four Dirac deltas from the decomposition of the divergent structures in $y$, $b$, $u$ and $t_5$, and therefore only requires a 2-dimensional integral over the remaining $v$ and $t_l$.

Likewise, its first subleading pole receives contributions from this 2-dimensional integral, combined with the linear term in the expansion of any of the other structures, X, Pre or F; or alternatively from the 3-dimensional integral one generates by collecting three Dirac delta and one plus-distributions.

We therefore expect that for $C_F C_A$ and $C_F^2$ the leading poles are fourth inverse regulator powers, and therefore only require 2-dimensional integrations. The third power divergent subleading poles require 2D and 3D integrations, and so forth, until the constant, regulator independent terms, which require all 6 integrations. For $C_F T_F n_f$ the scheme is similar, except that we start at $\epsilon^{-3}$ and $\epsilon^{-2}\alpha^{-1}$, so there is no 2D integration, we immediately start at 3D.

This reasoning can be pushed further, however, a quick look at the structure of the $C_F C_A$ and $C_F T_F n_f$ structures reveals that the only places where the variable $y$ appears is in the measurement function and the divergent structure. This means that the 6D integration, which naively is required for the constant terms $y_{20}$, $y_{10}$, $y_{00}$ ($\text{SCET}_{II}$) or $y_0$ ($\text{SCET}_I$), vanishes, as the absence of any poles from the divergent structures means only the leading orders of the Pre, X and F structures can contribute to the $y_{i0}$. But as the leading order of $F^{4\epsilon+2\alpha} \approx 1 + (4\epsilon + 2\alpha) \ln F + \ldots$ is 1, the entire integrand is just the plus-distribution in $y$ multiplied with $y$-independent terms, which vanishes upon integration.

We therefore conclude that at most we will need to perform 5D integrations to get all terms we want, and for higher poles even fewer integrations are necessary.

This entire discussion is relevant because a numerical integration's performance of course depends on the dimensionality. We expect faster convergence for a 2D integral than for a 5D one. Reducing the dimension therefore in general yields better results and smaller uncertainties in shorter time. In particular, since especially the prefactors mix contributions, a naive expansion à la SecDec evaluates the 2D integration as a 6D integration with 4 unused variables, and does so several times. First for the leading pole, of course, but also as a contribution to the subleading pole, with another constant prefactor.

It therefore makes sense to separate the integrand along the dimension of the integration domain, and then reassemble the bare soft function coefficients using the prefactors once the required integrations have been performed. For example, as soon as the 2D, 3D

and 4D integrations are finished in a run for a $C_F C_A$ structure, all required input for the first three leading poles is available.

## 6.3 C++ based approach

All of these points were enough to motivate us to write dedicated programs for the evaluation of the different colour structures of the bare soft functions, for both $\text{SCET}_I$ and $\text{SCET}_{II}$ observables.

The source codes for these programs can be found in appendix D, we will again explain our procedures along a typical program run.

First, since we no longer use a program whose job it is to find divergences in generic products of polynomials, we were free to expand and simplify the expressions which appear, and put them into library type source files, which encode all the static input, like numerators, Jacobians and Prefactors. The former two are collected in the `XFactorCA.cpp`, `XFactorPNf.cpp` and `XFactorNf.cpp` sources, where we separated the actual $C_F C_A$ and the Pseudo-$n_f$ structures we identified in section 5.7 into the first two files.

Second, we consolidated the input into one file, which takes the form of the measurement function in C++ syntax for all four regions A1, A2, B1 and B2, and also includes any parameters we introduce, as well as some integrator settings and a parameter $M$, which will be explained in chapter 7. Divonne consistently yields the best results in the SecDec approach and has a very convenient feature whose relevance we'll explore in chapter 7, so we hard code Divonne as the integrator choice. We already saw that the parametrisation using $u$ and $v$ instead of $a$ and $t$ was quite cumbersome, in chapter 7 we will find that this can get a lot worse. We will therefore ask for the measurement function in physical parametrisation, i.e. using the variables $a$, $b$, $y$, $t$, $t_5$ and $t_l$, and handle all conversions and reparametrisations to new variables internally.

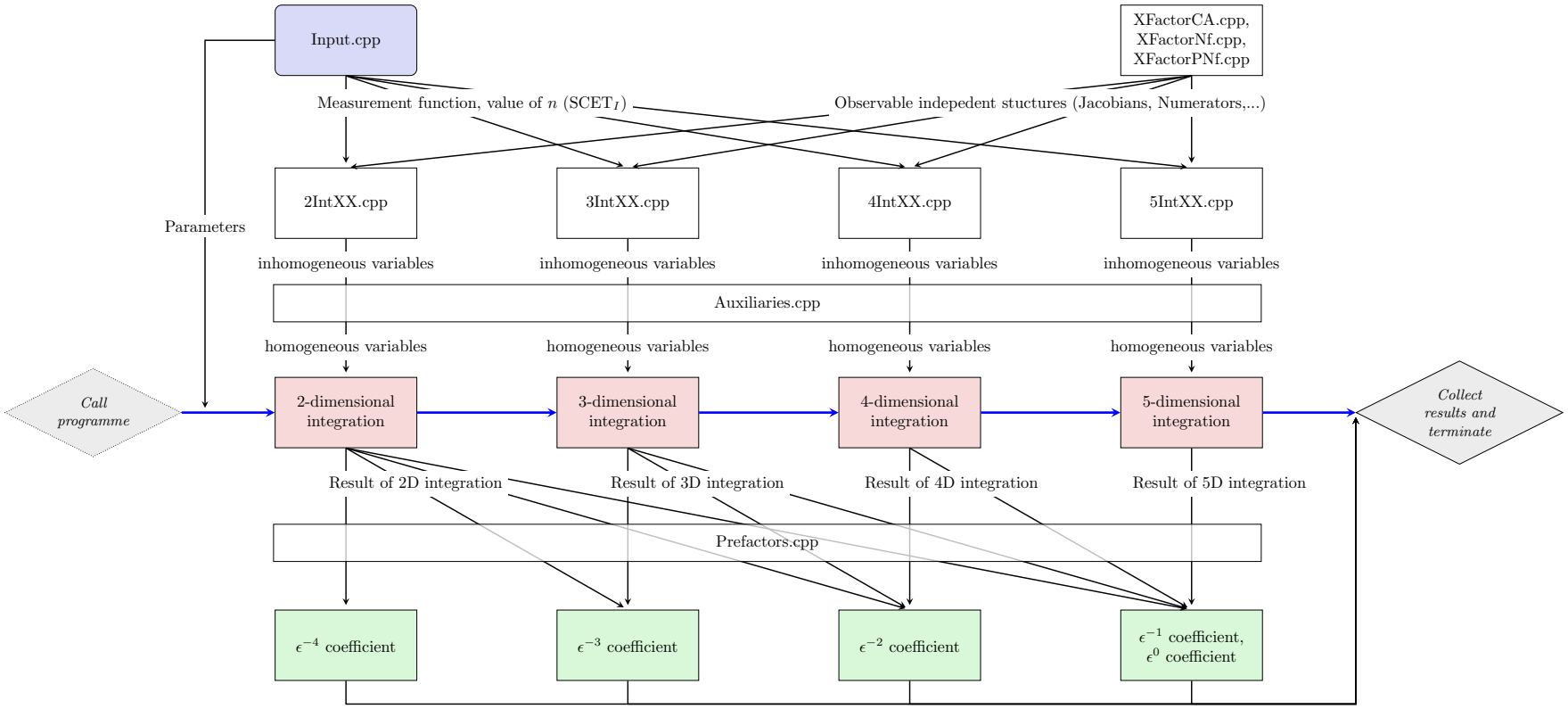


**Figure 6.3:** Program flow through the C++-based approach. The blue box marks the only file requiring user input, red boxes represent program steps, white boxes are library type source files. Green boxes denote results. The blue arrows denote the program flow, black arrows of the form $A \to B$ represent "Variable in A passed to B" or "Function defined in A called by B". The chart should be read left-to-right and top-down, and external libraries are again not included.

The flow through the program is again outlined in figure 6.3, using the nomenclature for a SCET$_I$ observable.

1. Prior to the program call, the program must of course be compiled from the sources, using the Cuba library as an external library. As the sources change whenever a new observable is computed, or when the integrator parameters are changed, we must recompile after every change.

2. Following the initial program call, the program runs through the differently dimensional integrations, starting with the 2D integration. To that end, the relevant $\epsilon$- and $\alpha$-orders are collected from the `XFactorXX.cpp` files, for appropriate colour structure $XX$, and combined with the measurement function in `2IntXX.cpp`, ..., `5IntXX.cpp`, again for appropriate $XX$ and depending on the dimension. For the higher dimensional integrations the integration variables need to be aligned, as there may be integrands with different integration variables. The $C_F C_A$ 3D integration, for example, has contributions which are integrated over $t_l$, $v$ and $y$, but also ones integrated over $t_l$, $v$ and $b$. The auxiliary source file `Auxiliaries.cpp` fulfils that job.

3. After the integration is completed, the program advances to the the next higher dimensional integration, but not before combining the results with the relevant prefactors to determine those pole coefficients for which enough information is already available.

As for SCET$_{II}$ more coefficients, and hence more integrals need to be computed, there is a second set of files alongside the `2IntXX.cpp`, `3IntXX.cpp`, `4IntXX.cpp` and `5IntXX.cpp` files, namely `2IntXXAM1.cpp` and its cousins. These contain the integrands accompanying an $\alpha^{-1}$ pole (AM1).

Using these programs the right way allows us to derive all the results in chapter 8 in usually less than a few hours.

However, if we tried to use the master formulae in terms of $u$ and $v$, i.e. with the parametrisation derived in chapter 5, nothing works properly: convergence rate is abysmal,

error estimates are off by orders of magnitude, and some observables flat out evaluate to `NaN`[3]. Illumination in this respect can be found in chapter 7.

## 6.4 Analytic approach

The insights gained during the C++ based approach are even powerful enough to allow the derivation of analytic formulas for the anomalous dimensions and anomaly coefficients, even if not the finite terms.

The strategy is here similar to the C++ case: The divergences are factorised, so we can apply a subtraction scheme and decompose divergent monomials into Dirac delta and plus-distributions. The delta distributions kill some of the integrations, which simplifies the computation.

It is, however, possible to go one step further, as many of the critical limits associated with a Dirac delta are tied to IRC safety - we used this to argue why nothing can go wrong. Here we can use IRC safety to reduce the NNLO measurement function in many instances to the NLO case. The NLO case is only dependent on one angle variable $t_k$ or $t_l$ and the rapidity $y$, so many integrations can be performed analytically because we know that e.g. the variables $a$ and $b$ cannot appear in the NLO measurement function, they are relative variables between the two NNLO emissions. Also, observable dependent information only enters via the parameter $n$ and the measurement function $F$, and the latter appears only in regulator expansions such as $1+2\epsilon \ln F + 2\epsilon^2 \ln^2 F + \ldots$. This means that terms in which only the leading term contributes are $F$-independent and therefore generic for all observables. This part in general still requires numerical integrations, but it must only be computed once and is generic for all observables.

We will find in chapter 8 that the anomalous dimensions for many observables are the same, this is tied to precisely this discussion - they depend on the observable only in certain limits, which are shared by all these observables.

The explicit form of the analytic formulae was not worked out by the author, but as they served as a check for most of the numerical results to be presented in chapter 8

[3] i.e. an undefined or unrepresentable result of a floating point operation in a computer program, like $\frac{0}{0}$.

for both $\text{SCET}_I$ and $\text{SCET}_{II}$ observables (the latter of which cannot be checked with SecDec), we feel that they should be mentioned.

*Though a program be but three lines long,*
*someday it will have to be maintained.*

— Geoffrey James
*The Tao of Programming*

# 7 Technical issues

Here we will explore in detail why a straightforward numerical integration fails if we use the parametrisation developed in chapter 5, and how to change the integrand to make it work.

## 7.1 Convergence and error estimates

As mentioned we find that a naive application of the two computational strategies yields abysmal convergence rates to the correct results and error estimates which are off by orders of magnitude.

To understand where this is coming from and how to solve it, we need to investigate Monte Carlo integration a bit more closely.

### 7.1.1 Monte Carlo integration

Assume we have a function $f(x)$ that we want to integrate numerically over an interval $\Omega$:

$$I[f] = \int_\Omega \mathrm{d}x\, f(x) \tag{7.1}$$

How can we estimate the value for the integral if we know the function, but can't integrate it analytically?

One way is to regard $I_f = \int_\Omega \mathrm{d}x\, f(x)$ as an expression for the mean of a random variable $f(x)$ living on a probability space $\Omega$ with uniform probability density. It is then clear that

$$I_N[f] = \frac{|\Omega|}{N} \sum_{i=1}^{N} f(x_i) =: |\Omega|\, \bar{f}_N \tag{7.2}$$

with random uniformly distributed $x_i$ is a good estimate achieved by sampling, and is expected to improve with increasing $N$. Here we defined $\bar{f}_N$ as the mean of the $N$ samples.

In fact, because the $f(x_i)$ can be seen as independent identically distributed random variables, the average $I_N[f]$ converges to the expected value $I[f]$, with uncertainty or statistical error of $\frac{\sigma_f}{\sqrt{N}}$ by the central limit theorem (CLT), provided the expected value $I[f]$ and variance $\sigma_f^2 = \int_\Omega \mathrm{d}x\, f^2(x) - I^2[f]$ are finite.

The variance is very likely also unknown if $I[f]$ is already unknown, but it can be estimated using the empirical variance (sample variance) $\sigma_N[f]$:

$$\sigma_N^2[f] = \sum_{i=1}^{N} \frac{|\Omega|}{N-1} \left(f_i - \bar{f}_N\right)^2 \tag{7.3}$$

This allows us to quantify the expected statistical uncertainty, and shows that we can reduce it by using more samples.

On the other hand, a complementary strategy would be to try and reduce the variance, a strategy that numerical integrators such as BASES or the Cuba integrators use, as well.

There are multiple ways of reducing the variance, we will just briefly mention two.

### 7.1.2 Variance reduction

The first is *importance sampling*, which in essence means that the distribution of the samples is changed to put more samples in regions where the integrand is large. Mathematically, this amounts to a change of

$$I[f] = \int_\Omega \mathrm{d}x\, f(x) = \int_\Omega \mathrm{d}x g(x) \frac{f(x)}{g(x)} = I^{(g)}\left[\frac{f}{g}\right], \tag{7.4}$$

where $I^{(g)}$ is the expectation value as evaluated with respect to the distribution $g$, and we assume that $g$ is a probability distribution function with support that coincides with that of $f$.

If now $g$ is "similar" to $f$, viz. the ratio $\frac{f}{g}$ is close to constant, then few samples will be enough for a good estimate, since estimating constant functions is not difficult.

In terms of the variance this means that

$$\begin{aligned} \sigma^2[f] - \left(\sigma^{(g)}\left[\frac{f}{g}\right]\right)^2 &= \int_\Omega \mathrm{d}x\, \left(f(x) - I[f]\right)^2 - \int_\Omega \mathrm{d}x g(x) \left(\frac{f(x)}{g(x)} - I[f]\right)^2 \\ &= \int_\Omega \mathrm{d}x\, f^2(x) \cdot \left(1 - \frac{1}{g(x)}\right) \end{aligned} \tag{7.5}$$

To get a positive difference and hence a reduced variance, $g$ should be small (and thereby increase the variance) if $f$ is small, and large where $f$ is large, demonstrating the similar behaviour of $f$ and $g$.

A second method is *stratified sampling*, for which we divide the integration region into strata, each of which is then sampled independently.

As an example, for the simplest option of splitting the integration domain into two halves $\Omega = \Omega_A + \Omega_B$, with $\frac{N}{2}$ samples each[99], and taking large $N$, so that $N - 1 \approx N$ we find a new estimate

$$I'_N[f] = \left[ \frac{|\Omega|}{2} \frac{2}{N} \sum_{i=1}^{\frac{N}{2}} f_i^{(A)} + \frac{|\Omega|}{2} \frac{2}{N} \sum_{i=1}^{\frac{N}{2}} f_i^{(B)} \right] = I^{(A)}_{\frac{N}{2}}[f] + I^{(B)}_{\frac{N}{2}}[f], \tag{7.6}$$

i.e. the sum of the estimates in the two halves.

For independent sampling the variances just add:

$$\sigma'_N[f] = \sigma^{(A)}_{\frac{N}{2}}[f] + \sigma^{(B)}_{\frac{N}{2}}[f], \tag{7.7}$$

whereas the sample variance for the combined set of $N$ samples is

$$\sigma^2_N[f] = \frac{|\Omega|}{N} \left[ \sum_i^{\frac{N}{2}} (f_i^{(A)} - \bar{f}_N)^2 + \sum_j^{\frac{N}{2}} (f_j^{(B)} - \bar{f}_N)^2 \right] \tag{7.8}$$

which, using $\bar{f}_N = \frac{1}{2}(\bar{f}^{(A)}_{\frac{N}{2}} + \bar{f}^{(B)}_{\frac{N}{2}})$ and the definitions for $\sigma^{(A/B)}_{\frac{N}{2}}$, becomes

$$\sigma^2_N[f] = \sigma'^2_N[f] + \frac{|\Omega|}{4} \left[ \left( \bar{f}^{(A)}_{\frac{N}{2}} + \bar{f}^{(B)}_{\frac{N}{2}} \right)^2 \right]. \tag{7.9}$$

So we see that the variance without stratification is the stratified variance plus a positive term. So stratification reduces the variance even for this simple example.

A detailed analysis for flexible strata shows[99] that oversampling in regions of high variance maximises variance reduction.

A quick look in the Cuba library's manual shows that the Vegas integrator uses importance sampling, and Divonne uses stratified sampling. Both are adaptive integrators, meaning that they try to construct the ideal probability distribution $g$ (for Vegas) or set of strata (Divonne) with the results that they already found as they go along.

### 7.1.3 The root of the problem

Now we can start to understand the problem. If we look at the naive integrand we derived at the end of chapter 5, we find that the angular parametrisations, among others, contribute a factor $t_l^{-\frac{1}{2}-\epsilon}(1-t_l)^{-\frac{1}{2}-\epsilon}$, which is divergent at 0 and 1. The divergence is an integrable pole, even at high regulator orders we find at best $\frac{\ln^i t_l}{\sqrt{t_l}}$ as the leading behaviour. However, thanks to this leading term the variance $\sigma_f^2$ for the integrand function is infinite, this integrable pole is not *square* integrable.

This in turn means that the central limit theorem's (CLT) requirements are violated and it is not applicable.

For the adaptive algorithms this throws hefty spanners in the works, as on the one hand the error estimates, based on the CLT, are no longer valid and not even sensible anymore — the sample variance for finitely many samples cannot be infinite — and on the other hand the variance reduction strategies now also look shady — Anything is a reduction if you start at $\infty$.

We expect that Vegas performs still a bit better than Divonne, since Vegas oversamples based on function values, which is still a suitable strategy. Divonne on the other hand will try to stratify according to the flawed sample variance, which does no longer reflect reality.

We can check this using a simple integral like $\int \mathrm{d}x\,\mathrm{d}x\,\frac{1}{\sqrt{x}\sqrt{y}}$, and indeed we find that both Vegas and Divonne severely underestimate their error, but Vegas converges to the correct value faster, it can cope better with the sub-optimal conditions.

We find a similar behaviour for our NNLO integrals. With infinite variance due to square root divergences Vegas and Divonne are roughly competitive, after eliminating the divergences Divonne outclasses Vegas.

### 7.1.4 Eliminating the divergences

Collecting all sources for square root divergences we find that $t_l$ and $v$ generate such divergences at 0, and $t_l$ and $u$ exhibit them at 1. While we're at it, we also note that many terms in the regulator expansions generate logarithmic divergences, we'll eliminate them in the process, the reasons will become clear in the next section.

Eliminating them is comparatively easy, if we have a divergence of the form

$$x^{-\frac{1}{a}}(1-x)^{-\frac{1}{b}} \tag{7.10}$$

we can use a substitution $x = 1-(1-\xi^m)^n$, which scales at leading order as $x \sim \xi^m$ and $(1-x) \sim (1-\xi)^n$. Together with the Jacobian this means that the leading behaviour of the divergence at 0 and 1 (dropping cluttering terms) turns into

$$x^{-\frac{1}{a}}\mathrm{d}x \to \xi^{m(1-\frac{1}{a})-1}\mathrm{d}\xi \qquad\qquad \bar{x}^{-\frac{1}{b}}\mathrm{d}x \to \bar{\xi}^{n(1-\frac{1}{b})-1}\mathrm{d}\xi \tag{7.11}$$

for $\xi$ near the respective interval boundaries 0 and 1. By choosing $n$ and $m$ appropriately we can therefore eliminate all such divergences.

Terms of the form $x^{-1}$ are invariant under these reparametrisations, but they can still have an effect on plus-distributions, whose modus operandi is that they effectively remove the leading term in a Taylor series to allow a cancellation:

$$\begin{aligned}\int_0^1 \mathrm{d}x \left[\frac{\ln x}{x}\right]_+ f(x) &= \int_0^1 \mathrm{d}x \,\frac{\ln x}{x}\cdot(f_0 + f_1 x + \frac{f_2}{2}x^2 + \ldots - f_0)\\ &= \int_0^1 \mathrm{d}x \left(f_1 + \frac{f_2}{2}x + \ldots\right)\cdot \ln x.\end{aligned} \tag{7.12}$$

Substituting $x = \xi^2$ suppresses the surviving ln divergence:

$$\begin{aligned}\int_0^1 \mathrm{d}x \left[\frac{\ln x}{x}\right]_+ f(x) &= 2\int_0^1 \mathrm{d}\xi \,\frac{2\ln \xi}{\xi}\cdot(f_0 + f_1 \xi^2 + \frac{f_2}{2}\xi^4 + \ldots - f_0)\\ &= \int_0^1 \mathrm{d}\xi \left(f_1 + \frac{f_2}{2}\xi^2 + \ldots\right)\cdot 4\xi\ln\xi.\end{aligned} \tag{7.13}$$

We therefore substitute the chapter 5 variables as follows:

$$\begin{aligned} &u \to 1-(1-z^2)^4 \qquad b \to c^2 \qquad y \to x^m\\ &v \to w^4 \qquad\qquad t_5 \to s_5^2 \qquad t_l \to 1-(1-s_l^4)^4\end{aligned} \tag{7.14}$$

and can rest assured that the integrand now vanishes in almost all interesting limits.

The unspecified exponent of $y \to x^m$ is due to the $y$-expansion of the measurement function (like in eq. 7.12), which can be of the form $F_{ij} \sim 1 + \sqrt{y}$, or even any other root. Then $m$ needs to be specified accordingly, and is observable dependent. We already mentioned this parameter in subsection 6.3, now we know why it is there, we will encounter it again in sections 8.9 and 8.8.

## 7.2 *Boost*ing the programs

The second major technical issue is tied to the nature of computers and C++ itself. It can occur when the measurement function contains large cancellations between terms.

As an example, take a simplified version of the measurement function we'll find for Transverse Thrust (TVT) in section 8.9. Schematically it is of the form

$$\frac{1}{\sqrt{x}}\left(\sqrt{\frac{1}{x}+2\Delta}-\sqrt{\frac{1}{x}}\right) \tag{7.15}$$

with

$$\lim_{x\to 0}\frac{1}{\sqrt{x}}\left(\sqrt{\frac{1}{x}+2\Delta}-\sqrt{\frac{1}{x}}\right)=\Delta. \tag{7.16}$$

For Transverse Thrust the crucial variable is indeed $x$, and $\Delta$ is a function of the other variables.

The problem is now that for very small values of $x$ the ratio between the two terms in the difference approaches unity, i.e. the relative difference between the two is small, irrespective of the value of $\Delta$. This is a problem for computer based methods, since any number a computer program uses is allocated a fixed amount of memory space, which cannot store numbers of arbitrary precision. `C++` and `FORTRAN77`, the two relevant programming languages for our two numerical strategies typically use 64bit/8byte `double` precision variables to store large decimal numbers, which amounts to roughly 15-17 decimal digit accuracy.

For the actual Transverse Thrust case, with all relevant variables evaluated at $10^{-8}$, the two terms in the difference above will match in the first 75 digits, and so any attempt to compute this difference using computers will evaluate it as 0, rather than close to the actual value $\Delta$.

This problem is unfortunately enhanced by our redefinitions in the section preceding this one, because we substitute the denominator of the roots to higher powers.

Naively one could expect this to be a niche issue, a corner case which doesn't really change much, but unfortunately this is not so:

The divergent monomials giving rise to the regulator poles also introduce plus-distributions, and so for small $x = \delta$ we inevitably find[1] expressions such as

$$\frac{\ln F(x) - \ln F(0)}{x} \to \begin{cases} \frac{\ln(\Delta+\varepsilon)-\ln\Delta}{\delta} \text{ analytically, which is finite} \\ \frac{\ln 0-\ln\Delta}{\delta} \text{ as seen by the program,} \end{cases} \tag{7.17}$$

which can arise from the collision of a plus-distribution $[\frac{1}{x}]_+$ with a $\ln F(x)$. The non-trivial limit at 0 identically must be caught by an `if`-clause, and will evaluate correctly, but for infinitesimal $x$ the program will find $F(x) = 0$ due to the insufficient resolution of digits.

As this problem is mainly due to the measurement function, which we by assumption do not know, we cannot solve the problem directly, but we can use other methods to circumvent it:

1. We can use the substitutions in subsection 7.1.4 to suppress the integrand at the boundary, which reduces its contribution to the integral and therefore assigns lower weight to this area, reducing the effect this problem has on the integral and error estimates.

2. Divonne has a feature which allows it to estimate the values of the integrand inside a user specified boundary region by extrapolating from two values outside this region[2].

3. We can increase the number of digits available for the computation.

If we manage to suppress the boundary region linearly using the substitutions in subsection 7.1.4, the boundary feature of Divonne can be used by default to avoid ever evaluating the integrand for small variable values and still get accurate results. This is one reason we introduce the substitution $y \to x^m$, bcause Transverse Thrust SCET$_I$ requires $m = 4$ to have the measurement function behave as $c_0 + c_2x^2 + \ldots$ for small values of $x$, and it is the main reason we hard code Divonne as the integrator choice in the C++ based approach.

Unless otherwise stated, all the observables we'll cover in chapter 8 lose their integrable divergence at $y = 0$ if we substitute $y \to x^2$, the parameter $m$ defined in 7.1.4 is therefore usually $m = 2$.

[1] Using that for continuous functions with $F(0) = \Delta$ we have $F(\delta) = \Delta + \varepsilon$, with $\varepsilon$ small.
[2] i.e. inside the bulk of the integration region.

For a harmless measurement function a linear interpolation into the boundary region, where the integrand is well approximated by its linearisation, is harmless, and for problematic functions it helps avoid the large cancellation. Using the boundary interpolation requires setting a non-zero `border` parameter in the Divonne function call, and while precise estimates are not possible[3], we expect that a `border` value lower than the expected error estimate should be sufficient to avoid overly large systematic errors. To check whether a chosen value for `border` is acceptable, varying it by one order of magnitude in both directions is helpful. If the integral estimate changes, it should be chosen smaller, as then the boundary region still contributes significantly. As a guiding data point: For Transverse Thrust we choose a value of $10^{-7}$ and reproduce the correct result.

Finally, to increase the number of digits we provide additional branches for the C++ based approach, where we use the *Boost*[100] library's `cpp_dec_float_100` type variable templates to define a 100 decimal digit precision data type `decimal`, which is then used to compute the measurement function. While we cannot guarantee that this will solve the problem - there could always be a measurement function for which 100 digits are not enough - it will shift the point where the problem appears to even smaller variable values. Using 100 digits slows the programs down considerably, and is therefore not recommended as the standard choice, but it can help avoid rounding error based catastrophes.

[3]We don't know the shape of the measurement function in detail

*I pass with relief from the tossing sea of Cause and Theory to the firm ground of Result and Fact.*

— Winston Churchill,
*The Story of the Malakand Field Force*

# 8 Example Results

The purpose of this chapter is not mainly to present results for various observables we can compute — most of the results we show are already known analytically — but to show a selection of different observable *types* whose soft functions — or at least soft anomalous dimensions/anomaly coefficients — we can now evaluate at NNLO. So if we present results for Thrust, we haven't regressed several decades and forgotten that a resummed result already exists, we instead want to show that observables that share their characteristics with Thrust can be treated.

We consider the NLO and NNLO 1-particle cut to be simple enough to be analytically computable for generic observables, and will therefore not compute them for the example observables here. We also only evaluate the $C_F C_A$ and $C_F T_F n_f$ structures of the NNLO 2-particle cut diagrams numerically and assume that the $C_F^2$ structure is either determined by non-abelian exponentiation (NAE) or can be computed analytically.

## 8.1 Results

Before we run through the collection of observables, we show the results in one comprehensive section.

Details for each observable can be found following the table. We list measurement functions where they are helpful to show new features, and list the full set of measurement functions in appendix C.

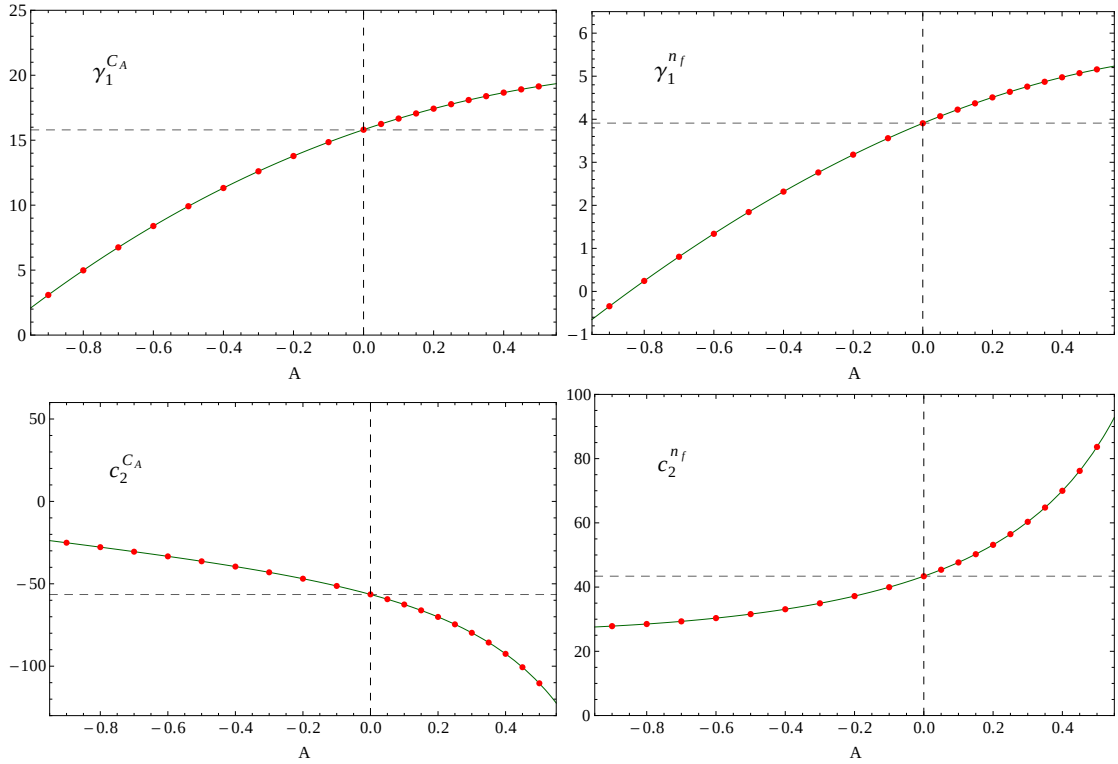


**Figure 8.1:** The numerical results for the Angularities observable's Laplace space anomalous dimension and NNLO constant contribution (dots) and the result of the analytic formulae (lines).

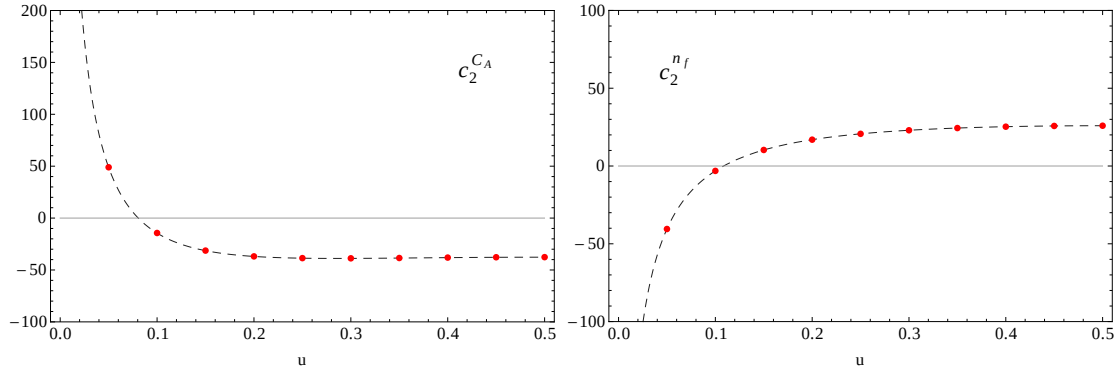


**Figure 8.2:** The finite terms for the hemisphere soft function. Dots are results of the C++ or SecDec programs, dashed lines are the literature result.

| SCET$_I$ Observable | $\gamma_1^{C_A}$ | $\gamma_1^{n_f}$ | $c_1^{C_A}$ | $c_1^{n_f}$ |
|---|---|---|---|---|
| C-Parameter | 15.7945(18)<br>15.7945 | 3.90982(74)<br>3.90981 | −57.9764(34)<br>$-58.16^{+0.26}_{-0.26}$ | 43.8182(15)<br>$43.74^{+0.06}_{-0.06}$ |
| Thrust | 15.7943(71)<br>15.7945 | 3.90985(72)<br>3.90981 | −56.5062(108)<br>−56.4990 | 43.3905(14)<br>43.3905 |
| Angularities | see below | see below | see below | see below |
| Hemispheres | 15.7943(71)<br>15.7945 | 3.90985(72)<br>3.90981 | see below | see below |
| Thrsh. Drell-Yan | 15.7942(23)<br>15.7945 | 3.90984(76)<br>3.90982 | 6.81357(627)<br>6.81287 | −10.6858(17)<br>−10.6857 |
| $W$ @ large $p_T$ | 15.8008(90)<br>15.7945 | 3.90985(72)<br>3.90981 | −2.6772(340)<br>−2.65010 | −25.3073(16)<br>−25.3073 |
| Transverse Thrust | −158.155(70)<br>$-148^{+20}_{-30}$ | 19.3995(46)<br>$18^{+2}_{-3}$ | — | — |

| SCET$_{II}$ Observable | $d_{2,C_A}$ | $d_{2,n_f}$ |
|---|---|---|
| Broadening | 7.0360(26)<br>7.0361 | −11.5394(15)<br>−11.5393 |
| $E_T$ Resummation | 15.9809(31)<br>see below | −18.7370(8)<br>see below |
| Transverse Thrust | 208.111(51)<br>208.0(1) | −37.174(4)<br>−37.191(6) |

**Table 8.1:** A list of all derived SCET$_I$ (upper) and SCET$_{II}$ (lower) results and their comparison to literature (grey, second lines). The colour structure assignment is such that e.g. $d_{2,n_f}$ is the $C_S T_F n_F$ colour structure, with $C_S$ dependent on the Wilson line configuration. Unless otherwise stated $C_S = C_F$, corresponding to Wilson lines in the fundamental representation.

## 8.2 C-Parameter

The computationally easiest observable we could find is the C-Parameter[101], an $e^+e^- \to$ *dijet* observable, whose N$^3$LL resummation is known[102], with the $\mathcal{O}(\alpha_s^2)$ renormalised soft function extracted using `EVENT2`[103]. Our programs can compute both the bare soft function's $\epsilon^0$ and $\epsilon^{-1}$ orders via the master formula in appendix B, so we can present a numerical result for the NNLO finite terms as well as the soft anomalous dimension.

The global definition of C-Parameter in terms of the final state momenta $p_i$ is

$$C = \frac{3}{2}\frac{\sum_{i,j}|\vec{p}_i|\,|\vec{p}_j|\sin\theta_{ij}}{\left(\sum_i|\vec{p}_i|\right)^2} \tag{8.1}$$

For massless soft particles this simplifies (in light cone coordinates) to[102]

$$C_s = \sum_j \frac{1}{Q}\frac{p_j^+ p_j^-}{p_j^+ + p_j^-} \tag{8.2}$$

which translates[1] to a measurement function $F_{A1}$ following chapter 5 of

$$F_{A1}^{(CP)} = \frac{ab}{a(a+b)+(1+ab)y} + \frac{a}{a+b+a(1+ab)y} \tag{8.3}$$

and $n = 1$, correctly signalling a SCET$_I$ observable. The reason we consider it the easiest observable is that it fits our idea of a generic observable perfectly, and doesn't add complexity. $n$ is positively finite and non-zero, and the function $F_{A1}$ and all functions $F_{Xi}$ that can be constructed from it are broken rational functions. The only bit of interest is the zero at $a = 1$, but as this is not a critical limit, it represents an integrable divergence.

The results for the coefficients $y_i$ we find by running our C++ program, it was checked with both the SecDec based and the analytic techniques, and provides a significant improvement over the `EVENT2` extraction that set the standard before.

## 8.3 Recoil-free Jet Broadening and $E_T$ Resummation

Jet Broadening as an $e^+e^- \to dijet$ event shape incorporates recoil effects, which can be eliminated by a convenient choice of the broadening axis[104], which leads to an observable definition of

$$B = \sum_i \frac{\sqrt{k_{i-}k_{i+}}}{2} \tag{8.4}$$

for *Recoil-free Broadening* in the soft region, where the sum runs over all soft emissions.

In physical parametrisation the measurement functions are given by

$$F^{(B)} = \sqrt{\frac{a}{(1+ab)(a+b)}}\,\frac{(1+b)}{2} \tag{8.5}$$

in all four regions A1 to B2, with $n = 0$.

[1] After multiplying with $Q$ to give it mass dimension 1

We find agreement with the literature result.

Although it is not strictly an event shape, we include the transverse energy distribution in Higgs production[105] here, as its measurement function differs from that of Recoil-free Broadening only by a factor of 2:

$$F^{(E)} = \sqrt{\frac{a}{(1+ab)(a+b)}}\,(1+b) \tag{8.6}$$

This observable is a hadron collider observable and the dominant contribution arises from gluon fusion, i.e. the Wilson lines expanding to the matrix element are incoming Wilson lines in the adjoint representation, rather than outgoing fundamental representation lines. Nevertheless, as the different $i\epsilon$-prescriptions do not change the matrix elements[92], and the adjoint representation just means $C_F \Rightarrow C_S = C_A$, we can compute it.

As it turns out results disagree with the literature[105]. We find for the NNLO results

$$d_2^{C_A} = 15.9809(31), \qquad d_2^{n_f} = -18.7370(8), \tag{8.7}$$

which corresponds in CTTW language to

$$B_g^{(2)} = 33.0083(18) \qquad \Leftrightarrow \qquad B_{g,literature}^{(2)} = -5.1 \pm 1.6 \tag{8.8}$$

This discrepancy is as of yet still unresolved, but the measurement functions for Recoil-free Broadening (which we reproduce flawlessly) and $E_T$ resummation match so closely that we are confident in our result, especially as our result is based on an analytic formula which just is evaluated numerically, while the literature result involves a fit to the low-$E_T$ end of a fixed-order result.

As mentioned in section 5.9 the soft function's finite terms are useless without the jet function's contribution, we will therefore not give results for them.

## 8.4 Thrust

Thrust, which is already familiar from chapter 2, is the first lepton collider event shape to add complexity, its NNLO measurement function is

$$F_{A1}^{(T)} = F_{A2}^{(T)} = \theta\left(\frac{a(a+b)}{1+ab} - y\right)\cdot 1 + \theta\left(y - \frac{a(a+b)}{1+ab}\right)\cdot\left(\frac{a}{a+b} + \frac{ab}{(1+ab)y}\right) \tag{8.9}$$

with $n = 1$, which originates from an observable definition in the soft region of

$$\tau_s = \sum_{k \in X_s} \theta(k_- - k_+)k_+ + \theta(k_+ - k_-)k_- \tag{8.10}$$

The Heaviside step functions signal that it measures different regions of integration space differently. We can easily implement such piece-wise defined measurement functions using `if`-clauses in both C++ and `FORTRAN77`. Consequently we reproduce the literature[106, 107] result to relative $10^{-4}$ accuracy.

## 8.5 Angularities

The Angularities represent the extension of our programs to include parameters. It is an observable which interpolates between Thrust and Recoil-free Broadening by the use of a continuous parameter $A$, and can even be extended beyond the edges of the interpolation.

Its definition in terms of momenta is given by

$$\omega = \sum_{k \in X_s} \theta(k_+ - k_-)k_-^{1-\frac{A}{2}} k_+^{\frac{A}{2}} + \theta(k_- - k_+)k_+^{1-\frac{A}{2}} k_-^{\frac{A}{2}}, \tag{8.11}$$

where $A < 2$ is required by IRC safety. It is easy to check that $A = 0$ corresponds to Thrust and $A = 1$ to Recoil-free Broadening. The measurement function is quite cumbersome, we relegate its definition to appendix C.

We can perform the calculations for fixed values of $A$ to sample the functional dependence on the parameter, which leads to the result illustrated in figure 8.3.

The dots represent the numerical results, the lines are the result from the analytic method, both in perfect agreement, error bars are negligible.

This result is the current crown jewel in the selection of observables, since not only is it a new result, but it actively enabled the NNLL' resummation for angularities[108], as the precise knowledge of the finite soft function terms allows the extraction of the finite terms for the jet function as well.

## 8.6 Hemisphere soft function

The Thrust axis defines two hemispheres, left and right, for which we can build the invariant masses of all emissions in these hemispheres $M^2_{L/R} = p^2_{L/R}$. Accordingly

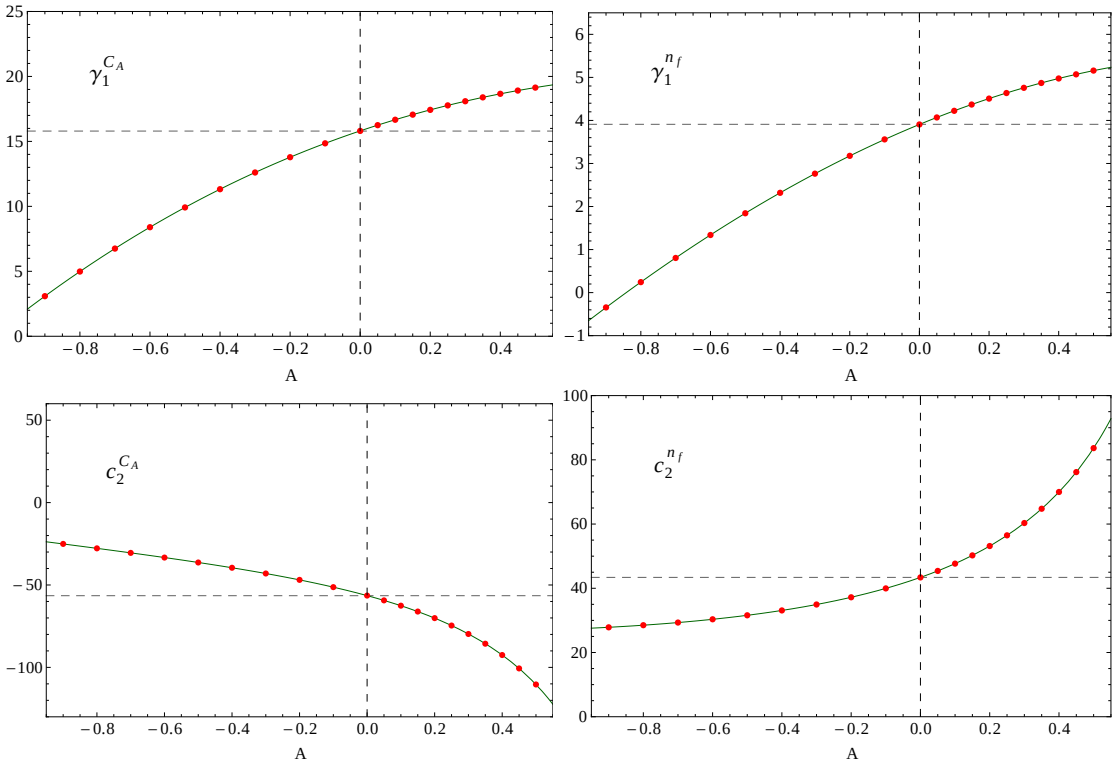


**Figure 8.3:** The numerical results for the Angularities observable's anomalous dimension and NNLO constant contribution.

the hemisphere soft function[106] is differential in two variables, precisely $M_L$ and $M_R$. The Laplace transformed hemisphere soft function then depends on two variables: $S(\tau_1, \tau_2)$, and can therefore not be accommodated in our approach directly. We can, however, define new variables

$$\tau = \tau_1 + \tau_2 \qquad u = \frac{\tau_1}{\tau_1 + \tau_2}, \tag{8.12}$$

and rasterise $u$ as a parameter, while keeping $\tau$ as the Laplace space variable. A fit through the resulting values for the anomalous dimension and finite terms can then reconstruct the functional dependence on both variables.

The anomalous dimension turns out to be $u$-independent and can be found in table 8.1, but the finite terms are parameter dependent and are shown in figure 8.4.

We find agreement with the Laplace transformed analytically known results, for those values of $u$ we rasterised.

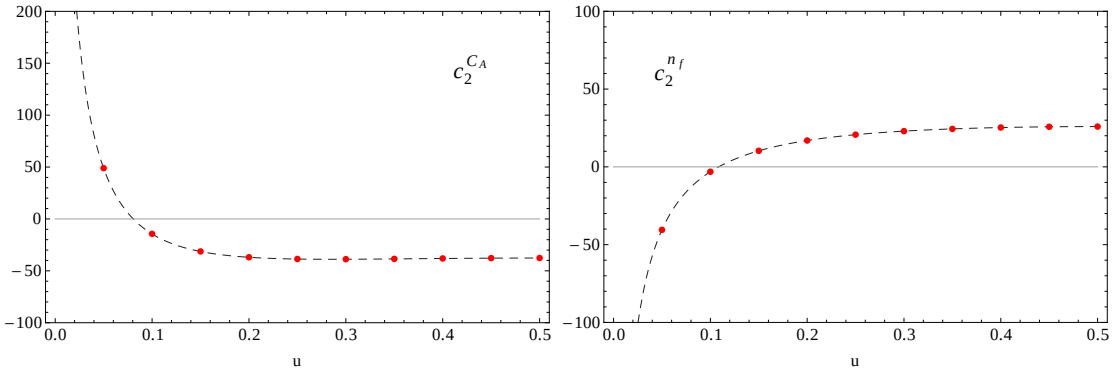


**Figure 8.4:** The finite terms for the hemisphere soft function. Dots are results of the C++ or SecDec programs, dashed lines are the literature result.

## 8.7 Drell-Yan production at Threshold

With Threshold Drell-Yan[109] we leave $e^+e^- \to dijet$ observables behind, as it is a hadronic 0-jet observable, and add a new feature because a straightforward calculation shows that the observable variable $\omega$, whose smallness requires resummation, is

$$\omega = E_k + E_l \qquad \Rightarrow \qquad y^{\frac{n}{2}} F = \frac{1+y}{\sqrt{y}} \qquad \Rightarrow \qquad n = -1, \quad F = 1+y, \tag{8.13}$$

which is slightly at odds with section 4.4. There we tied the behaviour of observables under changes in rapidity to their nature as $\text{SCET}_I$ or $\text{SCET}_{II}$ type observables. We found that $n = -1$ would lead to a collinear sector of the scaling $(1, \lambda^\infty, \lambda^\infty) = (1, 0, 0)$ and promised a solution here. This solution is[93] that for observables such as Threshold Drell-Yan no collinear sector in its usual sense contributes - we sit at threshold, there's no energy for its large component available. On the other hand, this is a hadronic observable, we should expect beams, i.e. boosted proton contents, collinear modes with small virtuality. Consequently the sectors to include are the soft sector $(\lambda, \lambda, \lambda)$, where $\lambda = 1 - x$ and $x$ is the momentum fraction of the proton the quark carries, and the beam sectors $(\varepsilon, \lambda, \sqrt{\varepsilon\lambda})$, where $\varepsilon = \frac{\Lambda^2_{QCD}}{Q^2}$, which we implicitly set to zero so far. So the assumption that the collinear sector scales as $\lambda^0$ in its *large* component is the reason we found inconsistencies, Drell-Yan is not exactly of the $\text{SCET}_I$ type illustrated in figure 3.1(a), here the soft sector has higher virtuality than the collinear sector.

Theoretical issues aside, $n = -1$ is just as good as any other value for a computer, we reproduce the literature to relative $10^{-4}$ accuracy.

## 8.8 $W$ production at large transverse momenta

The production of weak gauge bosons at large transverse momentum is similar to Threshold Drell-Yan, it has he same contributing sectors, and is interesting for two reasons: On a technical level it is the first observable showing angular dependence, on a theoretical level it violates the "Two Wilson lines" assumption, because a large-$p_T$ gauge boson must recoil against a jet, whose direction we denote as $n_j$. Nevertheless, it can be shown[110] that although the (momentum space) soft function is of the form

$$S(\omega) = \sum_{X_s} \langle 0| S_1^\dagger S_2^\dagger S_j^\dagger |X_s\rangle \langle X_s| S_j S_2 S_1 |0\rangle \delta(\omega - n_j \cdot p_{X_s}), \tag{8.14}$$

i.e. in principle dependent on emissions from three Wilson lines, reparametrisation invariance enforces that $S(\omega) \sim f(\sqrt{\frac{2n_1\cdot n_2}{n_1\cdot n_j n_2\cdot n_j}}\omega)$. The dependence on $n_1$ and $n_2$ can only arise from emissions attaching to the corresponding beam Wilson lines in the cut diagrams, and all 2-particle cut diagrams with 2 emissions attached to the beam Wilson lines have either no attachment to the jet Wilson line, or vanish because they include scaleless virtual sub-diagrams, or because of colour conservation. In other words: No diagrams involving the Wilson line along $n_j$ contribute, this observable is *effectively* of the "two Wilson lines" type, and we can compute its soft function.

The presence of the third Wilson line breaks the rotational invariance in transverse space, and so we get angular dependence in the measurement function. We find this by choosing our lightcone vectors appropriately. With $n_1 \cdot n_2 = n_1 \cdot n_j = n_2 \cdot n_j = 2$ and $n_j = n_1 + n_2 + n_{j\perp}$ with $n_{j\perp}^2 = -4$, we find that if we identify $n_1 = \bar{n}$ and $n_2 = n$, then for one emission we find

$$n_j \cdot k = k_+ + k_- + 2\,|k_\perp| \cos\vartheta, \tag{8.15}$$

where $\vartheta$ is the angle between $\vec{k}_\perp$ and $\vec{n}_{j\perp}$.

The presence of the third Wilson lines also changes the colour structure, we have $C_S = C_F - \frac{C_A}{2}$ for the $\bar{q}q \to g$ case, and $C_S = \frac{C_A}{2}$ for the $qg \to q$ case.

Generalised to 2 particles we find a Drell-Yan-like $n = -1$, and

$$F_A^{(W)} = F_B^{(W)} = 1 + y - 2\sqrt{\frac{ay}{(a+b)(1+ab)}}\,(b\,[1-2t_k] + 1 - 2t_l)\,, \tag{8.16}$$

where we substitute for $t_k$ one of the two choices in equation 5.22 to arrive at $F_{X1}$ and $F_{X2}$

Using this measurement with $m = 4$ (note the leading $\sqrt{y}$ in the measurement function), we again reproduce the literature value[110] at $10^{-2}$ accuracy. The loss of accuracy compared to other results can be traced to a large cancellation between NLO and NNLO contributions, the bare soft function is accurate to relative $10^{-4}$.

## 8.9 Transverse Thrust

Transverse Thrust is in many regards the most difficult of our observables — it has many of the features we already saw, plus a few new ones. First, it is a hadronic $2 \to 2$ event shape, but following [111] we can derive the necessary components for NNLL resummation from $0 \to 2$ and $2 \to 0$ observables, treating these two as separate. As this decomposition only holds on the level of the anomalous dimension, the finite terms are here irrelevant and can be discarded. For the soft anomalous dimension there are both an $\text{SCET}_I$ and $\text{SCET}_{II}$ type contribution. The $2 \to 0$ part is a standard $\text{SCET}_{II}$ observable with parametric dependence, and we therefore already know that we can treat it.

The $0 \to 2$ part is the more involved: It is an $n = 1$ $\text{SCET}_I$ observable, with measurement function

$$F_{Ai} = \frac{1}{4y}\Bigg[b\sqrt{\left(\frac{as}{1+ab} + \frac{2c(1-2t_k)\sqrt{ay}}{\sqrt{(a+b)(1+ab)}} - \frac{sy}{a+b}\right)^2 + \frac{16ayt_k\bar{t}_k}{(a+b)(1+ab)}} \tag{8.17}$$

$$- b\left|\frac{as}{1+ab} + \frac{2c(1-2t_k)\sqrt{ay}}{\sqrt{(a+b)(1+ab)}} - \frac{sy}{a+b}\right| \tag{8.18}$$

$$+ \sqrt{\left(\frac{s}{1+ab} + \frac{2c(1-2t_l)\sqrt{ay}}{\sqrt{(a+b)(1+ab)}} - \frac{asy}{a+b}\right)^2 + \frac{16ayt_l\bar{t}_l}{(a+b)(1+ab)}} \tag{8.19}$$

$$- \left|\frac{s}{1+ab} + \frac{2c(1-2t_k)\sqrt{ay}}{\sqrt{(a+b)(1+ab)}} - \frac{asy}{a+b}\right|\Bigg] \tag{8.20}$$

This function has a nontrivial limit as $y \to 0$, which we can catch in the measurement function using an `if`-clause, it is dependent on the parameters $c = \cos\theta$ and $s = \sin\theta$, where $\theta$ is the angle between beam and jet axes, it has different functional form in the four regions $A1$ to $B2$, and it exhibits the problematic large cancellation issue discussed in section 7.2. Also, its leading scaling in $y$ is of the form $F \sim c_0 + \sqrt{y}c_1 +$

..., meaning we need $m = 4$ to have linearly vanishing plus-distributions in $y$ (or rather $x$, following the substitution).

Nevertheless, putting nontrivial limits and extended C++ data types on the list of acceptable characteristics, we can again perform the calculations using the branch of the C++ program which uses the Boost library's data types, and produce results consistent with and improving on the `EVENT2` extracted literature result, albeit with reduced performance, the program runs slower. Although we expect the results to be dependent on the parameters $c$ and $s$, this dependence cancels, we are left with a number:

$$\begin{aligned} \gamma_1^{C_A} &= -158.155(70) \qquad \Leftrightarrow \qquad \gamma_1^{C_A} = -148^{+20}_{-30} \\ \gamma_1^{n_f} &= 19.3995(46) \qquad \Leftrightarrow \qquad \gamma_1^{n_f} = 18^{+2}_{-3}, \end{aligned} \tag{8.21}$$

where the right column are the `EVENT2` extracted values.

It should be noted here that having a semi-automated method to calculate generic soft functions can also serve as a means to cross-check results. Our computation for the Transverse Thrust soft function did serve as such a check and revealed a trivial inconsistency in the literature result.

## 8.10 Possible extensions

The master formulae we derived and programs we wrote are capable of computing soft functions for a wide range of observables at lepton and hadron colliders already, and the last eight sections attest to that. Nevertheless some areas where we can extend our framework are

- The $C_F^2$ colour structure. We didn't go into too much detail about the current status of $C_F^2$. Due to its divergence structure it should be possible to adapt our framework to $C_F^2$ structures for SCET$_{II}$ observables, for SCET$_I$ observables a bit more work is needed.

- Different Wilson line structures. If it proves possible to find parametrisations factorising the regulator poles, changing the setup from two lightlike Wilson lines to e.g. two spacelike ones does not change the overall approach or the programs, and can be implemented.

- Higher orders in the regulators. While not required for NNLL resummation, the orders starting at $\epsilon^1$ will be required for the renormalisation of the N$^3$LO soft anomalous dimension. We can extend our programs to higher orders at the expense of an additional integration dimension, i.e. slower programs.

- $\epsilon$-dependence in the measurement function. As only a finite number of regulator orders are required in the expansion of the integrand formulae, we can accommodate $\epsilon$-dependence at the cost of longer integrand formulae, i.e. slightly slower programs.

- Mass dimensions other than 1. This only changes constant factors in all integration formulae, and can easily be implemented.

*You can't always get what you want,*
*but if you try sometimes, well you just might find:*
*You get what you need.*

— The Rolling Stones,
*You can't always get what you want*

# 9 Conclusion

We have derived in this thesis a strategy for the numerical computation of the $C_F C_A$ and $C_F T_F n_f$ colour structures of NNLO soft functions of wide classes of observables. This strategy is based on the observation that the origin of all regulator poles can be traced to the matrix elements describing the emission of soft and collinear radiation, and is therefore independent of the observable.

We set up a generic computation for NNLO soft functions that involve two lightlike Wilson lines, and motivated and listed the restrictions that observables need to obey to be compatible with our approach by looking at the simpler NLO case. Subsequently we generalised to NNLO and factorised the regulator poles, thereby making them explicit for the two above mentioned colour structures. A working method to factorise the regulator poles for the $C_F^2$ structure was briefly mentioned, as well, to be explored in a future paper.

In the process, we discussed some of the implications of IRC safety and the effects it has on the behaviour of the soft function in critical limits associated with regulator poles in the different colour structures.

We highlighted two numerical implementations for the $C_F C_A$ and $C_F T_F n_f$ structures' computation for SCET$_I$ and SCET$_{II}$ observables' soft functions. Together with a third approach based on purely analytic methods we mentioned, we thus achieve redundancy to allow for cross checks. The computer based programs were set up using both the publicly available tool `SecDec` and our own specially tailored `C++`-based code. Following

a detailed explanation of the final programs, we highlighted some technical difficulties and the strategies to solve them. Finally we presented results both new and previously known, for various observables, thereby demonstrating the scope of the framework.

The computation of soft anomalous dimensions, which can be extracted using the NNLO soft functions, is a crucial step for the resummation of Sudakov logarithms to NNLL accuracy which is so far still performed analytically on a case-by-case basis. This thesis therefore represents an important step towards the automation of resummation to NNLL accuracy, as it eliminates one of the last analytic pen-and-paper steps required, which may ultimately result in computational tools to be used for phenomenological analyses, alongside the already existing computational arsenal - a definite benefit for collider experiments in the present and future.

*There are only two perfectly useless things in this world.*
*One is an appendix and the other is Poincaré.*

— Georges Clemenceau
*in Paris 1919 : Six Months That Changed the World*

# Appendices

# A

# Wilson line configurations

Here we derive the Wilson lines for radiation off different particle types, and the sign choices this entails.

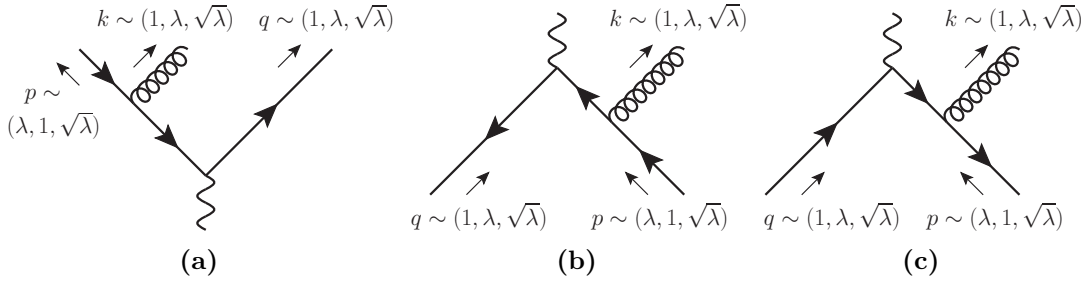


**Figure A.1:** Diagram types yielding different Wilson lines. Particles going to the left are anticollinear, to the right are collinear.

In chapter 3 we motivated the form for the Wilson line attached to an outgoing collinear quark. Even though it may not be obvious that the matching of a quark current $\bar{\psi}\gamma^\mu\psi$ to the SCET current $J$ depends on the physical situation, it is what we find:

Radiate from an incoming antiparticle (figure A.1c), and the correction due to one emission computes along the lines of (3.17) to

$$\bar{\psi} i g \bar{\mathcal{A}}^a T^a \frac{\bar{n}\!\!\!/ - p\!\!\!/}{(p-k)^2 + i\epsilon} \Gamma \psi \quad \to \quad \frac{igT^a}{\bar{n}\cdot k - i\epsilon \operatorname{sgn} n\cdot p} \bar{n}\cdot A_n^a \bar{\xi}_{\bar{n}} \Gamma \xi_n \tag{A.1}$$

Similarly we find for radiation off incoming quarks and outgoing antiquarks

$$-\frac{igT^a}{\bar{n}\cdot k - i\epsilon \operatorname{sgn} n\cdot p} \bar{n}\cdot A_n^a \bar{\xi}_n \Gamma \xi_{\bar{n}} \qquad \text{and} \qquad -\frac{igT^a}{\bar{n}\cdot k + i\epsilon \operatorname{sgn} n\cdot p} \bar{n}\cdot A_n^a \bar{\xi}_n \Gamma \xi_{\bar{n}}, \tag{A.2}$$

respectively.

To connect to the position space version and explain the integral boundaries, observe that the Fourier transform of e.g. the outgoing quark eikonal factor (assuming $n\cdot p > 0$) is

$$\begin{aligned} &\int \frac{\mathrm{d}^4 k}{(2\pi)^4} e^{ik\cdot x} \frac{i A_n(k)}{\bar{n}\cdot k + i\epsilon \operatorname{sgn} n\cdot p} = \int \frac{\mathrm{d}^4 k}{(2\pi)^4} \int_0^\infty \mathrm{d}s\, e^{ik\cdot x} A_n(k) e^{is(\bar{n}\cdot k + i\epsilon)} \\ &= \int_0^\infty \mathrm{d}s \int \frac{\mathrm{d}^4 k}{(2\pi)^4} e^{ik(x+s\bar{n})} A_n(k) = \int_0^\infty \mathrm{d}s\, A(x + s\bar{n}) \end{aligned} \tag{A.3}$$

Flipping the relative sign between the $\bar{n} \cdot k$ term and the $i\epsilon$ leads to the integral $\int_{-\infty}^{0} \mathrm{d}s$, which we find for incoming particles and antiparticles.

It is also the case, although we will only motivate, not demonstrate it[1], that Wilson lines attached to antiparticles are anti-path-ordered, rather than path ordered. When translating Feynman diagrams into formulae we follow the arrows on fermion lines backwards, which leads to a string of colour matrices ordered by their appearance along the particle trajectory. Antiparticles can be seen as particles travelling backwards, leading to anti-path-ordering.

In a differential geometry picture the Wilson line is a gauge link, a parallel transport of the gauge action along a trajectory. The path ordering then arises from the integration of the vanishing covariant derivative as a differential equation defining parallel transport, along the Wilson line's trajectory. This involves the successive summation of non-commuting, Lie algebra valued infinitesimal displacements.

So to summarise we find that the collinear Wilson lines appearing in the matching of the current necessarily depend on the process that we describe using this current. This means that the soft functions we want to compute are constructed from four types of Wilson lines:

$$\begin{aligned}
S^{\dagger}_{out}(x) &= P\, exp\left(igT^a \int_0^{\infty} \mathrm{d}s\, \bar{n} \cdot A^a_n(x + s\bar{n})\right) && \text{for outgoing particles,} \\
\bar{S}_{out}(x) &= \bar{P}\, exp\left(-igT^a \int_0^{\infty} \mathrm{d}s\, \bar{n} \cdot A^a_n(x + s\bar{n})\right) && \text{for outgoing antiparticles,} \\
S_{in}(x) &= P\, exp\left(igT^a \int_{-\infty}^{0} \mathrm{d}s\, \bar{n} \cdot A^a_n(x + s\bar{n})\right) && \text{for incoming particles, and} \\
\bar{S}^{\dagger}_{in}(s) &= \bar{P}\, exp\left(-igT^a \int_{-\infty}^{0} \mathrm{d}s\, \bar{n} \cdot A^a_n(x + s\bar{n})\right) && \text{for incoming antiparticles.}
\end{aligned} \tag{A.4}$$

The NNLO matrix elements only depend via the imaginary part of the 1-particle cut on the different Wilson lines, but at NNLO only the real part contributes[92], which allows us to cover all cases with two light-like back-to-back Wilson lines in one setting.

[1] A demonstration would require 2 particle emission including non-abelian diagrams.

# B
# Master formulae

Here we list the master formulae for the three colour structures, in the physical and computing parametrisations, as derived in chapters 5 and 7 and used in the programs described in chapter 6. We have suppressed the dependence of the functions F on the six integration variables in the formulae below, and mark sources for regulator poles in blue.

## B.1 $C_F T_F n_f$

The integrands are derived from (5.17), after assumptions about the measurement function and the angular parametrisation are taken into account, and integrate to the $y_i$ or $y_{ij}$ in the square brackets of (5.26) or (5.33).

### B.1.1 Physical parametrisation

$$\begin{aligned} S_{n_f} = \int_0^1 \mathrm{d}a\,\mathrm{d}b\,\mathrm{d}t\,\mathrm{d}y\,\mathrm{d}t_5\,\mathrm{d}t_l\, & \frac{2^{7-4\epsilon}\epsilon\Gamma[-2\alpha-4\epsilon]}{e^{2\epsilon\gamma_e}\pi^{\frac{3}{2}}\Gamma[\frac{1}{2}-\epsilon]\Gamma[1-\epsilon]} y^{-1+\alpha+2n\epsilon}\, t_5^{-1-\epsilon}(2-t_5)^{-1-\epsilon} \\ & \cdot a^{2-\alpha-2\epsilon} b^{-\alpha-2\epsilon} \left(t\bar{t}\right)^{-\frac{1}{2}-\epsilon} \left(t_l\bar{t}_l\right)^{-\frac{1}{2}-\epsilon} \left(F_{A1}^{4\epsilon+2\alpha}+F_{A2}^{4\epsilon+2\alpha}+F_{B1}^{4\epsilon+2\alpha}+F_{B2}^{4\epsilon+2\alpha}\right) \\ & \cdot \frac{(1-a)^2(1-b)^2-4t(a+b)(1+ab)}{\left((1-a)^2+4at\right)^2} (a+b)^{-2+2\epsilon}(1+ab)^{-2+2\alpha+2\epsilon} \end{aligned} \tag{B.1}$$

### B.1.2 Computing parametrisation - Integrable poles removed

$$\begin{aligned} S_{n_f} = \int_0^1 \mathrm{d}z\,\mathrm{d}c\,\mathrm{d}w\,\mathrm{d}x\,\mathrm{d}s_5\,\mathrm{d}s_l\, & \frac{2^{17-4\epsilon} m\epsilon\Gamma[-2\alpha-4\epsilon]}{e^{2\epsilon\gamma_e}\pi^{\frac{3}{2}}\Gamma[\frac{1}{2}-\epsilon]\Gamma[1-\epsilon]} z^{-1-4\epsilon}\, x^{-1+m\alpha+2nm\epsilon}\, s_5^{-1-2\epsilon} \\ & \cdot \frac{1}{(1+w^4)^3} c^{1-2\alpha-4\epsilon} w^{1-4\epsilon} s_l^{1-4\epsilon} \left(F_{A1}^{4\epsilon+2\alpha}+F_{A2}^{4\epsilon+2\alpha}+F_{B1}^{4\epsilon+2\alpha}+F_{B2}^{4\epsilon+2\alpha}\right) (2-s_5^2)^{-1-\epsilon} \\ & \cdot (1-z^2)^{1-4\epsilon}(1-s_l^4)^{1-4\epsilon} \left((2-s_l^4)(2-2s_l^4+s_l^8)\right)^{-\frac{1}{2}-\epsilon} \left((2-z^2)(2-2z^2+z^4)\right)^{-1-2\epsilon} \\ & \cdot \left(1+w^4z^2(2-z^2)(2-2z^2+z^4)\right)^{-\frac{1}{2}-\epsilon} \left((1-z^2)^4+w^4z^2(2-z^2)(2-2z^2+z^4)\right)^{1-\alpha} \\ & \cdot \left(1+c^2\left((1-z^2)^4+w^4z^2(2-z^2)(2-2z^2+z^4)\right)\right)^{-2+2\alpha+2\epsilon} \end{aligned}$$

$$\cdot\left(c^2+(1-z^2)^4+w^4z^2(2-z^2)(2-2z^2+z^4)\right)^{-2+2\epsilon}\Big[-4w^4\Big(c^2+w^4z^2\Big(2-z^2\Big)$$
$$\cdot\Big(z^4-2z^2+2\Big)+\Big(1-z^2\Big)^4\Big)\Big(1+c^2\Big(w^4z^2(2-z^2)(z^4-2z^2+2)+(1-z^2)^4\Big)\Big)$$
$$-(1-c^2)^2(1-w^4)^2\Big(w^4z^2(2-z^2)(z^4-2z^2+2)+(1-z^2)^4\Big)\Big]$$

## B.2 $C_F C_A$

We split this colour structure into the sum of *Pseudo-$n_f$*(PNF) and *Real* $C_A$(RCA) structures. The Pseudo-$n_f$ structure has the same divergence pattern as the $n_f$ structure, splitting allows some terms to cancel in both PNF and RCA.

### B.2.1 Physical parametrisation

$$S_{PNF}=\int_0^1 \mathrm{d}a\,\mathrm{d}b\,\mathrm{d}t\,\mathrm{d}y\,\mathrm{d}t_5\,\mathrm{d}t_l\,\frac{(1-\epsilon)2^{5-4\epsilon}\epsilon\Gamma[-2\alpha-4\epsilon]}{e^{2\epsilon\gamma_e}\pi^{\frac{3}{2}}\Gamma[\frac{1}{2}-\epsilon]\Gamma[1-\epsilon]}y^{-1+\alpha+2n\epsilon}\,t_5^{-1-\epsilon}(2-t_5)^{-1-\epsilon}$$
$$\cdot a^{1-\alpha-2\epsilon}b^{1-\alpha-2\epsilon}\left(t\bar{t}\right)^{-\frac{1}{2}-\epsilon}\left(t_l\bar{t}_l\right)^{-\frac{1}{2}-\epsilon}\left(F_{A1}^{4\epsilon+2\alpha}+F_{A2}^{4\epsilon+2\alpha}+F_{B1}^{4\epsilon+2\alpha}+F_{B2}^{4\epsilon+2\alpha}\right)$$
$$\cdot\frac{(1-a^2)^2}{\left((1-a)^2+4at\right)^2}(a+b)^{-2+2\epsilon}(1+ab)^{-2+2\alpha+2\epsilon} \tag{B.2}$$

$$S_{RCA}=\int_0^1 \mathrm{d}a\,\mathrm{d}b\,\mathrm{d}t\,\mathrm{d}y\,\mathrm{d}t_5\,\mathrm{d}t_l\,\frac{-2^{5-4\epsilon}\epsilon\Gamma[-2\alpha-4\epsilon]}{e^{2\epsilon\gamma_e}\pi^{\frac{3}{2}}\Gamma[\frac{1}{2}-\epsilon]\Gamma[1-\epsilon]}y^{-1+\alpha+2n\epsilon}\,t_5^{-1-\epsilon}\,b^{-1-\alpha-2\epsilon}$$
$$\cdot(2-t_5)^{-1-\epsilon}a^{-\alpha-2\epsilon}\left(t\bar{t}\right)^{-\frac{1}{2}-\epsilon}\left(t_l\bar{t}_l\right)^{-\frac{1}{2}-\epsilon}\left(F_{A1}^{4\epsilon+2\alpha}+F_{A2}^{4\epsilon+2\alpha}+F_{B1}^{4\epsilon+2\alpha}+F_{B2}^{4\epsilon+2\alpha}\right)$$
$$\cdot\frac{(1-2t)\left(a^2b+2a\left(b^2+1\right)+b\right)-2ab}{(1-a)^2+4at}(a+b)^{-1+2\epsilon}(1+ab)^{-1+2\alpha+2\epsilon} \tag{B.3}$$

### B.2.2 Computing parametrisation - Integrable poles removed

$$S_{PNF}=\int_0^1 \mathrm{d}z\,\mathrm{d}c\,\mathrm{d}w\,\mathrm{d}x\,\mathrm{d}s_5\,\mathrm{d}s_l\,\frac{(\epsilon-1)2^{4(4-\epsilon)}m\epsilon\Gamma[-2\alpha-4\epsilon]}{e^{2\epsilon\gamma_e}\pi^{\frac{3}{2}}\Gamma[\frac{1}{2}-\epsilon]\Gamma[1-\epsilon]}z^{-1-4\epsilon}\,x^{-1+m\alpha+2nm\epsilon}\,s_5^{-1-2\epsilon}$$
$$\cdot\frac{1}{(1+w^4)^3}c^{3-2\alpha-4\epsilon}w^{1-4\epsilon}s_l^{1-4\epsilon}\left(F_{A1}^{4\epsilon+2\alpha}+F_{A2}^{4\epsilon+2\alpha}+F_{B1}^{4\epsilon+2\alpha}+F_{B2}^{4\epsilon+2\alpha}\right)(2-s_5^2)^{-1-\epsilon}$$
$$\cdot(1-z^2)^{1-4\epsilon}(1-s_l^4)^{1-4\epsilon}\left((2-s_l^4)(2-2s_l^4+s_l^8)\right)^{-\frac{1}{2}-\epsilon}\left((2-z^2)(2-2z^2+z^4)\right)^{-1-2\epsilon}$$
$$\cdot\left(1+w^4z^2(2-z^2)(2-2z^2+z^4)\right)^{-\frac{1}{2}-\epsilon}\left((1-z^2)^4+w^4z^2(2-z^2)(2-2z^2+z^4)\right)^{1-\alpha}$$
$$\cdot\left(1+c^2((1-z^2)^4+w^4z^2(2-z^2)(2-2z^2+z^4))\right)^{-2+2\alpha+2\epsilon}$$
$$\cdot\left(c^2+(1-z^2)^4+w^4z^2(2-z^2)(2-2z^2+z^4)\right)^{-2+2\epsilon}$$

$$\cdot\left[2+w^4z^2\left(2-z^2\right)\left(2-2z^2+z^4\right)-z^2\left(2-z^2\right)\left(2-2z^2+z^4\right)\right]^2$$

$$\begin{aligned}
S_{RCA} = \int_0^1 \mathrm{d}z\,\mathrm{d}c\,\mathrm{d}w\,\mathrm{d}x\,\mathrm{d}s_5\,\mathrm{d}s_l\,&\frac{2^{4(4-\epsilon)}m\epsilon\Gamma[-2\alpha-4\epsilon]}{e^{2\epsilon\gamma_e}\pi^{\frac{3}{2}}\Gamma[\frac{1}{2}-\epsilon]\Gamma[1-\epsilon]}z^{-1-4\epsilon}\,x^{-1+m\alpha+2nm\epsilon}\,s_5^{-1-2\epsilon}\\
&\cdot c^{-1-2\alpha-4\epsilon}\frac{1}{(1+w^4)}w^{1-4\epsilon}s_l^{1-4\epsilon}\left(F_{A1}^{4\epsilon+2\alpha}+F_{A2}^{4\epsilon+2\alpha}+F_{B1}^{4\epsilon+2\alpha}+F_{B2}^{4\epsilon+2\alpha}\right)(2-s_5^2)^{-1-\epsilon}\\
&\cdot(1-z^2)^{1-4\epsilon}(1-s_l^4)^{1-4\epsilon}\left((2-s_l^4)(2-2s_l^4+s_l^8)\right)^{-\frac{1}{2}-\epsilon}\left((2-z^2)(2-2z^2+z^4)\right)^{-1-2\epsilon}\\
&\cdot\left(1+w^4z^2(2-z^2)(2-2z^2+z^4)\right)^{-\frac{1}{2}-\epsilon}\left((1-z^2)^4+w^4z^2(2-z^2)(2-2z^2+z^4)\right)^{-\alpha}\\
&\cdot\left(1+c^2((1-z^2)^4+w^4z^2(2-z^2)(2-2z^2+z^4))\right)^{-1+2\alpha+2\epsilon}\\
&\cdot\left(c^2+(1-z^2)^4+w^4z^2(2-z^2)(2-2z^2+z^4)\right)^{-1+2\epsilon}\\
&\cdot\Bigg[2c^2\left(w^4z^2\left(2-z^2\right)\left(z^4-2z^2+2\right)+\left(1-z^2\right)^4\right)\\
&\quad-\left(1-\frac{2w^4z^4(2-z^2)^2(2-2z^2+z^4)^2}{w^4z^2(2-z^2)(2-2z^2+z^4)+(1-z^2)^4}\right)\Bigg(c^2\\
&\quad+2\left(1+c^4\right)\left(w^4z^2(2-z^2)\left(z^4-2z^2+2\right)+\left(1-z^2\right)^4\right)\\
&\quad+c^2\left(w^4z^2(2-z^2)\left(2-2z^2+z^4\right)+\left(1-z^2\right)^4\right)^2+c^2\Bigg)\Bigg]
\end{aligned}$$

# C
# Measurement functions

Here we list all measurement functions for the observables computed in chapter 8. We suppress the dependence on the six integration variables, all functions should in their full form read "$F_{Xi}(a,b,y,t,t_5,t_l)$", rather than just "$F_{Xi}$".

## C.1 C-Parameter

$$
\begin{aligned}
&n=1\\
F_{A1}=F_{A2}&=\frac{ab}{a(a+b)+(1+ab)y}+\frac{a}{a+b+a(1+ab)y}\\
F_{B1}=F_{B2}&=\frac{a}{a(1+ab)+(a+b)y}+\frac{ab}{1+ab+a(a+b)y}
\end{aligned}
\tag{C.1}
$$

## C.2 Recoil-free Broadening

$$
\begin{aligned}
&n=0\\
\text{all } F_{Xi}&=\sqrt{\frac{a}{(a+b)(1+ab)}}\,\frac{1+b}{2}
\end{aligned}
\tag{C.2}
$$

## C.3 $E_T$ Resummation

$$
\begin{aligned}
&n=0\\
\text{all } F_{Xi}&=\sqrt{\frac{a}{(a+b)(1+ab)}}\,(1+b)
\end{aligned}
\tag{C.3}
$$

## C.4 Thrust

$$
\begin{aligned}
&n=1\\
F_{A1}=F_{A2}&=\theta\left(\frac{a(a+b)}{1+ab}-y\right)\cdot 1+\theta\left(y-\frac{a(a+b)}{1+ab}\right)\cdot\left(\frac{a}{a+b}+\frac{ab}{(1+ab)y}\right)\\
F_{B1}=F_{B2}&=\theta\left(\frac{a(1+ab)}{a+b}-y\right)\cdot 1+\theta\left(y-\frac{a(1+ab)}{a+b}\right)\cdot\left(\frac{a}{y(a+b)}+\frac{ab}{1+ab}\right)
\end{aligned}
\tag{C.4}
$$

## C.5 Angularities

$$
\begin{aligned}
&n=1\\
F_{A1}=F_{A2}&=\theta\left(\frac{a(a+b)}{1+ab}-y\right)\cdot a^{1-\frac{A}{2}}(a+b)^{\frac{A}{2}-1}(1+ab)^{-\frac{A}{2}}\left(ba^{A-1}+1\right)\\
&+\theta\left(y-\frac{a(a+b)}{1+ab}\right)\cdot a^{1-\frac{A}{2}}(a+b)^{\frac{A}{2}-1}(1+ab)^{\frac{A}{2}-1}\left((1+ab)^{1-A}+b\left(\frac{a+b}{y}\right)^{1-A}\right)\\
F_{B1}=F_{B2}&=\theta\left(\frac{a(1+ab)}{a+b}-y\right)\cdot a^{1-\frac{A}{2}}(a+b)^{-\frac{A}{2}}(1+ab)^{\frac{A}{2}-1}\left(a^{A-1}+b\right)\\
&+\theta\left(y-\frac{a(1+ab)}{a+b}\right)\cdot a^{1-\frac{A}{2}}(a+b)^{\frac{A}{2}-1}(1+ab)^{\frac{A}{2}-1}\left(b(a+b)^{1-A}+\left(\frac{1+ab}{y}\right)^{1-A}\right)
\end{aligned}
\tag{C.5}
$$

## C.6 Hemisphere masses

$$
\begin{aligned}
&n=1\\
F_{A1}=F_{A2}&=\theta\left(y-\frac{a(a+b)}{1+ab}\right)\left((1-u)\frac{ab}{y(1+ab)}+u\frac{a}{a+b}\right)+\theta\left(\frac{a(a+b)}{1+ab}-y\right)u\\
F_{B1}=F_{B2}&=\theta\left(y-\frac{a(1+ab)}{a+b}\right)\left((1-u)\frac{a}{y(a+b)}+u\frac{ab}{1+ab}\right)+\theta\left(\frac{a(1+ab)}{a+b}-y\right)u
\end{aligned}
\tag{C.6}
$$

## C.7 Threshold Drell-Yan

$$
\begin{aligned}
n&=-1\\
\text{all } F_{Xi}&=1+y
\end{aligned}
\tag{C.7}
$$

## C.8 $W$ production at large transverse momentum

$$
\begin{aligned}
&n=-1\\
F_{Ai}=F_{Bi}&=1+y-2\sqrt{\frac{ay}{(a+b)(1+ab)}}\,(b[1-2t_{ki}]+[1-2t_l])
\end{aligned}
\tag{C.8}
$$

Substitute one of

$$
\begin{aligned}
t_{k1}&=t+t_l-2tt_l-2\sqrt{t\bar{t}t_l\bar{t}_l}\,(1-t_5)\\
t_{k2}&=t+t_l-2tt_l-2\sqrt{t\bar{t}t_l\bar{t}_l}\,(t_5-1)
\end{aligned}
\tag{C.9}
$$

for $t_{ki}$ to arrive at $F_{X1}$ and $F_{X2}$.

## C.9 Transverse Thrust, SCET$_I$

$$
\begin{aligned}
F_{Ai} = \frac{1}{4y}\Bigg[ & b\sqrt{\left(\frac{as}{1+ab}+\frac{2c(1-2t_{ki})\sqrt{ay}}{\sqrt{(a+b)(1+ab)}}-\frac{sy}{a+b}\right)^2+\frac{16ayt_{ki}\bar{t}_{ki}}{(a+b)(1+ab)}} \\
& -b\left|\frac{as}{1+ab}+\frac{2c(1-2t_{ki})\sqrt{ay}}{\sqrt{(a+b)(1+ab)}}-\frac{sy}{a+b}\right| \\
& +\sqrt{\left(\frac{s}{1+ab}+\frac{2c(1-2t_l)\sqrt{ay}}{\sqrt{(a+b)(1+ab)}}-\frac{asy}{a+b}\right)^2+\frac{16ayt_l\bar{t}_l}{(a+b)(1+ab)}} \\
& -\left|\frac{s}{1+ab}+\frac{2c(1-2t_l)\sqrt{ay}}{\sqrt{(a+b)(1+ab)}}-\frac{asy}{a+b}\right|\Bigg] \\
F_{Bi} = \frac{1}{4y}\Bigg[ & b\sqrt{\left(\frac{asy}{1+ab}+\frac{2c(1-2t_{ki})\sqrt{ay}}{\sqrt{(a+b)(1+ab)}}-\frac{s}{a+b}\right)^2+\frac{16ayt_{ki}\bar{t}_{ki}}{(a+b)(1+ab)}} \\
& -b\left|\frac{asy}{1+ab}+\frac{2c(1-2t_{ki})\sqrt{ay}}{\sqrt{(a+b)(1+ab)}}-\frac{s}{a+b}\right| \\
& +\sqrt{\left(\frac{sy}{1+ab}+\frac{2c(1-2t_l)\sqrt{ay}}{\sqrt{(a+b)(1+ab)}}-\frac{as}{a+b}\right)^2+\frac{16ayt_l\bar{t}_l}{(a+b)(1+ab)}} \\
& -\left|\frac{sy}{1+ab}+\frac{2c(1-2t_l)\sqrt{ay}}{\sqrt{(a+b)(1+ab)}}-\frac{as}{a+b}\right|\Bigg],
\end{aligned}
\tag{C.10}
$$

with $c$ and $s$ parameters as outlined in the appropriate section. Substitute one of

$$
\begin{aligned}
t_{k1} &= t+t_l-2tt_l-2\sqrt{t\bar{t}t_l\bar{t}_l}\,(1-t_5) \\
t_{k2} &= t+t_l-2tt_l-2\sqrt{t\bar{t}t_l\bar{t}_l}\,(t_5-1)
\end{aligned}
\tag{C.11}
$$

for $t_{ki}$ to arrive at $F_{X1}$ and $F_{X2}$.

## C.10 Transverse Thrust, SCET$_{II}$

$$
\begin{aligned}
& n=0 \\
& F_{Ai}=F_{Bi}=\sqrt{\frac{a}{(a+b)(1+ab)}}\,\left(b\left(1-|1-2t_{ki}|\right)+1-|1-2t_l|\right)
\end{aligned}
\tag{C.12}
$$

Substitute one of

$$
\begin{aligned}
t_{k1} &= t+t_l-2tt_l-2\sqrt{t\bar{t}t_l\bar{t}_l}\,(1-t_5) \\
t_{k2} &= t+t_l-2tt_l-2\sqrt{t\bar{t}t_l\bar{t}_l}\,(t_5-1)
\end{aligned}
\tag{C.13}
$$

for $t_{ki}$ to arrive at $F_{X1}$ and $F_{X2}$.

# D
# Source files

The CD glued to the back cover contains all the source files for the NNLO programmes we described in chapter 6, and which we used to derive the results in chapter 8.

*With just enough of learning to misquote.*

— Lord Byron

# References


[1] Georges Aad et al. 'Observation of a new particle in the search for the Standard Model Higgs boson with the ATLAS detector at the LHC'. In: *Phys. Lett.* B716 (2012), pp. 1–29. arXiv: 1207.7214 [hep-ex].

[2] Serguei Chatrchyan et al. 'Observation of a new boson at a mass of 125 GeV with the CMS experiment at the LHC'. In: *Phys. Lett.* B716 (2012), pp. 30–61. arXiv: 1207.7235 [hep-ex].

[3] David J. Gross and Frank Wilczek. 'Ultraviolet Behavior of Non-Abelian Gauge Theories'. In: *Phys. Rev. Lett.* 30 (26 June 1973), pp. 1343–1346. URL: http://link.aps.org/doi/10.1103/PhysRevLett.30.1343; H. David Politzer. 'Reliable Perturbative Results for Strong Interactions?' In: *Phys. Rev. Lett.* 30 (26 June 1973), pp. 1346–1349. URL: http://link.aps.org/doi/10.1103/PhysRevLett.30.1346; David J. Gross and Frank Wilczek. 'Asymptotically Free Gauge Theories. I'. In: *Phys. Rev. D* 8 (10 Nov. 1973), pp. 3633–3652. URL: http://link.aps.org/doi/10.1103/PhysRevD.8.3633; David J. Gross and Frank Wilczek. 'Asymptotically free gauge theories. II'. In: *Phys. Rev. D* 9 (4 Feb. 1974), pp. 980–993. URL: http://link.aps.org/doi/10.1103/PhysRevD.9.980.

[4] John C. Collins, Davison E. Soper and George F. Sterman. 'Factorization of Hard Processes in QCD'. In: *Adv. Ser. Direct. High Energy Phys.* 5 (1989), pp. 1–91. arXiv: hep-ph/0409313 [hep-ph].

[5] Mao Zeng. 'Drell-Yan process with jet vetoes: breaking of generalized factorization'. In: *JHEP* 10 (2015), p. 189. arXiv: 1507.01652 [hep-ph].

[6] Jonathan R. Gaunt. 'Glauber Gluons and Multiple Parton Interactions'. In: *JHEP* 07 (2014), p. 110. arXiv: 1405.2080 [hep-ph].

[7] Carola F. Berger et al. 'An Automated Implementation of On-Shell Methods for One-Loop Amplitudes'. In: *Phys. Rev.* D78 (2008), p. 036003. arXiv: 0803.4180 [hep-ph].

[8] Walter T. Giele and Giulia Zanderighi. 'On the Numerical Evaluation of One-Loop Amplitudes: The Gluonic Case'. In: *JHEP* 06 (2008), p. 038. arXiv: 0805.2152 [hep-ph]; R. Keith Ellis, Walter T. Giele, Zoltan Kunszt, Kirill Melnikov and Giulia Zanderighi. 'One-loop amplitudes for $W^+$ 3 jet production in hadron collisions'. In: *JHEP* 01 (2009), p. 012. arXiv: 0810.2762 [hep-ph].

[9] Giuseppe Bevilacqua et al. 'HELAC-NLO'. In: *Comput. Phys. Commun.* 184 (2013), pp. 986–997. arXiv: 1110.1499 [hep-ph].

[10] Fabio Cascioli, Philipp Maierhöfer and Stefano Pozzorini. 'Scattering Amplitudes with Open Loops'. In: *Phys. Rev. Lett.* 108 (2012), p. 111601. arXiv: 1111.5206 [hep-ph].

[11] Simon Badger, Benedikt Biedermann, Peter Uwer and Valery Yundin. 'Numerical evaluation of virtual corrections to multi-jet production in massless QCD'. In: *Comput. Phys. Commun.* 184 (2013), pp. 1981–1998. arXiv: 1209.0100 [hep-ph].

[12] Gavin Cullen et al. 'G*OSAM*-2.0: a tool for automated one-loop calculations within the Standard Model and beyond'. In: *Eur. Phys. J.* C74.8 (2014), p. 3001. arXiv: 1404.7096 [hep-ph].

[13] Johan Alwall et al. 'The automated computation of tree-level and next-to-leading order differential cross sections, and their matching to parton shower simulations'. In: *JHEP* 07 (2014), p. 079. arXiv: 1405.0301 [hep-ph].

[14] Jürgen Reuter et al. 'Automation of NLO processes and decays and POWHEG matching in WHIZARD'. In: *17th International workshop on Advanced Computing and Analysis Techniques in physics research (ACAT 2016) Valparaiso, Chile, January 18-22, 2016*. 2016. arXiv: 1602.06270 [hep-ph]. URL: https://inspirehep.net/record/1422629/files/arXiv:1602.06270.pdf.

[15] Stefano Actis, Ansgar Denner, Lars Hofer, Andreas Scharf and Sandro Uccirati. 'Recursive generation of one-loop amplitudes in the Standard Model'. In: *JHEP* 04 (2013), p. 037. arXiv: 1211.6316 [hep-ph]; Stefano Actis et al. *RECOLA: REcursive Computation of One-Loop Amplitudes*. 2016. arXiv: 1605.01090 [hep-ph].

[16] M. Bahr et al. 'Herwig++ Physics and Manual'. In: *Eur. Phys. J.* C58 (2008), pp. 639–707. arXiv: 0803.0883 [hep-ph]; Johannes Bellm et al. 'Herwig 7.0/Herwig++ 3.0 release note'. In: *Eur. Phys. J.* C76.4 (2016), p. 196. arXiv: 1512.01178 [hep-ph].

[17] Torbjörn Sjöstrand et al. 'An Introduction to PYTHIA 8.2'. In: *Comput. Phys. Commun.* 191 (2015), pp. 159–177. arXiv: 1410.3012 [hep-ph].

[18] Tanju Gleisberg et al. 'Event generation with SHERPA 1.1'. In: *JHEP* 02 (2009), p. 007. arXiv: 0811.4622 [hep-ph]; *Sherpa 2.2.1*. https://sherpa.hepforge.org. Accessed: 21th September 2016, Version 2.2.1.

[19] John M. Campbell, R. Keith Ellis and Walter T. Giele. 'A Multi-Threaded Version of MCFM'. In: *Eur. Phys. J.* C75.6 (2015), p. 246. arXiv: 1503.06182 [physics.comp-ph].

[20] Simone Alioli et al. 'Combining Higher-Order Resummation with Multiple NLO Calculations and Parton Showers in GENEVA'. In: *JHEP* 09 (2013), p. 120. arXiv: 1211.7049 [hep-ph].

[21] Stefano Catani, Frank Krauss, Rudolf Kuhn and Bryan R. Webber. 'QCD matrix elements + parton showers'. In: *JHEP* 11 (2001), p. 063. arXiv: hep-ph/0109231 [hep-ph].

[22] Matt Dobbs. 'Phase space veto method for next-to-leading order event generators in hadronic collisions'. In: *Phys. Rev.* D65 (2002), p. 094011. arXiv: hep-ph/0111234 [hep-ph].

[23] Yoshimasa Kurihara et al. 'QCD event generators with next-to-leading order matrix elements and parton showers'. In: *Nucl. Phys.* B654 (2003), pp. 301–319. arXiv: hep-ph/0212216 [hep-ph].

[24] Zoltan Nagy and Davison E. Soper. 'Matching parton showers to NLO computations'. In: *JHEP* 10 (2005), p. 024. arXiv: hep-ph/0503053 [hep-ph].

[25] Michael Krämer, Stephen Mrenna and Davison E. Soper. 'Next-to-leading order QCD jet production with parton showers and hadronization'. In: *Phys. Rev.* D73 (2006), p. 014022. arXiv: hep-ph/0509127 [hep-ph].

[26] Stefano Frixione and Bryan R. Webber. 'Matching NLO QCD computations and parton shower simulations'. In: *JHEP* 06 (2002), p. 029. arXiv: hep-ph/0204244 [hep-ph].

[27] Paolo Nason. 'A New method for combining NLO QCD with shower Monte Carlo algorithms'. In: *JHEP* 11 (2004), p. 040. arXiv: hep-ph/0409146 [hep-ph].

[28] Keith Hamilton, Paolo Nason, Carlo Oleari and Giulia Zanderighi. 'Merging H/W/Z + 0 and 1 jet at NLO with no merging scale: a path to parton shower + NNLO matching'. In: *JHEP* 05 (2013), p. 082. arXiv: 1212.4504 [hep-ph].

[29] Keith Hamilton, Paolo Nason, Emanuele Re and Giulia Zanderighi. 'NNLOPS simulation of Higgs boson production'. In: *JHEP* 10 (2013), p. 222. arXiv: 1309.0017 [hep-ph].

[30] Simone Alioli et al. 'Matching Fully Differential NNLO Calculations and Parton Showers'. In: *JHEP* 06 (2014), p. 089. arXiv: 1311.0286 [hep-ph].

[31] Nils Lavesson and Leif Lönnblad. 'Extending CKKW-merging to One-Loop Matrix Elements'. In: *JHEP* 12 (2008), p. 070. arXiv: 0811.2912 [hep-ph]; Stefan Höche, Ye Li and Stefan Prestel. 'Drell-Yan lepton pair production at NNLO QCD with parton showers'. In: *Phys. Rev.* D91.7 (2015), p. 074015. arXiv: 1405.3607 [hep-ph].

[32] Andrea Banfi, Gavin P. Salam and Giulia Zanderighi. 'Principles of general final-state resummation and automated implementation'. In: *JHEP* 03 (2005), p. 073. arXiv: hep-ph/0407286 [hep-ph].

[33] Andrea Banfi, Heather McAslan, Pier Francesco Monni and Giulia Zanderighi. 'A general method for the resummation of event-shape distributions in $e^+e^-$ annihilation'. In: *JHEP* 05 (2015), p. 102. arXiv: 1412.2126 [hep-ph].

[34] Christian W. Bauer, Sean Fleming, Dan Pirjol and Iain W. Stewart. 'An Effective field theory for collinear and soft gluons: Heavy to light decays'. In: *Phys. Rev.* D63 (2001), p. 114020. arXiv: hep-ph/0011336 [hep-ph].

[35] Christian W. Bauer, Dan Pirjol and Iain W. Stewart. 'Soft collinear factorization in effective field theory'. In: *Phys. Rev.* D65 (2002), p. 054022. arXiv: hep-ph/0109045 [hep-ph].

[36] Christian W. Bauer, Sean Fleming, Dan Pirjol, Ira Z. Rothstein and Iain W. Stewart. 'Hard scattering factorization from effective field theory'. In: *Phys. Rev.* D66 (2002), p. 014017. arXiv: hep-ph/0202088 [hep-ph].

[37] Martin Beneke, Alexander P. Chapovsky, Markus Diehl and Thorsten Feldmann. 'Soft collinear effective theory and heavy to light currents beyond leading power'. In: *Nucl. Phys.* B643 (2002), pp. 431–476. arXiv: hep-ph/0206152 [hep-ph].

[38] Thomas Becher, Matthias Neubert and Gang Xu. 'Dynamical Threshold Enhancement and Resummation in Drell-Yan Production'. In: *JHEP* 07 (2008), p. 030. arXiv: 0710.0680 [hep-ph].

[39] Thomas Becher and Matthew D. Schwartz. 'A precise determination of $\alpha_s$ from LEP thrust data using effective field theory'. In: *JHEP* 07 (2008), p. 034. arXiv: 0803.0342 [hep-ph].

[40] Valentin Ahrens, Thomas Becher, Matthias Neubert and Li Lin Yang. 'Renormalization-Group Improved Prediction for Higgs Production at Hadron Colliders'. In: *Eur. Phys. J.* C62 (2009), pp. 333–353. arXiv: 0809.4283 [hep-ph].

[41] Yang-Ting Chien and Matthew D. Schwartz. 'Resummation of heavy jet mass and comparison to LEP data'. In: *JHEP* 08 (2010), p. 058. arXiv: 1005.1644 [hep-ph].

[42] Riccardo Abbate, Michael Fickinger, Andre H. Hoang, Vicent Mateu and Iain W. Stewart. 'Thrust at $N^3LL$ with Power Corrections and a Precision Global Fit for alphas(mZ)'. In: *Phys. Rev.* D83 (2011), p. 074021. arXiv: 1006.3080 [hep-ph].

[43] Alessandro Broggio, Matthias Neubert and Leonardo Vernazza. 'Soft-gluon resummation for slepton-pair production at hadron colliders'. In: *JHEP* 05 (2012), p. 151. arXiv: 1111.6624 [hep-ph].

[44] Thomas Becher, Guido Bell, Christian Lorentzen and Stefanie Marti. 'Transverse-momentum spectra of electroweak bosons near threshold at NNLO'. In: *JHEP* 02 (2014), p. 004. arXiv: 1309.3245 [hep-ph].

[45] Thomas Becher, Guido Bell, Christian Lorentzen and Stefanie Marti. 'The transverse-momentum spectrum of Higgs bosons near threshold at NNLO'. In: *JHEP* 11 (2014), p. 026. arXiv: 1407.4111 [hep-ph].

[46] André H. Hoang, Daniel W. Kolodrubetz, Vicent Mateu and Iain W. Stewart. '$C$-parameter distribution at N$^3$LL' including power corrections'. In: *Phys. Rev.* D91.9 (2015), p. 094017. arXiv: 1411.6633 [hep-ph].

[47] Stefan Kluth. 'Tests of Quantum Chromo Dynamics at e+ e- Colliders'. In: *Rept. Prog. Phys.* 69 (2006), pp. 1771–1846. arXiv: hep-ex/0603011 [hep-ex].

[48] Richard A. Davison and Bryan R. Webber. 'Non-Perturbative Contribution to the Thrust Distribution in e+ e- Annihilation'. In: *Eur. Phys. J.* C59 (2009), pp. 13–25. arXiv: 0809.3326 [hep-ph].

[49] Thomas Gehrmann, Gionata Luisoni and Pier Francesco Monni. 'Power corrections in the dispersive model for a determination of the strong coupling constant from the thrust distribution'. In: *Eur. Phys. J.* C73.1 (2013), p. 2265. arXiv: 1210.6945 [hep-ph].

[50] André H. Hoang, Daniel W. Kolodrubetz, Vicent Mateu and Iain W. Stewart. 'Precise determination of $\alpha_s$ from the $C$-parameter distribution'. In: *Phys. Rev.* D91.9 (2015), p. 094018. arXiv: 1501.04111 [hep-ph].

[51] K. A. Olive et al. 'Review of Particle Physics'. In: *Chin. Phys.* C38 (2014), p. 090001.

[52] David d'Enterria and Peter Z. Skands, eds. *Proceedings, High-Precision $\alpha_s$ Measurements from LHC to FCC-ee*. CERN. Geneva: CERN, 2015. arXiv: 1512.05194 [hep-ph]. URL: https://inspirehep.net/record/1409920/files/arXiv:1512.05194.pdf.

[53] Zvi Bern, Lance J. Dixon, David A. Kosower and Adrian Signer. 'Multiparton loop amplitudes and next-to-leading order jet cross-sections'. In: *QCD corrections and new physics. Proceedings, International Symposium, Hiroshima, Japan, October 27-29, 1997*. 1998. arXiv: hep-ph/9802264 [hep-ph]. URL: http://weblib.cern.ch/abstract?CERN-TH-98-39.

[54] Amitava Datta, Anindya Datta and Sujoy Poddar. 'Enriching the exploration of the mUED model with event shape variables at the {CERN} {LHC}'. In: *Physics Letters B* 712.3 (2012), pp. 219–225. URL: http://www.sciencedirect.com/science/article/pii/S0370269312002754.

[55] Monoranjan Guchait and Dipan Sengupta. 'Event-shape selection cuts for supersymmetry searches at the LHC with 7 TeV energy'. In: *Phys. Rev.* D84 (2011), p. 055010. arXiv: 1102.4785 [hep-ph].

[56] Lisa Randall and David Tucker-Smith. 'Dijet Searches for Supersymmetry at the Large Hadron Collider'. In: *Phys. Rev. Lett.* 101 (22 Nov. 2008), p. 221803. URL: http://link.aps.org/doi/10.1103/PhysRevLett.101.221803.

[57] Mrinal Dasgupta and Gavin P. Salam. 'Event shapes in e+ e- annihilation and deep inelastic scattering'. In: *J. Phys.* G30 (2004), R143. arXiv: hep-ph/0312283 [hep-ph].

[58] Andrea Banfi, Gavin P. Salam and Giulia Zanderighi. 'Phenomenology of event shapes at hadron colliders'. In: *JHEP* 06 (2010), p. 038. arXiv: 1001.4082 [hep-ph].

[59] Siegmund Brandt, Charles Peyrou, Ryszard Sosnowski and Andrzej Wroblewski. 'The principal axis of jets — an attempt to analyse high-energy collisions as two-body processes'. In: *Physics Letters* 12.1 (1964), pp. 57–61. URL: http://www.sciencedirect.com/science/article/pii/003191636491176X; Edward Farhi. 'Quantum Chromodynamics Test for Jets'. In: *Phys. Rev. Lett.* 39 (25 Dec. 1977), pp. 1587–1588. URL: http://link.aps.org/doi/10.1103/PhysRevLett.39.1587.

[60] James D. Bjorken and Stanley J. Brodsky. 'Statistical Model for Electron-Positron Annihilation into Hadrons'. In: *Phys. Rev. D* 1 (5 Mar. 1970), pp. 1416–1420. URL: http://link.aps.org/doi/10.1103/PhysRevD.1.1416.

[61] Vernon D. Barger, J. Ohnemus and Roger J. N. Phillips. 'Event shape criteria for single lepton top signals'. In: *Phys. Rev.* D48 (1993), pp. 3953–3956. arXiv: hep-ph/9308216 [hep-ph].

[62] R. Keith Ellis, Douglas A. Ross and Anthony E. Terrano. 'The Perturbative Calculation of Jet Structure in e+ e- Annihilation'. In: *Nucl. Phys.* B178 (1981), pp. 421–456.

[63] Siegfried Bethke. 'Hadron Physics in Electron-Positron Annihilation'. In: *High Energy Phenomenology*. Scottish Graduate Series (1994). Ed. by Ken J. Peach and Lance L.J. Vick. URL: https://books.google.co.uk/books?id=If3SkYMbDGAC.

[64] Aude Gehrmann-De Ridder, Thomas Gehrmann, E. W. Nigel Glover and Gudrun Heinrich. 'NNLO corrections to event shapes in e+ e- annihilation'. In: *JHEP* 12 (2007), p. 094. arXiv: 0711.4711 [hep-ph].

[65] Stefano Catani, Luca Trentadue, G. Turnock and Bryan R. Webber. 'Resummation of large logarithms in e+ e- event shape distributions'. In: *Nucl. Phys.* B407 (1993), pp. 3–42.

[66] Leandro G. Almeida et al. 'Comparing and counting logs in direct and effective methods of QCD resummation'. In: *JHEP* 04 (2014), p. 174. arXiv: 1401.4460 [hep-ph].

[67] John Ellis, Mary K. Gaillard and Graham G. Ross. 'Search for gluons in e+e- annihilation'. In: *Nuclear Physics B* 111.2 (1976), pp. 253–271. URL: http://www.sciencedirect.com/science/article/pii/0550321376905423.

[68] Howard Georgi and Marie Machacek. 'Simple Quantum-Chromodynamics Prediction of Jet Structure in $e^+e^-$ Annihilation'. In: *Phys. Rev. Lett.* 39 (20 Nov. 1977), pp. 1237–1239. URL: http://link.aps.org/doi/10.1103/PhysRevLett.39.1237.

[69] Andrew J. Larkoski, Duff Neill and Jesse Thaler. 'Jet shapes with the broadening axis'. In: *Journal of High Energy Physics* 2014.4 (2014), pp. 1–50. URL: http://dx.doi.org/10.1007/JHEP04(2014)017.

[70] Giuseppe Marchesini. 'From QCD Lagrangian to Monte Carlo simulation'. In: *Lect. Notes Phys.* 737 (2008), pp. 159–180. arXiv: hep-ph/0701268 [hep-ph].

[71] John C. Collins, Davison E. Soper and George F. Sterman. 'Transverse Momentum Distribution in Drell-Yan Pair and W and Z Boson Production'. In: *Nucl. Phys.* B250 (1985), pp. 199–224.

[72] Iain W. Stewart. *Lectures on the Soft-Collinear Effective Theory*. 2013. URL: http://ocw.mit.edu/courses/physics/8-851-effective-field-theory-spring-2013/lecture-notes/MIT8_851S13_scetnotes.pdf.

[73] Christian Bauer and Matthias Neubert. 'Heavy-Quark and Soft-Collinear Effective Theory (rev.)' In: *Chin. Phys. C 38*. Ed. by K.A. Olive et al. (Particle Data Group), (2014) and 2015 update. URL: http://pdg.lbl.gov/2015/reviews/rpp2015-rev-heavy-quark-eff-th.pdf.

[74] Thomas Becher, Alessandro Broggio and Andrea Ferroglia. *Introduction to Soft-Collinear Effective Theory*. Lecture Notes in Physics. Springer International Publishing, 2015. URL: https://books.google.co.uk/books?id=JSURBwAAQBAJ.

[75] Matthew D. Schwartz. *Quantum Field Theory and the Standard Model*. Cambridge University Press, 2014. URL: http://www.cambridge.org/us/academic/subjects/physics/theoretical-physics-and-mathematical-physics/quantum-field-theory-and-standard-model.

[76] Enrico Fermi. 'Tentativo di una Teoria Dei Raggi $\beta$'. Italian. In: *La Ricerca Scientifica* 2.12 (1933), pp. 491–495; Enrico Fermi. 'Tentativo di una Teoria Dei Raggi $\beta$'. Italian. In: *Il Nuovo Cimento* 11.1 (1934), pp. 1–19. URL: http://dx.doi.org/10.1007/BF02959820; Enrico Fermi. 'Versuch einer Theorie der $\beta$-Strahlen. I'. German. In: *Zeitschrift für Physik* 88.3 (1934), pp. 161–177. URL: http://dx.doi.org/10.1007/BF01351864.

[77] Werner Heisenberg and Heinrich Euler. 'Folgerungen aus der Diracschen Theorie des Positrons'. In: *Zeitschrift für Physik* 98.11 (1936), pp. 714–732. URL: http://dx.doi.org/10.1007/BF01343663.

[78] Steven Weinberg. 'Phenomenological Lagrangians'. In: *Physica* A96 (1979), pp. 327–340; Heinz Pagels. 'Departures from Chiral Symmetry: A Review'. In: *Phys. Rept.* 16 (1975), p. 219; Jürg Gasser and Heinrich Leutwyler. 'Chiral perturbation theory to one loop'. In: *Annals of Physics* 158.1 (1984), pp. 142–210. URL: http://www.sciencedirect.com/science/article/pii/0003491684902422.

[79] Thomas Becher and Guido Bell. 'Analytic Regularization in Soft-Collinear Effective Theory'. In: *Phys. Lett.* B713 (2012), pp. 41–46. arXiv: 1112.3907 [hep-ph].

[80] Jui-yu Chiu, Andreas Fuhrer, Andre H. Hoang, Randall Kelley and Aneesh V. Manohar. 'Soft-Collinear Factorization and Zero-Bin Subtractions'. In: *Phys. Rev.* D79 (2009), p. 053007. arXiv: 0901.1332 [hep-ph].

[81] Jui-yu Chiu, Ambar Jain, Duff Neill and Ira Z. Rothstein. 'The Rapidity Renormalization Group'. In: *Phys. Rev. Lett.* 108 (2012), p. 151601. arXiv: 1104.0881 [hep-ph]; Jui-Yu Chiu, Ambar Jain, Duff Neill and Ira Z. Rothstein. 'A Formalism for the Systematic Treatment of Rapidity Logarithms in Quantum Field Theory'. In: *JHEP* 05 (2012), p. 084. arXiv: 1202.0814 [hep-ph].

[82] Thomas Becher and Matthias Neubert. 'Drell-Yan Production at Small $q_T$, Transverse Parton Distributions and the Collinear Anomaly'. In: *Eur. Phys. J.* C71 (2011), p. 1665. arXiv: 1007.4005 [hep-ph].

[83] Christian W. Bauer, Dan Pirjol and Iain W. Stewart. 'Soft collinear factorization in effective field theory'. In: *Phys. Rev.* D65 (2002), p. 054022. arXiv: hep-ph/0109045 [hep-ph].

[84] Sean Fleming, Andre H. Hoang, Sonny Mantry and Iain W. Stewart. 'Top Jets in the Peak Region: Factorization Analysis with NLL Resummation'. In: *Phys. Rev.* D77 (2008), p. 114003. arXiv: 0711.2079 [hep-ph].

[85] Michal Czakon. 'The Four-loop QCD beta-function and anomalous dimensions'. In: *Nucl. Phys.* B710 (2005), pp. 485–498. arXiv: hep-ph/0411261 [hep-ph]; Timo van Ritbergen, Jozef A. M. Vermaseren and Sergey A. Larin. 'The Four loop beta function in quantum chromodynamics'. In: *Phys. Lett.* B400 (1997), pp. 379–384. arXiv: hep-ph/9701390 [hep-ph].

[86] Vladimir A. Smirnov and E. R. Rakhmetov. 'The Strategy of regions for asymptotic expansion of two loop vertex Feynman diagrams'. In: *Theor. Math. Phys.* 120 (1999). [Teor. Mat. Fiz.120,64(1999)], pp. 870–875. arXiv: hep-ph/9812529 [hep-ph].

[87] Martin Beneke and Thorsten Feldmann. 'Factorization of heavy to light form-factors in soft collinear effective theory'. In: *Nucl. Phys.* B685 (2004), pp. 249–296. arXiv: hep-ph/0311335 [hep-ph].

[88] Andreas Vogt. 'Next-to-next-to-leading logarithmic threshold resummation for deep inelastic scattering and the Drell-Yan process'. In: *Phys. Lett.* B497 (2001), pp. 228–234. arXiv: hep-ph/0010146 [hep-ph]; Carola F. Berger. 'Higher orders in A(alpha(s))/[1-x]+ of nonsinglet partonic splitting functions'. In: *Phys. Rev.* D66 (2002), p. 116002. arXiv: hep-ph/0209107 [hep-ph]; Sven-Olaf Moch, Jozef A. M. Vermaseren and Andreas Vogt. 'Three-loop results for quark and gluon form-factors'. In: *Phys. Lett.* B625 (2005), pp. 245–252. arXiv: hep-ph/0508055 [hep-ph]; Andrey Grozin, Johannes M. Henn, Gregory P. Korchemsky and Peter Marquard. 'Three Loop Cusp Anomalous Dimension in QCD'. In: *Phys. Rev. Lett.* 114.6 (2015), p. 062006. arXiv: 1409.0023 [hep-ph].

[89] Thomas Becher and Matthias Neubert. 'On the Structure of Infrared Singularities of Gauge-Theory Amplitudes'. In: *JHEP* 06 (2009). [Erratum: JHEP11,024(2013)], p. 081. arXiv: 0903.1126 [hep-ph]; Sven-Olaf Moch, Jozef A. M. Vermaseren and Andreas Vogt. 'The Quark form-factor at higher orders'. In: *JHEP* 08 (2005), p. 049. arXiv: hep-ph/0507039 [hep-ph]; Sven-Olaf Moch, Jozef A. M. Vermaseren and Andreas Vogt. 'Three-loop results for quark and gluon form-factors'. In: *Phys. Lett.* B625 (2005), pp. 245–252. arXiv: hep-ph/0508055 [hep-ph]; Pavel A. Baikov, Konstantin G. Chetyrkin, Alexander V. Smirnov, Vladimir A. Smirnov and Matthias Steinhauser. 'Quark and gluon form factors to three loops'. In: *Phys. Rev. Lett.* 102 (2009), p. 212002. arXiv: 0902.3519 [hep-ph].

[90] Thomas Becher, Rikkert Frederix, Matthias Neubert and Lorena Rothen. 'Automated NNLL + NLO resummation for jet-veto cross sections'. In: *Eur. Phys. J.* C75.4 (2015), p. 154. arXiv: 1412.8408 [hep-ph].

[91] David Farhi, Ilya Feige, Marat Freytsis and Matthew D. Schwartz. 'Streamlining resummed QCD calculations using Monte Carlo integration'. In: *JHEP* 08 (2016), p. 112. arXiv: 1507.06315 [hep-ph].

[92] Daekyoung Kang, Ou Z. Labun and Christopher Lee. 'Equality of hemisphere soft functions for $e^+e^-$, DIS and $pp$ collisions at $\mathcal{O}(\alpha_s^2)$'. In: *Phys. Lett.* B748 (2015), pp. 45–54. arXiv: 1504.04006 [hep-ph].

[93] Thomas Becher, Matthias Neubert and Ben D. Pecjak. 'Factorization and Momentum-Space Resummation in Deep-Inelastic Scattering'. In: *JHEP* 01 (2007), p. 076. arXiv: hep-ph/0607228 [hep-ph].

[94] Thomas Becher, Guido Bell and Matthias Neubert. 'Factorization and Resummation for Jet Broadening'. In: *Phys. Lett.* B704 (2011), pp. 276–283. arXiv: 1104.4108 [hep-ph].

[95] Jonathon Carter and Gudrun Heinrich. 'SecDec: A general program for sector decomposition'. In: *Comput. Phys. Commun.* 182 (2011), pp. 1566–1581. arXiv: 1011.5493 [hep-ph]; Sophia Borowka, Jonathon Carter and Gudrun Heinrich. 'Numerical Evaluation of Multi-Loop Integrals for Arbitrary Kinematics with SecDec 2.0'. In: *Comput. Phys. Commun.* 184 (2013), pp. 396–408. arXiv: 1204.4152 [hep-ph]; Sophia Borowka and Gudrun Heinrich. 'Massive non-planar two-loop four-point integrals with SecDec 2.1'. In: *Comput. Phys. Commun.* 184 (2013), pp. 2552–2561. arXiv: 1303.1157 [hep-ph]; Sophia Borowka et al. 'SecDec-3.0: numerical evaluation of multi-scale integrals beyond one loop'. In: *Comput. Phys. Commun.* 196 (2015), pp. 470–491. arXiv: 1502.06595 [hep-ph].

[96] Klaus Hepp. 'Proof of the Bogoliubov-Parasiuk theorem on renormalization'. In: *Communications in Mathematical Physics* 2.1 (1966), pp. 301–326. URL: http://dx.doi.org/10.1007/BF01773358; Thomas Binoth and Gudrun Heinrich. 'An automatized algorithm to compute infrared divergent multiloop integrals'. In: *Nucl. Phys.* B585 (2000), pp. 741–759. arXiv: hep-ph/0004013 [hep-ph]; Thomas Binoth and Gudrun Heinrich. 'Numerical evaluation of multiloop integrals by sector decomposition'. In: *Nucl. Phys.* B680 (2004), pp. 375–388. arXiv: hep-ph/0305234 [hep-ph].

[97] Thomas Hahn. 'CUBA: A Library for multidimensional numerical integration'. In: *Comput. Phys. Commun.* 168 (2005), pp. 78–95. arXiv: hep-ph/0404043 [hep-ph]. URL: http://www.feynarts.de/cuba/.

[98] Setsuya Kawabata. 'A new Monte Carlo event generator for high energy physics'. In: *Computer Physics Communications* 41.1 (1986), pp. 127–153. URL: http://www.sciencedirect.com/science/article/pii/0010465586900251; Setsuya Kawabata. 'A new version of the multi-dimensional integration and event generation package BASES/SPRING'. In: *Computer Physics Communications* 88.2 (1995), pp. 309–326. URL: http://www.sciencedirect.com/science/article/pii/001046559500028E.

[99] William H. Press, Saul A. Teukolsky, William T. Vetterling and Brian P. Flannery. *Numerical Recipes 3rd Edition: The Art of Scientific Computing*. 3rd ed. New York, NY, USA: Cambridge University Press, 2007.

[100] *Boost C++ Libraries*. http://www.boost.org/. Accessed: 17th September 2016, Version 1.61.0.

[101] Giorgio Parisi. 'Super Inclusive Cross-Sections'. In: *Phys. Lett.* B74 (1978), pp. 65–67; John F. Donoghue, Francis E. Low and So-Young Pi. 'Tensor Analysis of Hadronic Jets in Quantum Chromodynamics'. In: *Phys. Rev.* D20 (1979), p. 2759.

[102] André H. Hoang, Daniel W. Kolodrubetz, Vicent Mateu and Iain W. Stewart. '$C$-parameter distribution at N$^3$LL' including power corrections'. In: *Phys. Rev.* D91.9 (2015), p. 094017. arXiv: 1411.6633 [hep-ph].

[103] Stefano Catani and Michael H. Seymour. 'The Dipole formalism for the calculation of QCD jet cross-sections at next-to-leading order'. In: *Phys. Lett.* B378 (1996), pp. 287–301. arXiv: hep-ph/9602277 [hep-ph]; Stefano Catani and Michael H. Seymour. 'A General algorithm for calculating jet cross-sections in NLO QCD'. In: *Nucl. Phys.* B485 (1997). [Erratum: Nucl. Phys.B510,503(1998)], pp. 291–419. arXiv: hep-ph/9605323 [hep-ph].

[104] Thomas Becher and Guido Bell. 'NNLL Resummation for Jet Broadening'. In: *JHEP* 11 (2012), p. 126. arXiv: 1210.0580 [hep-ph].

[105] Massimiliano Grazzini, Andreas Papaefstathiou, Jennifer M. Smillie and Bryan R. Webber. 'Resummation of the transverse-energy distribution in Higgs boson production at the Large Hadron Collider'. In: *JHEP* 09 (2014), p. 056. arXiv: 1403.3394 [hep-ph].

[106] Randall Kelley, Matthew D. Schwartz, Robert M. Schabinger and Hua Xing Zhu. 'The two-loop hemisphere soft function'. In: *Phys. Rev.* D84 (2011), p. 045022. arXiv: 1105.3676 [hep-ph].

[107] Pier Francesco Monni, Thomas Gehrmann and Gionata Luisoni. 'Two-Loop Soft Corrections and Resummation of the Thrust Distribution in the Dijet Region'. In: *JHEP* 08 (2011), p. 010. arXiv: 1105.4560 [hep-ph].

[108] Guido Bell, Andrew Hornig, Chris Lee and Jim Talbert. 'Resummation of e+e- angularities at NNLL'. Presentation given at SCET2016, Hamburg, 22 March 2016. 2016. URL: https://indico.desy.de//event/scet2016.

[109] Andrei V. Belitsky. 'Two loop renormalization of Wilson loop for Drell-Yan production'. In: *Phys. Lett.* B442 (1998), pp. 307–314. arXiv: hep-ph/9808389 [hep-ph].

[110] Thomas Becher, Guido Bell and Stefanie Marti. 'NNLO soft function for electroweak boson production at large transverse momentum'. In: *JHEP* 04 (2012), p. 034. arXiv: 1201.5572 [hep-ph].

[111] Thomas Becher and Xavier Garcia i Tormo. 'Factorization and resummation for transverse thrust'. In: *JHEP* 06 (2015), p. 071. arXiv: 1502.04136 [hep-ph]; Thomas Becher, Xavier Garcia i Tormo and Jan Piclum. 'Next-to-next-to-leading logarithmic resummation for transverse thrust'. In: *Phys. Rev.* D93.5 (2016). [Erratum: Phys. Rev.D93,no.7,079905(2016)], p. 054038. arXiv: 1512.00022 [hep-ph].

# Quotes

Harold North Fowler. *Theaetetus ; Sophist.* Vol. 12/12. Plato. London: Heinemann, 1921.

James Gleick. *Chaos : Making a New Science.* London: Heinemann, 1988.

Johann Wolfgang von Goethe. *Wilhelm Meisters Wanderjahre, oder Die Entsagenden.* German. Stuttgart: Cotta, 1829.

Wing-Tsit Chan. *A source book in Chinese philosophy.* Chinese (translation) ; English. 1st Princeton pbk. ed. Source Books in Asian Philosophy 2. Princeton, N.J.: Princeton University Press, 1969, c1963.

Agniezka Holland. *The Secret Garden.* Film. Screenplay by Caroline Thompson. Based on the book by Frances Hodgson Burnett. Warner Bros. Family Entertainment, 1993.

Zbyněk Žába. *Les Maximes de Ptahhotep.* Prague: Československa akademie věd, 1956; Miriam Lichtheim. *The Old and Middle Kingdoms.* English. Vol. 1/3. Ancient Egyptian Literature, a Book of Readings. Berkeley: University of California Press, 1973.

Geoffrey James. *The Tao of Programming.* Santa Monica: Infobooks, 1987.

Winston Churchill. *The story of the Malakand field force : an episode of frontier war.* New York; London: Longmans, Green, and Co., 1898.

Mick Jagger and Keith Richards. *You can't always get what you want.* Song. Track 9/9. Let it bleed. London: Decca, 1969.

Margaret MacMillan and Richard Holbrooke. *Paris 1919: Six Months That Changed the World*. New York: Random House Publishing Group, 2002.

Byron, George Gordon, 6th Baron. *English Bards and Scotch Reviewers*. London: James Cawthorn, 1809.